POLYMER AND CARBON NANOTUBE MATERIALS FOR CHEMICAL SENSORS AND ORGANIC ELECTRONICS
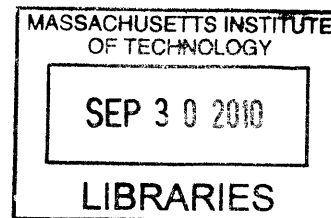
BY

FEI WANG

B.S. in Chemistry
Peking University, 2005

Submitted to the Department of Materials Science and Engineering
in Partial Fulfillment of the Requirements for the Degree of

DOCTOR OF PHILOSOPHY

at the

MASSACHUSETTS INSTITUTE OF TECHNOLOGY

June 2010

Signature of Author: _____ _____

Department of Materials Science and Engineering
May 14, 2010

Certified by: _____

Timothy M. Swager
Thesis Advisor

Michael F. Rubner
Thesis Co-Advisor

Accepted by: _____

Christine Ortiz
Chair, Departmental Committee on Graduate Students

To my family

POLYMER AND CARBON NANOTUBE MATERIALS FOR CHEMICAL SENSORS AND ORGANIC ELECTRONICS

BY

FEI WANG

Submitted to the Department of Materials Science and Engineering on May 14, 2010
in Partial Fulfillment of the Requirements for the Degree of
Doctor of Philosophy in Materials Science and Engineering

ABSTRACT

This thesis details the development of new materials for high-performance chemical sensing as well as organic electronic applications. In Chapter 2, we develop a chemiresistive material based on single-walled carbon nanotubes (SWCNTs) and hexafluoroisopropanol (HFIP) functionalized polythiophene, with a largely simplified fabrication process. The sensor shows high sensitivity and selectivity for a nerve reagent stimulant. A series of mechanistic studies indicate that the sensing response occurs via charge transfer, the introduction of scattering sites and configurational changes in the polymers. Temkin isotherm is utilized to successfully explain the relationship between the analyte concentration and sensor response.

In Chapter 3, we develop a chemiresistive material based on SWCNTs wrapped with a calixarene-substituted polythiophene. The material displays a selective and sensitive response to xylene isomers. The selectivity is verified by nuclear magnetic resonance spectroscopy, quartz crystal microbalance measurements, and fluorescence spectroscopy. Mechanistic studies, including field effect investigations and Raman spectroscopy, are also reported.

In Chapter 4, we present a multi-walled carbon nanotube (MWCNT) array with a series of cross-sensitive recognition groups covalently attached to the MWCNTs. These functional groups greatly enhance the sensitivity and selectivity to the target analytes. The distinct response pattern of each chemical was subjected to statistical analysis, leading to a clear separation and accurate identification of 100 % of the compounds. We also present a highly sensitive humidity indicator consisting of a platinum-CNT composite.

In Chapter 5, we design and synthesize several HFIP-containing polythiophenes. The photophysical properties and the fluorescence quenching of the polymers are systematically investigated. An interesting enhancement of the energy transfer constants is observed between these polymers and phenyl-C61-butyric acid methyl ester (PCBM), resulting from the strong hydrogen bonding interaction. Further X-ray diffraction studies of the polymers and their mixtures with PCBM demonstrate that the HFIP substitution prevents clean phase separation between the polythiophene and the PCBM. These results together prove the power of molecular interactions in changing the donor-acceptor interactions and in controlling the polymer morphology.

Thesis Supervisor: Timothy M. Swager
Title: John D. MacArthur Professor of Chemistry and Department Head

Table of Contents

List of Figures

List of Tables

List of Schemes

Chapter 1

Introduction

1.1 Chemiresistors

The development of a low cost, low power and portable sensing device is needed for various applications, such as homeland security and monitoring of agricultural, medical, and manufacturing environments. A chemiresistor, which is a chemical sensor that detects analyts via changes in its resistance, offers significant promise. In particular, chemiresistors can be easily fabricated and implemented, since high precision resistance measurements can be realized using very simple electronics.

Over the past decades, several materials have been utilized as gas sensors. Among these, metal oxides-based materials are the most popular.[1] Although these materials function as effective sensors for several reductive gases, their high resistance necessitates high power consumption. In addition, these materials cannot discriminate between similar gases. Organic semiconductors, usually conjugated polymers, have been studied as highly selective chemiresistor materials.[2-4] The integration of molecular recognition units in the polymer structures is attractive; however these materials suffer from electrostatic/dielectric interferences and fragile organic-metal interfaces. Recently carbon nanotube field effect transistors have been investigated as sensors for biological and vapor analytes.[5-8] Carbon nanotubes are ideal for sensing applications because their electrical properties are very sensitive to the local chemical environment. However, there are still some limitations to the widespread application of CNTs, such as the lack of selectivity. In this chapter we will introduce the basic chemistry of carbon nanotubes that is directly relevant to this thesis, without attempting a comprehensive review.

1.2 Carbon Nanotube Materials

Since their first report by Iijima in 1991,[9] carbon nanotubes (CNTs) have been a subject of intensive research.[10-13] CNTs can be conceptualized as rolled-up graphene sheets. Their structures consist of either a single wall of graphene(single-walled CNTs, SWCNTs) or multiple concentric graphene walls (multi-walled CNTs, MWCNTs) (Figure 1.1a). The rolling-up of the graphene sheets can be described with a roll-up vector (n,m), whose beginning and end join together during the folding of the graphene sheet.[14] The magnitude of the numbers n and m indicates the diameter of the tube. The direction of the vector determines the atomic orientation along the tube circumference, thus leading to different types such as armchair ($n = m$), zigzag ($m = 0$) or chiral ($n \neq m$) nanotubes (Figure 1.1b). The difference of the n and m number determines the electronic properties of the SWCNTs. For metallic nanotubes, $n\text{-}m = 3q$ where q is an integer or zero, and for semiconductive nanotubes, $n\text{-}m \neq 3q$ or zero. Naturally, SWCNTs are synthesized with a metallic/semiconductive ratio of 1/2. The efficient separation of these two types of nanotubes is an active area of research interest.[15-18]
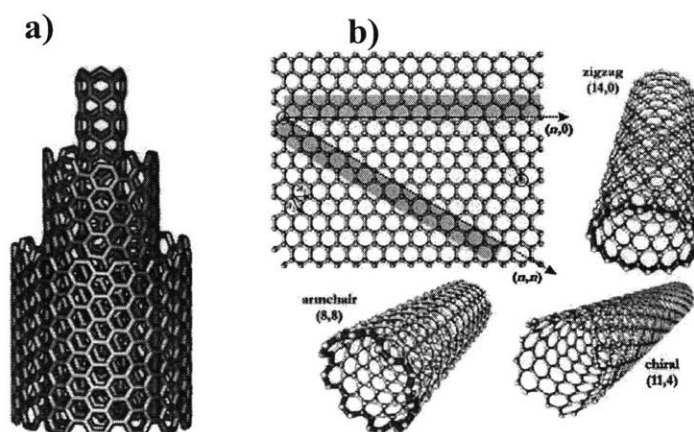
Figure 1.1. Structure of a MWCNT (a) and the rolling-up method (b). Adapted from reference 14.

CNTs have unique mechanical, optical, thermal and electrical properties. CNTs are one of the strongest and stiffest materials in nature, with a tensile strength of 11-150 GPa (0.38-1.55 GPa for stainless steel) and a Young's modulus on the order of 270-950 GPa[19,20] (200 GPa for stainless steel). The emission wavelength of SWCNTs falls into the near-infrared range[21,22] (0.8-2.1 μm, depending on the nanotube structure) and is very sensitive to the local environment, thus facilitating the biological detection.[23,24] Moreover, CNTs have been used as the active channel in transistors and conductors due to their high mobilities (up to 10,000 cm^2Vs^{-1} at room temperature),[25] electrical conductivities,[26,27] current-carrying capacities (up to 10^9 A cm^{-2})[28] and thermal conductivities (up to 3,500 $Wm^{-1} K^{-1}$).[29]

CNTs are ideal candidates for sensing applications because their electronic properties are extremely sensitive to changes in their local chemical environments. Since the first study of the response of a SWCNT field effect transistor toward ammonia and nitrogen dioxide,[30] CNTs have found widespread applications in detecting chemical vapors[5,6] and biological molecules.[7,8] Moreover, the incorporation of recognition groups into such sensors can largely enhance the selectivity and sensitivity. As conceptualized in Figure 1.2, sensor **a** with bare nanotubes is responds both to the target analyte (green triangles) and the contaminants (purple squares and blue circles), sensor **b**, with rational recognition groups, has an increased response to the target analyte and almost no response to the contaminants.

a) No Functionalization

b) Functionalized with Recognition Groups
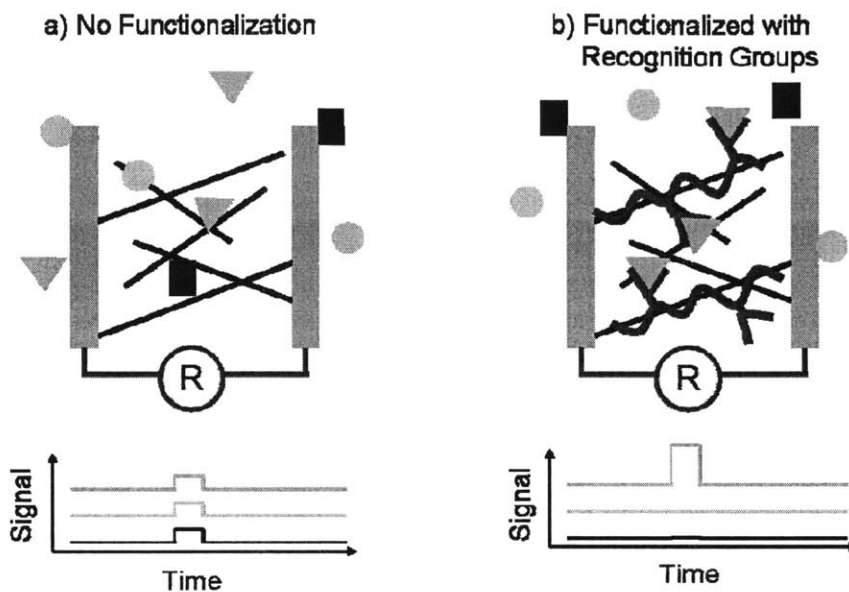
Figure 1.2. Increasing sensitivity and selectivity by incorporation of recognition groups.

In most previous cases, recognition groups were introduced onto the CNT-based sensor after its fabrication, which can be complicated by the bundled nature of CNTs. [5-8] Our goal is to simultaneously introduce enhanced sensitivity/sensitivity to the sensors and to simplify the fabrication process. Therefore, rational functionalization of the CNTs, either by their interaction with a conjugated polymer or by covalent functionalization, accomplishes both goals. We will discuss each of these functionalization methods in more detail.

1.3 CNT/Conjugated Polymer Interactions

Conjugated polymers are polymers whose backbone contains alternating single and multiple bonds. [31,32] Several examples of conjugated polymers are shown in Figure 1.3. The interactions between the molecular orbitals along the polymer backbone result in an extended system of delocalized π-electrons, which leads to many interesting electronic and optical

properties. The 2000 Nobel Prize in Chemistry recognized the important discovery that doped

conjugated polymers display conductive properties.[33-35]
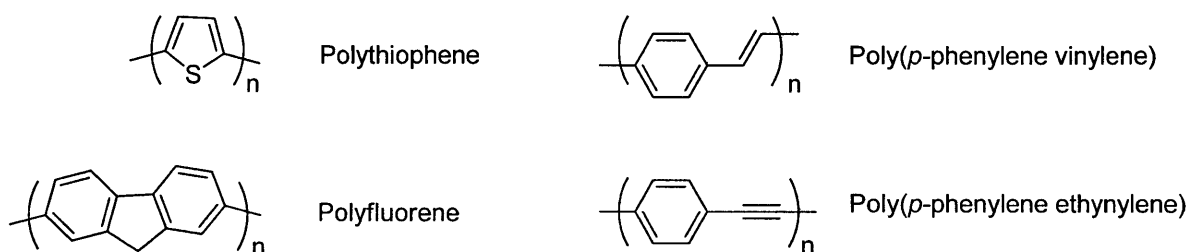
Figure 1.3. Examples of conjugated polymers.

The most important advantage of conjugated polymers over other conductive or

semiconductive materials is the ease of processability. Another advantage is the polymers'

properties can be fine-tuned through controlled organic synthesis. This is extremely important

in sensor development, because enhanced sensing performance can be achieved with optimized

recognition groups.[2,3] Figure 1.4 shows two examples of conjugated polymers with

recognition groups that have been used for chemical sensing. Binding of the crown ether in

polymer **1** to potassium cations resulted in the aggregation of the polymer and a red-shift in its

fluorescence emission.[36] Binding of a neutral organic molecule onto the calixarene motif in

polymer **2** enhanced the conductivity of the polymer film.[37]
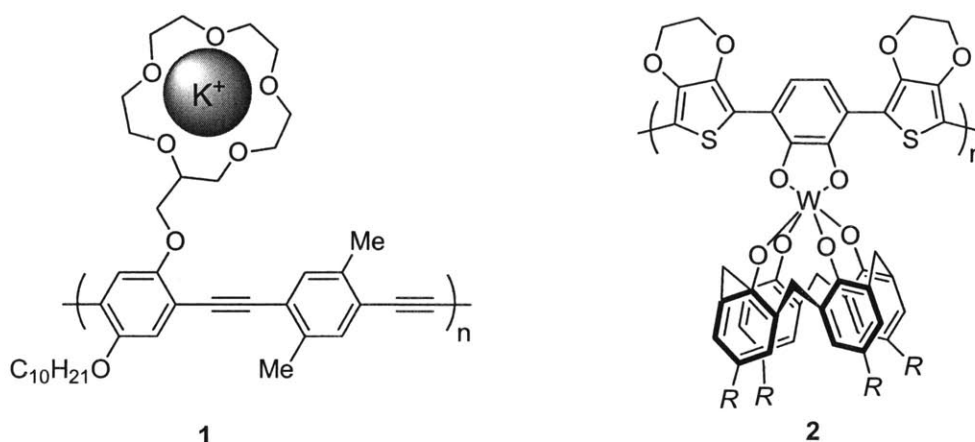
Figure 1.4. Examples of conjugated polymers with recognition groups.

Conjugated polymers were demonstrated to have strong $\pi-\pi$ interactions with CNTs,[38,39] and can stabilize CNT dispersions via steric effect.[40] Compare to the electrostatic stabilization by surfactants that is more effective at low concentration of the dispersion, the steric stabilization are effective both at low and high concentrations. As shown in Figure 1.5, a very stable dispersion of SWCNTs can be achieved by sonication of the nanotubes with a poly(3-hexylthiophene) (P3HT) solution.[41] In addition to nanotubes, conjugated polymers also stabilize graphene, and have been utilized to obtain single graphene sheets. [42]
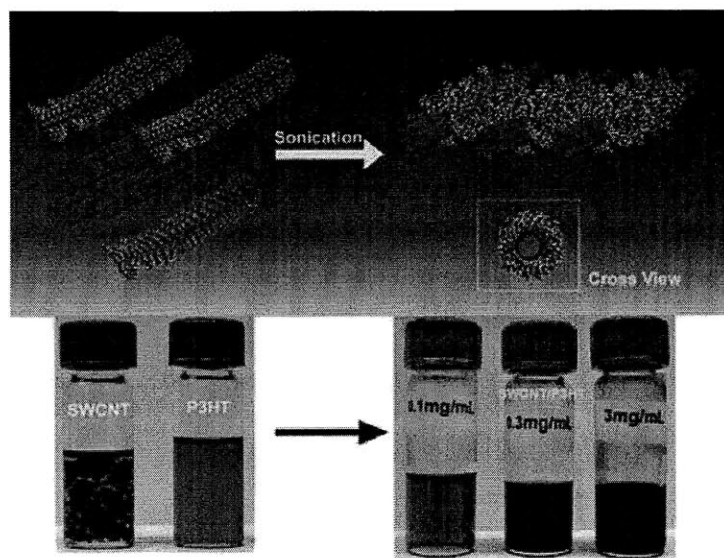
Figure 1.5. Stable SWCNT dispersions obtained in the presence of a conjugated polymer. Adapted from reference 41.

1.4 Covalent Functionalization of CNTs

Covalent functionalization of CNTs has been accomplished via oxidative reactions, thermally activated addition at nanotube sidewalls, and substitution reaction on fluorinated nanotubes.[14,43] However, the incorporation of recognition groups onto nanotubes by these methods are limited because the reactions usually proceed under harsh conditions. For example, high temperature, high pressure, or highly reactive reagents (concentrated HNO_3, lithium diisopropylamide, *etc.*), limit the functional group tolerance of many of these reactions.

Our group recently developed a highly efficient modular functionalization approach of CNTs and fullerenes.[44,45] The proposed reaction mechanism is shown in Scheme 1.1 with a fullerene substrate. Initially, the very reactive zwitterionic complex, which is formed between 4-dimethylaminopyridine (DMAP) and dimethyl acetylene dicarboxylate (DMAD) adds to the double bonds of fullerenes. The fullerene-centered anion then attacks the carbonyl carbon of

the ester group, affording a charged intermediate **3**. Further addtion of methanol replaces the

DMAP with methoxy group, providing the fullerene-DMAD adduct **4**.
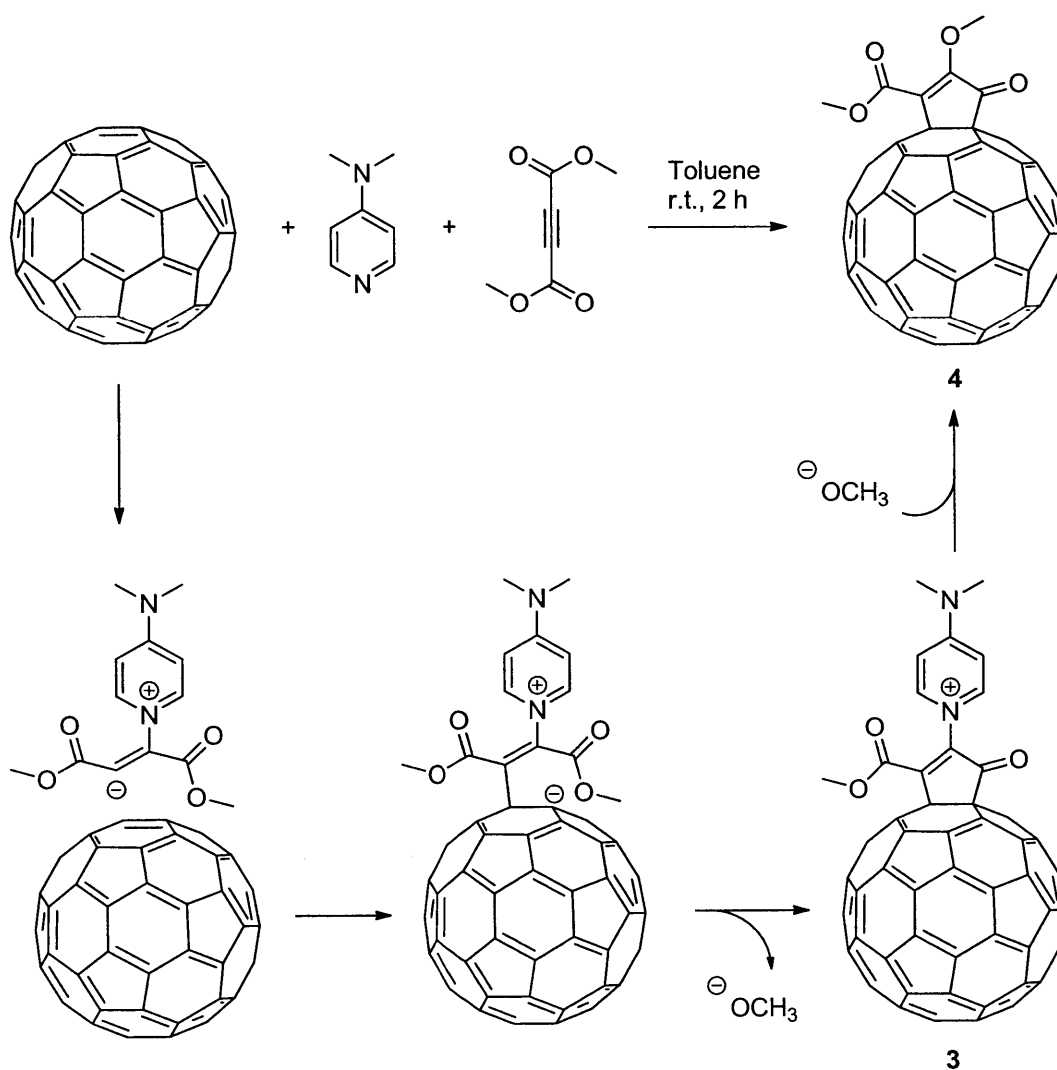
Scheme 1.1. Proposed mechanism for zwitterion-initiated functionalization of fullerenes.

Diverse functionalization can be introduced into the system through three strategies. First, charge trapping of the zwitterionic intermediate with added nucleophiles can readily afford various functional groups. Second, demethylation of the cyclopentenones of the CNTs can yield highly water-soluble CNTs functionalized with free hydroxyl groups. Third, CNTs can be functionalized with other disubstitued acetylene dicarboxylates, including those with chloroethyl, allyl, and propargyl groups. These groups can be further transformed by SN_2 substitution, thiol addition or 1,3-dipolar cycloadditions, respectively.

1.5 Outline of Thesis

In this thesis, we present our work on developing new materials for resistance-based sensing as well as organic electronic applications. In Chapters 2 and 3, we develop CNT/polythiophene hybrid materials for the selective and sensitive detection of a chemical warfare agent stimulant and structural isomers of xylenes, respectively. We also study their sensing mechanisms and explore the signal transduction mechanism. In Chapter 4, we develop a sensor array with covalently functionalized MWCNTs that can clearly identify organic volatile compounds by their functional groups. In Chapter 5, we develop several HFIP-containing polymers and investigat the hydrogen bonding effect in polythiophene/PCBM hybrid materials.

1.6 References and Notes

(1)   Henrich, V. E.; Cox, P. A. *The Surface Science of Metal Oxides*; Cambridge University Press, 1996.

(2)   Thomas, S. W.; Joly, G. D.; Swager, T. M. *Chem. Rev.* **2007**, *107*, 1339-1386.

(3)   McQuade, D. T.; Pullen, A. E.; Swager, T. M. *Chem. Rev.* **2000**, *100*, 2537-2574.

(4)   Swager, T. M. *Acc. Chem. Res.* **1998**, *31*, 201-207.

(5)   Kauffman, D. R.; Star, A. *Angew. Chem. Int. Ed.* **2008**, *47*, 6550-6570.

(6)   Snow, E. S.; Perkins, F. K.; Robinson, J. A. *Chem. Soc. Rev.* **2006**, *35*, 790-798.

(7)   Allen, B. L.; Kichambare, P.; Star, A. *Adv. Mater.* **2007**, *19*, 1439-1451.

(8)   Kim, S. N.; Rusling, J.; Papadimitrakopoulos, F. *Adv. Mater.* **2007**, *19*, 3214-3228.

(9)   Iijima, S. *Nature* **1991**, *354*, 56-58.

(10)   O'Connell, M. J. *Carbon Nanotubes: Properties and Applications*; 1st ed.; CRC Press, 2006.

(11)   Harris, P. J. F. *Carbon Nanotube Science: Synthesis, Properties and Applications*; 1st ed.; Cambridge University Press, 2009.

(12)   Jorio, A. *Carbon Nanotubes: Advanced Topics in the Synthesis, Structure, Properties and Applications*; 1st ed.; Springer, 2008.

(13)   Saito, R.; Dresselhaus, G.; Dresselhaus, M. S. *Physical Properties of Carbon Nanotubes*; 1st ed.; World Scientific Publishing Company, 1998.

(14)   Balasubramanian, K.; Burghard, M. *Small* **2005**, *1*, 180-192.

(15)   Strano, M. S.; Dyke, C. A.; Usrey, M. L.; Barone, P. W.; Allen, M. J.; Shan, H.; Kittrell, C.; Hauge, R. H.; Tour, J. M.; Smalley, R. E. *Science* **2003**, *301*, 1519-1522.

(16)   Zheng, M.; Jagota, A.; Strano, M. S.; Santos, A. P.; Barone, P.; Chou, S. G.; Diner, B. A.; Dresselhaus, M. S.; Mclean, R. S.; Onoa, G. B.; Samsonidze, G. G.; Semke, E. D.; Usrey, M.; Walls, D. J. *Science* **2003**, *302*, 1545-1548.

(17)   Kim, W.; Lee, C. Y.; O'brien, K. P.; Plombon, J. J.; Blackwell, J. M.; Strano, M. S. *J. Am. Chem. Soc.* **2009**, *131*, 3128-3129.

(18)   LeMieux, M. C.; Roberts, M.; Barman, S.; Jin, Y. W.; Kim, J. M.; Bao, Z. *Science* **2008**, *321*, 101-104.

(19)   Demczyk, B. G.; Wang, Y. M.; Cumings, J.; Hetman, M.; Han, W.; Zettl, A.; Ritchie, R. O. *Mat. Sci. Eng. A-Struct.* **2002**, *334*, 173-178.

(20)   Yu, M.; Lourie, O.; Dyer, M. J.; Moloni, K.; Kelly, T. F.; Ruoff, R. S. *Science* **2000**, *287*, 637-640.

(21)   Iakoubovskii, K.; Minami, N.; Kazaoui, S.; Ueno, T.; Miyata, Y.; Yanagi, K.; Kataura, H.; Ohshima, S.; Saito, T. *J. Phys. Chem. B* **2006**, *110*, 17420-17424.

(22)   Iakoubovskii, K.; Minami, N.; Ueno, T.; Kazaoui, S.; Kataura, H. *J. Phys. Chem. C* **2008**, *112*, 11194-11198.

(23)   Heller, D. A.; Jeng, E. S.; Yeung, T.; Martinez, B. M.; Moll, A. E.; Gastala, J. B.; Strano, M. S. *Science* **2006**, *311*, 508-511.

(24)   Kim, J.; Heller, D. A.; Jin, H.; Barone, P. W.; Song, C.; Zhang, J.; Trudel, L. J.; Wogan, G. N.; Tannenbaum, S. R.; Strano, M. S. *Nat. Chem.* **2009**, *1*, 473-481.

(25)   Zhou, X.; Park, J.; Huang, S.; Liu, J.; McEuen, P. L. *Phys. Rev. Lett.* **2005**, *95*, 146805.

(26)   Quinn, B. M.; Lemay, S. *Adv. Mater.* **2006**, *18*, 855-859.

(27)   White, C. T.; Todorov, T. N. *Nature* **1998**, *393*, 240-242.

(28)   Yao, Z.; Kane, C. L.; Dekker, C. *Phys. Rev. Lett.* **2000**, *84*, 2941.

(29)   Pop, E.; Mann, D.; Wang, Q.; Goodson, K.; Dai, H. *Nano Lett.* **2006**, *6*, 96-100.

(30)   Kong, J.; Franklin, N. R.; Zhou, C.; Chapline, M. G.; Peng, S.; Cho, K.; Dai, H. *Science* **2000**, *287*, 622-625.

(31)   Skotheim, T. A.; Reynolds, J. R. *Conjugated polymers*; CRC Press, 2007.

(32)   Inzelt, G. *Conducting Polymers*; 2008.

(33)   Shirakawa, H. *Angew. Chem. Int. Ed.* **2001**, *40*, 2574-2580.

(34)   MacDiarmid, A. G. *Angew. Chem. Int. Ed.* **2001**, *40*, 2581-2590.

(35)   Heeger, A. J. *Angew. Chem. Int. Ed.* **2001**, *40*, 2591-2611.

(36)   Kim, J.; McQuade, D.; McHugh, S.; Swager, T. *Angew. Chem. Int. Ed.* **2000**, *112*, 4026-4030.

(37)   Vigalok, A.; Zhu, Z.; Swager, T. M. *J. Am. Chem. Soc.* **2001**, *123*, 7917-7918.

(38)   Star, A.; Stoddart, J. F.; Steuerman, D.; Diehl, M.; Boukai, A.; Wong, E. W.; Yang, X.; Chung, S.; Choi, H.; Heath, J. R. *Angew. Chem. Int. Ed.* **2001**, *40*, 1721-1725.

(39)   Li, X.; Zhang, L.; Wang, X.; Shimoyama, I.; Sun, X.; Seo, W.; Dai, H. *J. Am. Chem. Soc.* **2007**, *129*, 4890-4891.

(40)   Hiemenz, P. C.; Rajagopalan, R. *Principles of Colloid and Surface Chemistry*; 3rd ed.; CRC Press, 1997.

(41)   Gu, H.; Swager, T. M. *Adv. Mater.* **2008**, *20*, 4433-4437.

(42)   Li, X.; Wang, X.; Zhang, L.; Lee, S.; Dai, H. *Science* **2008**, *319*, 1229-1232.

(43)   Tasis, D.; Tagmatarchis, N.; Bianco, A.; Prato, M. *Chem. Rev.* **2006**, *106*, 1105-1136.

(44)   Zhang, W.; Swager, T. M. *J. Am. Chem. Soc.* **2007**, *129*, 7714-7715.

(45)   Zhang, W.; Sprafke, J. K.; Ma, M.; Tsui, E. Y.; Sydlik, S. A.; Rutledge, G. C.; Swager, T. M. *J. Am. Chem. Soc.* **2009**, *131*, 8446-8454.

Chapter 2

Hexafluoroisopropanol Functionalized Polythiophene/ Carbon Nanotube Resistive Sensors for Chemical Warfare Agent Detection

2.1 Introduction

Carbon nanotube (CNT) field effect transistors have been studied as chemical[1,2] and biological[3,4] sensors. They are sensitive because their resistance can change drastically in the presence of analytes via charge transfer (doping), carrier pinning, and/or modification of the Schottky barrier at the nanotube/metal contact. However, their applications have largely been limited by the complexity associated with device fabrication. Recently, chemiresistors based on polymer/CNT systems have been reported.[5-9] In these cases, polymers are deposited onto single CNT devices or pre-patterned CNT networks. The polymer coatings generally provide increased selectivity, but have not simplified the fabrication process.

We are interested in creating a material with both high sensitivity/selectivity and good processability. The material of interest is a conjugated polymer/CNT composite. As discussed in Chapter 1, conjugated polymers, especially polythiophenes, have strong $\pi-\pi$ interactions with CNTs and can stabilize CNT dispersion.[10]

We choose to attach a hexafluoroisopropanol group to polythiophene because it can hydrogen bond with phosphate esters that are common in a number of chemical warfare agents, including sarin gas.[6,11-13] We utilize non-toxic dimethyl methylphosphonate (DMMP) as a simulant for more toxic nerve gases, because DMMP has a similar hydrogen bonding characteristic and vapor pressure (160 Pa at 25 °C) of to sarin.

In this chapter, we report that CNTs dispersed with a HFIP-functionalized polythiophene produce highly sensitive and selective chemiresistor sensors using a greatly simplified fabrication process.

2.2 Monomer Synthesis

We designed the structure of an HFIP-substituted terthiophene monomer to achieve a satisfactory oxidative potential for oxidative polymerization and to prevent the twisting of polymer backbone. While electron withdrawing fluorine groups usually make the parent molecule more difficult to oxideze, increasing a molecule's conjugation length can lower the oxidative potential and the band gap of the conjugated molecule by introducing energy splitting. Moreover, since the bulky hexafluoroisopropanol (HFIP) groups tend to twist the polymer backbone, two bare thiophenes are needed as spacers between HFIP-functionalied ones.
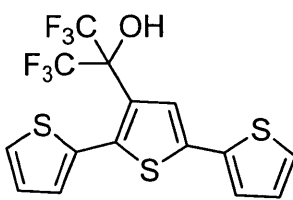
Scheme 2.1. Structure of HFIP-substituted terthiophene monomer.

The synthesis of the HFIP-substituted terthiophene is summarized in Scheme 2.1. A bromoterthiophene **2** was first synthesized by a Stille-type cross-coupling reaction between a stannylated thiophene and a tribromothiophene **1**, in satisfying yield. **2** was then transformed to the monomer **3** via lithiation followed by quenching with hexafluoroacetone.
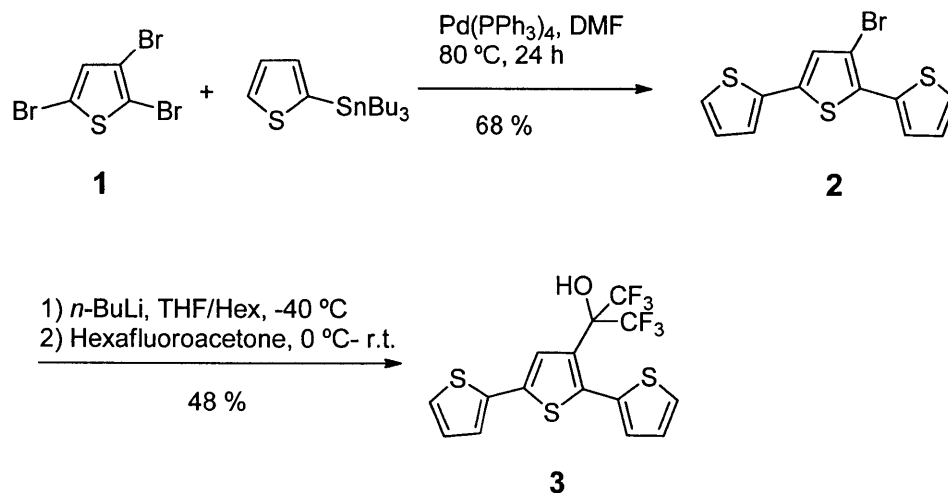
Scheme 2.2. Synthesis of monomer

2.3 Polymer Synthesis

HFIP-PT **P1** was synthesized via oxidative polymerization of monomer **3** by iron chlororide (Scheme 2.2). The number average molecular weight is 25.3 K, with a polydispersity index of 2.3. Although the HFIP-PT does not have long chain side groups, it is quite soluble in hydrogen bond acceptor solvents such as tetrahydrofuran, due to the enthalpically favored hydrogen-bonding between the HFIP group and the solvent.
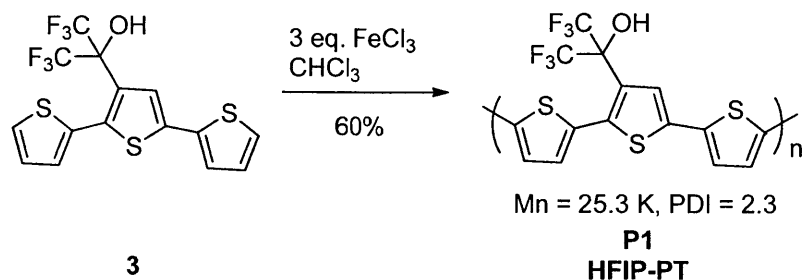
Scheme 2.3. Synthesis of HFIP-PT polymer

2.4 Dispersing Nanotubes with HFIP-PT

We successfully dispersed SWCNTs in HFIP-PT solution by sonication in the presence 50 wt. % of a HFIP-PT or poly(3-hexylthiophene) (P3HT). As shown in Figure 2.1, a transparent solution of HFIP-PT/SWCNT system was observed, which remains stable for at least three years. Since this polymer/SWCNT system is very soluble, traditional polymer-processing methods, such as spin-coating and ink-jet printing, can be utilized to fabricate devices.
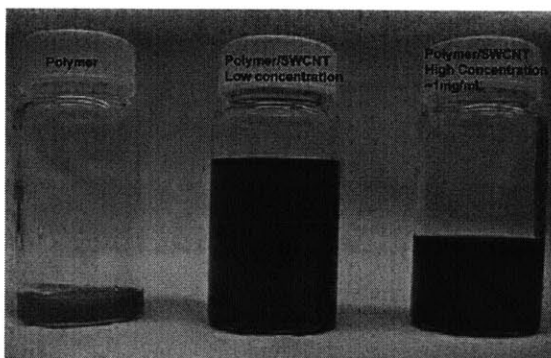
Figure 2.1. Photograph of polymer solution (left) and HFIP-PT/SWNT solutions (middle, [SWCNT]~0.05 mg/mL; right, [SWCNT]~1mg/mL) in THF.

The quality of the CNT dispersions is very important and ensures that the CNTs form a percolative network of largely individual tubes. As shown in Figure 2.2, the AFM image of a CNT network drop-casted from 0.02 wt. % solutions indicates that the CNTs are well debundled and dispersed by HFIP-PT. To study the quality of CNT dispersion, a section analysis was measured with atomic force microscopy (AFM). As shown in Figure 2.3, the average height of the nanotubes is 1.5 nm with a standard deviation of 0.4 nm (neglecting the

polymer aggregation at 2.1 μm). This data indicates that the polymer/nanotube suspension is largely comprised of individual nanotubes.
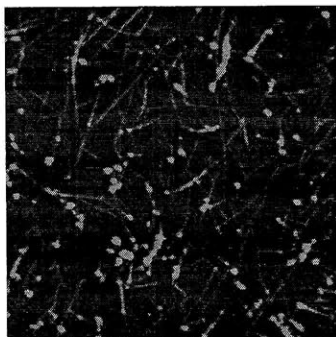
Figure 2.2. AFM image of SWCNT network drop casted from 0.02 wt.% solutions.
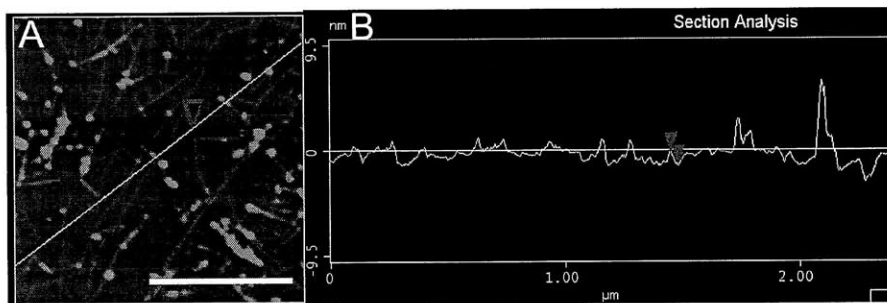
Figure 2.3. Height profile of CNT network. A) Enlarged image of AFM image in Figure 2.2. The scale bar is 1 μm. B) Section analysis of A).

We further studied the quality of the dispersion by Raman spectroscopy. The relative low intensity of the (10, 2) radial breathing mode (RBM) at 264 cm^{-1} of HFIP-PT/SWCNT (red) compared with bare SWCNTs (black) in Figure 2.4 (insert) further demonstrates the decrease in the SWCNT bundling when dispersed by HFIP-PT.[14] Moreover, no significant changes have been observed in the disorder mode or tangential mode, indicating that the chemical

property of pristine tubes has not been changed by sonication process. The peaks at 1030 and 914 cm^{-1} are THF solvent peaks.
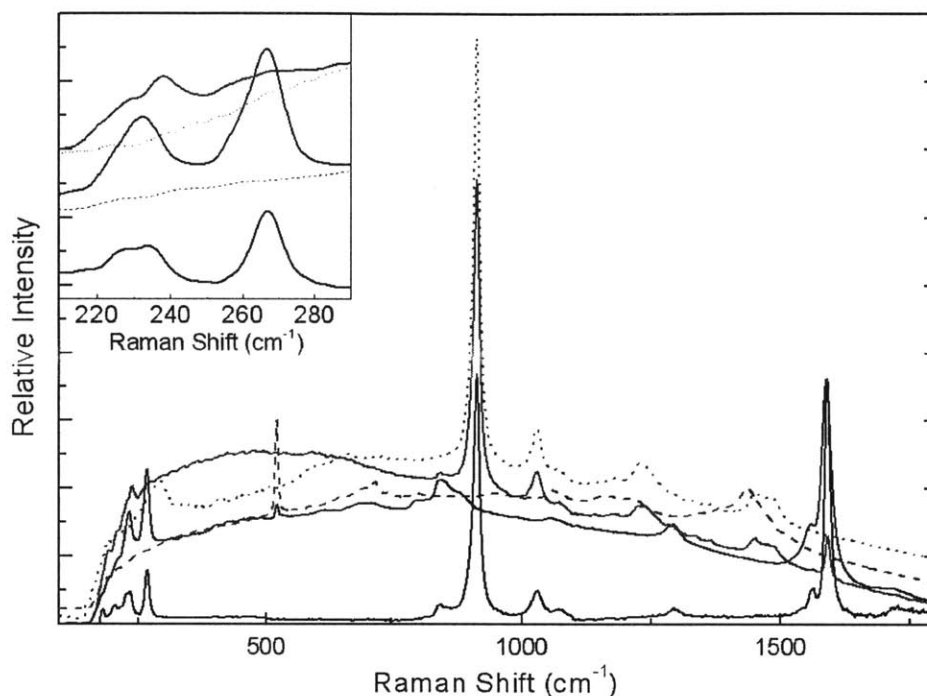
Figure 2.4. Raman spectra of SWCNTs taken from THF suspensions sonicated for 2 hours with HFIP-PT (red curve, stable suspension) and without HFIP-PT (black curve, unstable suspension), and the dried drop cast HFIP-PT/SWCNT dispersion (blue). The other curves are HFIP-PT without SWCNTs (dotted: solution, dashed: solid). Enlarged spectra in the range of 210-290 nm is shown on the top left. Excitation wavelength is 785 nm.

2.5 Device Fabrication

The fabrication of our sensory device is quite simple and straightforward. Polymer/SWCNT films (50 nm thick) were spin-coated from 0.2 wt. % solutions (THF for HFIP-PT and CHCl$_3$ for P3HT) onto a glass substrate, and two gold strip electrodes (50 nm

thick) were then sputter-coated on to the film. The active area of the HFIP/SWCNT film is 5 mm × 5 mm. The resistance of HFIP-PT/SWCNT devices ranged from 0.5 to 1.5 MΩ.
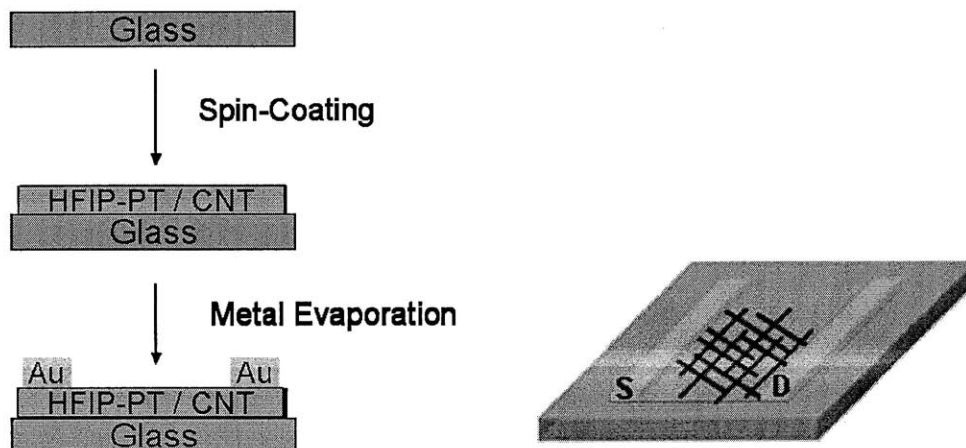
Figure 2.5. Schematic views of the sensor fabrication process (left) and the device consisting of a percolative network of carbon nanotubes between two gold electrodes, deposited by casting a HFIP-PT stabilized dispersion (right).

2.6 Sensing Results

The sensory response investigated is a conductance measurement between the two electrodes at a constant bias voltage (0.1 V). Our chemiresistors based on an HFIP-PT/SWCNT hybrid system were shown to be highly sensitive and selective for DMMP detection. As shown in Figure 2.6, the sensor response is fast and reproducible even at low analyte concentrations. For instance, it gives an 8 % conductance change upon exposure to 0.6 ppm of DMMP. A conductance change of 1 % was observed in response to 0.05 ppm of DMMP, which qualifies the sensor a ppb level sensing. Moreover, the sensor displays a linear

logarmithic response to analyte concentration over 2 decades of concentration (Figure 2.6, right).
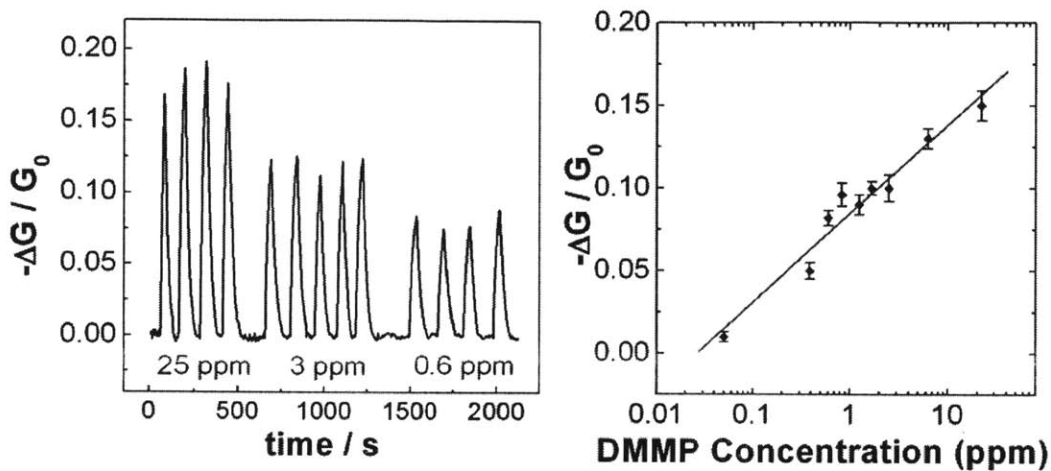
Figure 2.6. Conductance change *(-ΔG/G₀)* of the sensor upon exposure to varying concentrations of DMMP (left), and the calibration curve of the sensor at DMMP concentration of 0.05-25 ppm (right). The bias voltage is fixed at 0.1 V, and the temperature is 70 °C.

Figure 2.7 shows a comparison of the selectivity and sensitivity for SWCNTs deposited from HFIP-PT, P3HT-stabilized dispersions, and non-stabilized dispersions. The selectivity is excellent considering that the equilibrium vapor pressure of methanol (167,000 ppm) is more than 100 times that of DMMP (1,600 ppm). Moreover, the H-bonding ability of HFIP-PT/SWCNTs greatly increased the response and selectivity for DMMP, as compared to P3HT/SWCNTs and bare SWCNTs. The enhancement due to the HFIP-PT is most impressive at low analyte concentrations. At equilibrium vapor pressures of DMMP, the HFIP-

PT/SWCNT sensor has only a ~40 % larger response than the P3HT/SWNCT, whereas at 1ppm of DMMP, the HFIP/SWCNT is nine times more sensitive than that of P3HT.
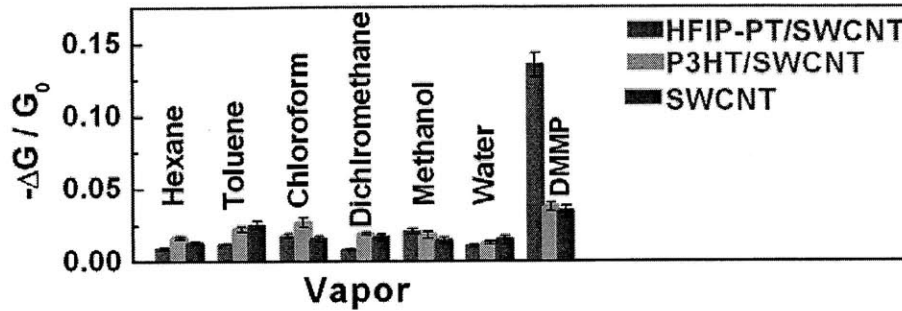
Figure 2.7. Conductance changes of the SWCNT sensors in response to common organic solvents and DMMP diluted to 1 % of saturated vapor conditions at room temperature, with a bias voltage fixed at 0.1 V.

2.7 Mechanistic Study

To explore the mechanism of the DMMP response in our HFIP-PT/SWCNT sensors, we first performed sensory studies in a field effect transistor architecture. Figure 2.8 shows the images of these devices. A 300 nm thick silicon nitride insulating layer was coated onto a doped silicon back gate. Interdigitated electrodes (Ti/Pt, 20 nm/100 nm) were evaporated onto the insulating layer, with 2 μm digits and spaces. The active interdigitated area is 2 mm (digit length) by 800 μm (100 digit pairs). The electrodes (with the exception of the active area and contact area) were protected with a negative photoresist SU8-2. The polymer/SWCNT dispersion was then drop-coated onto the interdigitated electrodes and tested.
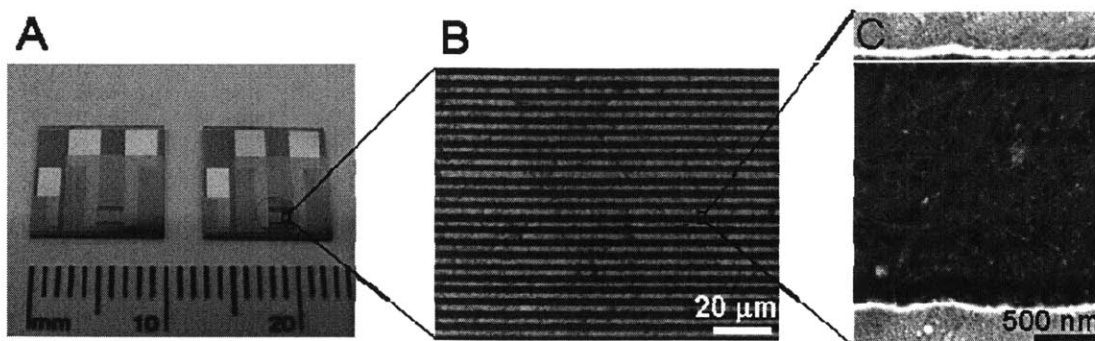
Figure 2.8. A) Optical image of FET devices with (right) and without (left) drop-coated HFIP-PT/SWCNT. The active interdigitated area is 2 mm (digit length) by 800 μm (100 digit pairs). B) Optical image of an interdigitated electrodes active area drop-coated with HFIP-PT/SWCNT. C) Scanning electron microscope (SEM) image of HFIP-PT/SWCNT network bridging two adjacent electrodes.

As shown in Figure 2.9, the source-drain current I_{ds} increases with more negative gate voltages and saturates at ~5 V V_g, indicating a p-type behavior, although the outputs do not resemble a standard field effect transistor due to the contribution of the metallic SWCNTs. We also noted a negative shift of the threshold voltage and a decrease in transconductance with exposure to saturated DMMP vapor. Such behaviors have been found in other SWCNT devices, and the shift of threshold voltage[15,16] and the decrease in transconductance[8,16] are attributed to a charge transfer process associated with the analyte and introduction of scattering sites, respectively.
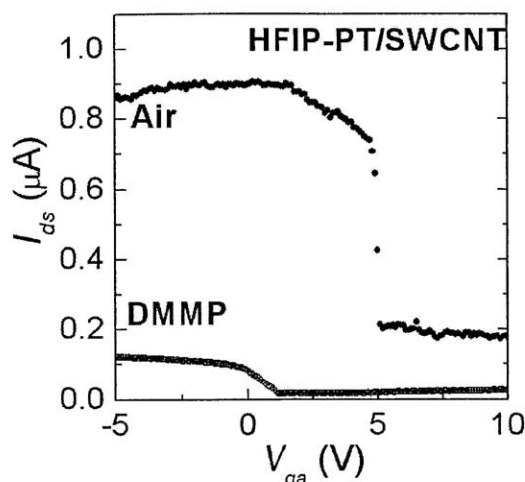
Figure 2.9. The source-drain current vs gate voltage of the sensor under conditions of air and saturated DMMP vapors. The source-drain bias voltage is fixed at 1 mV. The gate voltage was scanned from 10 V to -5 V.

Another possible cause of the resistance changes is that DMMP changes the nature of the Schottky barrier of HFIP-PT/SWCNT-Au contact. This effect has been eliminated from consideration by passivating the electrode interfaces. Specifically, we observed similar results to DMMP when the electrodes interfaces were coated with a 50 μm thick film polymethylmethacrylate (PMMA). The effectiveness of PMMA to block the diffusion of DMMP to the sensor was demonstrated by passivating the entire device and under these conditions no response is observed with exposure to DMMP for 60 s.

Figure 2.10 presents the UV-vis absorption and fluorescence emission spectra of polymers HFIP-PT in solution and in thin films. The thin-film spectra from polymer HFIP-PT show a broadened absorption (from 435 nm with an extinction coefficient of $1.96 \times 10^4 \text{ M}^{-1} \text{ cm}^{-1}$ in solution to 447 nm in film) and emission (from 546 nm in solution to 570 nm in the thin

film). The shifts to longer wavelength are typical of conjugated polymers and likely represent a combination of aggregation and planarization of the polymer backbones.
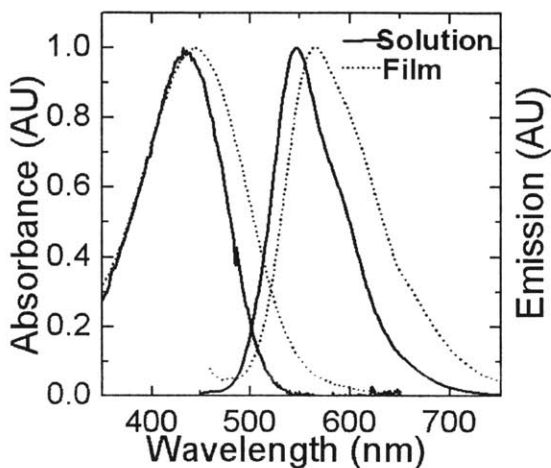
Figure 2.10. UV-vis absorption and fluorescence emission spectra of polymer HFIP-PT in chloroform solution (solid lines) and as thin films (dotted lines).

The presence of the HFIP group was intended to promote strong interactions between DMMP and HFIP-PT. To probe this interaction, we monitored changes in the fluorescence intensity of the polymer in response to DMMP.[17,18] HFIP-PT is an emissive polymer with a quantum yield of 28 % in THF and absorption and emission maxima of 435 and 546 nm, respectively. The dispersions with SWCNTs have a quenched HFIP-PT fluorescence with a decreased quantum yield (corrected for the optical absorptions of the SWCNTs) of 11 %. Spin-coated films containing only HFIP-PT prepared in the same fashion as the sensory devices display absorption and emission maxima at 447 and 570 nm, respectively. From comparative studies with thin films of HFIP-PT/SWCNTs we estimate that 60 % of the emission is quenched by the SWCNTs, thereby indicating that most of the polymer is closely

associated with the SWCNTs. The thin film of HFIP-PT exhibits some self-quenching due to interchain interactions and the extended conformation of the PT, and extended exposure to DMMP increased this emission at 570 nm by 55 %. In the case of HFIP-PT/SWCNT films (Figure 2.11), the emission at 570 nm was very constant in air without DMMP, showing this polymer is rather stable to photo bleaching. Upon exposure to DMMP vapor, the fluorescence is enhanced by 76 %. This increase indicates that the polymer bound to the SWNCT is still capable of interacting with the DMMP and that quenching by the SWCNT is attenuated. Hence, a working model for our sensory mechanism is a combination of charge transfer, introduction of scattering sites, and an increased physical separation of the SWCNTs caused by the interaction of HFIP-PT and DMMP.
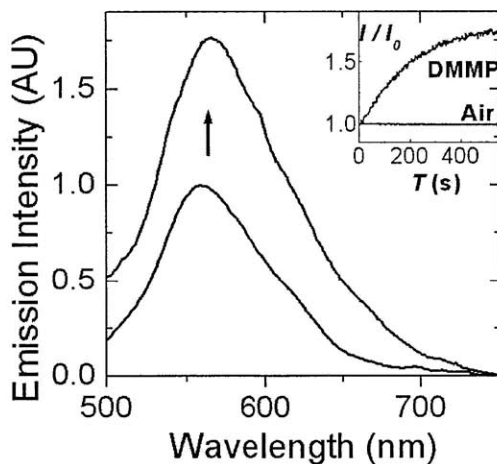
Figure 2.11. Fluorescent emission of HFIP-PT/SWCNT film under air (black) and 10 min exposure to saturated DMMP vapors (blue). Insertion: fluorescence intensity change at 570 nm (I/I_0) vs exposure time (T) in both conditions. An excitation wavelength of 450 nm was used.

2.8 Understanding the Sensing Response with Temkin Isotherm

We are interested in understanding the transduction mechanism mathematically. Strano et al[19] investigated the dynamics of the sensing processes using continuum site balance equations and a mass action model. They assumed that the analyte adsorption process is the rate-limiting step of the sensing response. They also assume that the sensing response S is directly proportional to the occupied site density. The nanotube sensor can thus be conceptualized as a number of sites which are able to adsorb analytes. The total number of adsorption sites is denoted as $T\theta$, unoccupied sites as θ, occupied sites as $A\theta$, where the analyte is denoted as A.

Utilizing the same assumptions, we found that the response in Figure 2.6 can be described with Temkin isotherm, which is an empirical modeling of adsorption onto an energetically heterogeneous surface.[20,21]

$$S = mA\theta = ma \lg bC_A = ma\log C_A + ma\log b \qquad (1)$$

In this equation, S is sensing response, $A\theta$ is the number of occupied adsorption sites, C_A is the analyte concentration, and a, b and m are constants. Apparently the sensing response is proportional to the logarithm of analytes' concentration. Figure 2.12 shows the fitting of the data in Figure 2.6 to equation (1), confirming the capability of quantitative detection with the HFIP-PT/SWNCT sensor.
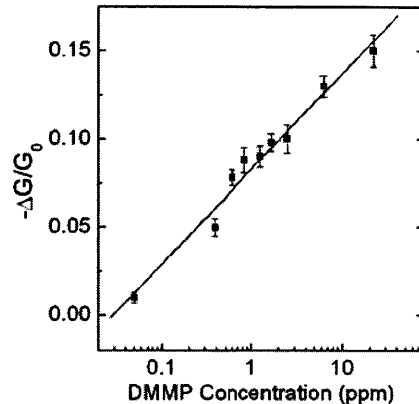
Figure 2.12. Conductance change (black squares) of the HFIP-PT sensor upon exposure to varying concentrations of DMMP. The data were fitted to equation (1) with *ma* and *b* determined to be 0.0541 and 1.1 ppm^{-1}, respectively.

2.9 Conclusions

In conclusion, we have fabricated a high-performance polymer/SWCNT chemical sensor using a very simple spin-casting technique. The dispersing polymer provides increased sensitivity due to strong H-bonding interactions with the analyte. The effectiveness of this approach suggests that carbon nanotubes dispersed with receptor-containing polymers are a promising approach for the production of low cost chemiresistive sensors.

2.10 Experimental Section

Materials

All solvents were of spectroscopic grade unless otherwise noted. Anhydrous tetrahydrofuran was obtained using a solvent purification system (Innovative technologies) immediately before using. Anhydrous DMF was purchased from Aldrich as Sure-Seal Bottles and used as received. All chemicals were of reagent grade from Sigma-Aldrich or Alfa Aesar and used as received. Single-walled carbon nanotubes were acquired from Carbon Nanotechnologies Inc. (CNI lot# R0204) and were synthesized by the high-pressure catalytic decomposition of carbon monoxide (HIPCO) method.

General Methods and Instrumentation

NMR spectra were obtained on Varian Mercury (300 MHz). NMR chemical shifts are referenced to $CHCl_3$/TMS (7.27 ppm for ^1H, 77.23 ppm for ^{13}C). For ^{19}F NMR spectra, trichlorofluoromethane was used as an external standard (0 ppm), and upfield shifts are reported as negative values. In some cases, signals associated with the CF_3 groups and proximal quaternary centers were not reported in the ^{13}C NMR spectra due to C-F coupling and low signal-to-noise ratios. High-resolution mass spectra (HRMS) were obtained at the MIT Department of Chemistry Instrumentation Facility (DCIF) using a peak-matching protocol to determine the mass and error range of the molecular ion. Fourier Transform infrared (FT-IR) spectroscopy was performed on a Perkin-Elmer model 2000 FT-IR spectrophotometer using the Spectrum v. 2.00 software package. Polymer molecular weights were determined at room temperature on a HP series 1100 GPC system in THF at 1.0 mL/min (1 mg/mL sample concentrations). UV/Vis spectra were recorded on an Agilent 8453 diode-array

spectrophotometer. Emission spectra were acquired on a SPEX Fluorolog fluorometer (model FL-321, 450 W xenon lamp) using either right-angle detection (solution measurements) or front-face detection (thin-film measurements). Fluorescence quantum yields were achieved by comparison with Rhodamine 101 as standard.[22] Melting points were measured with a Meltemp II apparatus and are reported uncorrected. Raman spectra were measured with a Kaiser Hololab 5000R Modular Research Raman Spectrometer with Microprobe from MIT Center for Materials Science and Engineering. AFM images were taken with a D3100S-1 atomic force microscope (Digital Instrument). SEM images were taken with a LEO A scanning electron microscope. Analytes of specific concentrations were generated with a KIN-TEK gas-generating system. Source-drain current changes in response to analyte were measured with an AUTOLAB PGSTAT 20 potentiostat (Eco Chemie) at a constant potential (typically 0.1 V). The source-drain current dependence on gate voltage was measured with a Keithley 4200 semiconductor characterization system.

Synthesis of Compound 2

In a 100 mL round-bottom flask were added 2,3,5-tribromothiophene (1.4 mL, 11 mmol), 2-(tributylstannyl)thiophene (7 mL, 22 mmol), tetrakis(triphenylphosphine)palladium(0) (0.1 g, 0.1 mmol) and dimethylformamide (30 mL). The mixture was stirred at 80 °C for 24 h under anitrogen atmosphere. It was then diluted with ether (100 mL), washed with HCl and then brine, dried over $MgSO_4$, and evaporated under reduced pressure. The resulting crude product was purified by column chromatography (hexane), providing 2.46 g of a light yellow, viscous oil (yield 68 %). ^{1}H NMR (300 MHz, $CDCl_3$) δ: 7.43 (dd, 1H, J = 1.2, 3.6 Hz), 7.36 (dd, 1H, J = 1.2, 5.1 Hz), 7.27 (dd, 1H, J = 1.2, 5.1 Hz), 7.19 (dd, 1H, J = 1.2, 3.6 Hz), 7.09

(dd, 1H, J =3.6, 5.1 Hz), 7.08 (s), 7.04 (dd, 1H, J = 3.6, 5.1 Hz). ^{13}C NMR (75 MHz, CDCl$_3$) δ:

135.7, 135.6, 134.1, 130.7, 128.0, 127.6, 127.2, 126.5, 126.1, 125.3, 124.3, 107.8. IR (KBr) $v/$

cm^{-1}: 3105, 3080, 1664, 1493, 1420, 1223, 1048, 848, 815, 710.

Synthesis of Compound 3

Into a 100 mL round-bottom flask was added 0.327 g (1.0 mmol) of **2** and 10 mL of

hexane under nitrogen atmosphere. The mixture was cooled to -78 ℃, and 0.75 mL of a 1.6 M

solution (1.2 mmol) of *n*-butyllithium in hexanes was added slowly by syringe. After the

addition was complete, 1 mL of tetrahydrofuran was added. After 0.5 h, 2 mL of more hexane

was added and the solution was allowed to warm to 0 ℃ for 30 min. The addition funnel was

quickly replaced with a Dewar-type condenser under a heavy flow of argon. The condenser

was charged with dry ice and acetone and an excess of anhydrous gaseous hexafluoroacetone

was then condensed into the flask. The reaction mixture was allowed to warm to room

temperature, and the hexafluoroacetone was allowed to reflux at RT for 3 h. Excess

hexafluoroacetone was removed by flushing the apparatus with argon for several hours. A

bubbler filled with 10 % aqueous NaOH solution was used to trap the reactive vapor. The

reaction mixture was treated with a 5 % HCl solution (25 mL) and extracted with diethyl ether

(200 mL). The organic extracts were washed with water (100 mL × 2) and brine (100 mL) and

dried over MgSO$_4$. The residue was purified by column chromatography (8% ethyl acetate in

hexanes) to yield 0.20 g (48.3 %) of a crystalline solid; mp 85-86℃. ^{1}H NMR (300 MHz,

CDCl$_3$) δ: 7.42 (dd, 1H, J = 1.2, 3.6 Hz), 7.33 (m, 2H), 7.18 (dd, 1H, J =1.2, 5.1 Hz), 7.08 (s,

1H), 6.99 (dd, 1H, J = 3.6, 5.1 Hz), 6.94 (dd, 1H, J = 3.6, 5.1 Hz), 3.86 (s, 1H). ^{13}C NMR (75

MHz, CDCl$_3$) δ: 139.00, 135.43, 134.38, 131.30, 130.13, 128.15, 127.82, 126.95, 126.03,

125.19, 123.21, 123.14. ^{19}F NMR (282 MHz, CDCl$_3$) δ: -76.41. FT-IR (KBr) ν/cm^{-1}: 3473, 3092, 2921, 1804, 1628, 1570, 1540, 1507, 1467, 1428, 1415, 1359, 1260, 1238, 1219, 1158, 1118, 1045, 1006, 956, 886, 836, 797, 712. HRMS (EI): calcd for C$_{15}$H$_8$F$_6$OS$_3$ (M$^+$), 413.9636, found 413.9638.

Synthesis of Polymer P1 (HFIP-PT)

To a 25 mL round-bottom flask with anhydrous iron trichloride (20 mg, 0.4 mmol) in chloroform (15 mL) was added **3** (41 mg, 0.1 mmol) in a chloroform solution (0.5 mL). The mixture was sonicated for 2 h, and then stirred at room temperature for 24 h. It was then diluted with tetrahydrofuran (100 mL), reduced with sodium thiosulphate (0.5 g), then washed sequentially with water (100 mL), 0.1 M hydrazine aqueous solution (100 mL), water (100 mL), brine (100 mL), dried over MgSO$_4$, filtered with a 0.2 μm PTFE filter and evaporated to 10 mL under reduced pressure. The polymer solution was then precipitated into 30 mL of hexane. The precipitate was isolated by centrifugation and decantation of the liquid. The precipitate was dissolved in tetrahydrofuran (5 mL) and precipitated into hexane again. The precipitation was repeated once more. The material was dried under vacuum to yield a orange-red solid (20 mg, 50%). According to gel-permeation chromatography (polystyrene standards), **HFIP-PT** has an *Mn* = 25.3K and a polydispersity index (*PDI*) = 2.3. ^{1}H NMR (300 MHz, CDCl$_3$) δ: 7.26(aromatic C-H), 7.19 (aromatic C-H), 7.15(aromatic C-H), 3.97(O-H). ^{19}F NMR (282 MHz, CDCl$_3$) δ: -76.24. FT-IR (KBr) ν/cm^{-1}: 3451, 2361, 1637, 1468, 1309, 1260, 1224, 1189, 1120, 1102, 1075, 960, 794, 740, 726.

Dispersing SWNCTs with HFIP-PT

Purified SWCNT (5 mg) and HFIP-PT (5 mg) were mixed in 5 mL tetrahydrofuran and ultrasonicated for 2 hours. This HFIP-PT/SWCNT mixture was purified by high speed centrifugation (4500 rpm, 60 minutes), to achieve a uniform SWCNT dispersion. The upper 80% of supernatant was collected, leaving ~0.3mg of undissolved SWCNT precipitated.

Sensor Fabrication

Polymer/SWCNT films (50 nm thick) were spin-coated from 0.2 wt. % solutions (THF for HFIP-PT and CHCl$_3$ for P3HT) on to a glass substrate, and two gold strip electrodes (50 nm thick) were then sputter-coated on to the film. The active area of the HFIP/SWCNT film is 5 mm × 5 mm. The resistance of HFIP-PT/SWCNT devices range from 0.5 to 1.5 MΩ.

2.11 References and Notes

(1)   Kauffman, D. R.; Star, A. *Angew. Chem. Int. Ed.* **2008**, *47*, 6550-6570.

(2)   Snow, E. S.; Perkins, F. K.; Robinson, J. A. *Chem. Soc. Rev.* **2006**, *35*, 790-798.

(3)   Allen, B. L.; Kichambare, P.; Star, A. *Adv. Mater.* **2007**, *19*, 1439-1451.

(4)   Kim, S. N.; Rusling, J.; Papadimitrakopoulos, F. *Adv. Mater.* **2007**, *19*, 3214-3228.

(5)   Qi, P.; Vermesh, O.; Grecu, M.; Javey, A.; Wang, Q.; Dai, H.; Peng, S.; Cho, K. J. *Nano Lett.* **2003**, *3*, 347-351.

(6)   Snow, E. S.; Perkins, F. K.; Houser, E. J.; Badescu, S. C.; Reinecke, T. L. *Science* **2005**, *307*, 1942-1945.

(7)   Wei, C.; Dai, L.; Roy, A.; Tolle, T. B. *J. Am. Chem. Soc.* **2006**, *128*, 1412-1413.

(8)   Star, A.; Han, T.; Joshi, V.; Gabriel, J.; Grüner, G. *Adv. Mater.* **2004**, *16*, 2049-2052.

(9)   Lee, C.; Sharma, R.; Radadia, A.; Masel, R.; Strano, M. *Angew. Chem. Int. Ed.* **2008**, *47*, 5018-5021.

(10)   Gu, H.; Swager, T. M. *Adv. Mater.* **2008**, *20*, 4433-4437.

(11)   Grate, J. W. *Chem. Rev.* **2000**, *100*, 2627-2648.

(12)   Grate, J. W. *Chem. Rev.* **2008**, *108*, 726-745.

(13)   Toal, S. J.; Trogler, W. C. *J. Mater. Chem.* **2006**, *16*, 2871-2883.

(14)   O'Connell, M. J. *Carbon Nanotubes: Properties and Applications*; 1st ed.; CRC Press, 2006.

(15)   Kong, J.; Franklin, N. R.; Zhou, C.; Chapline, M. G.; Peng, S.; Cho, K.; Dai, H. *Science* **2000**, *287*, 622-625.

(16)   Star, A.; Gabriel, J. P.; Bradley, K.; Grüner, G. *Nano Lett.* **2003**, *3*, 459-463.

(17)   Kim, J.; Swager, T. M. *Nature* **2001**, *411*, 1030-1034.

(18)   Farchioni, R.; Grosso, G. *Organic Electronic Materials : Conjugated Polymers and Low Molecular Weight Organic Solids*; 1st ed.; Springer, 2001.

(19)   Lee, C. Y.; Strano, M. S. *Langmuir* **2005**, *21*, 5192-5196.

(20)   Adamson, A. W.; Gast, A. P. *Physical Chemistry of Surfaces, 6th Edition*; 6th ed.; Wiley-Interscience, 1997.

(21)   Wongwiriyapan, W.; Inoue, S.; Okabayashi, Y.; Ito, T.; Shimazaki, R.; Maekawa, T.; Suzuki, K.; Ishikawa, H.; Honda, S.; Mori, H.; Oura, K.; Katayama, M. *Appl. Phys. Express* **2009**, *2*, 095008.

(22)   Lakowicz, J. R. *Principles of Fluorescence Spectroscopy*; 2nd ed.; Springer, 1999.

Chapter 3

Calixarene-Functionalized Polythiophene/Carbon Nanotube

Resistive Sensors for Molecular Recognition

3.1 Introduction

Distinguishing structural isomers and stereo isomers is a challenging but critical task for biotechnology, pharmaceutical industry, and environmental monitoring. One of the great promises of host-guest chemistry is to impart selectivity to sensors necessary to detect these small structural differences.[1,2] Although several transduction techniques have been developed for host-guest chemistry based sensors[3] (e.g. optical, electrochemical, quartz crystal microbalance and surface acoustic wave sensors), alternative low-cost chemiresistor devices are simple and require minimal power.

Carbon nanotube (CNT) is a leading candidate for chemiresistor material because of its unique electrical properties. In the last decade, CNT sensors have been widely explored to sensitively detect chemical[4-8] and biological[9-11] analytes. Of these sensors, chemical modification enhances their selectivity and sensitivity, but does not contribute to the ease of fabrication. In chapter 2, we presented a single walled CNT (SWCNT)/polythiophene based resistor made with a greatly simplified fabrication process from a stable polymer/SWCNT dispersion. The polymer component offers great flexibility in its design and synthesis, thus enabling the incorporation of various recognition groups. We report herein a resistance sensor based upon SWCNTs wrapped with calixarene substituted polythiophenes capable of a differential response to xylene isomers.

3.2 Polymer Synthesis

The isomers of xylenes are extensively used by the chemical industry and are difficult to distinguish due to their similar physical properties such as boiling point and vapor pressure.[12] We considered calixarenes as a promising receptor[13,14] to differentiate these

isomers due to the shape presistent hydrophobic binding pockets of these materials in their

cone confromation. Of particular relevance is the fact that *p-tert*-butyl[4]calixarene can

preferably extract *p*-xylene from a 1:1:1 mixture of xylene isomers.[15]

In this chapter, a *p*-tert-butylcalix[4]arene substituted polythiophene **P1** has been

synthesized via a Stille-type cross-coupling reaction between distannylated monomers and

calixarene-functionalized dibrominated monomer **1** which was prepared by monoalkylation of

p-tert-butylcalix[4]arene (Scheme 3.1). **P1** has a number average molecular weight (*Mn*) of

9.2 KDa and a polydispersity index (*PDI*) of 1.4.
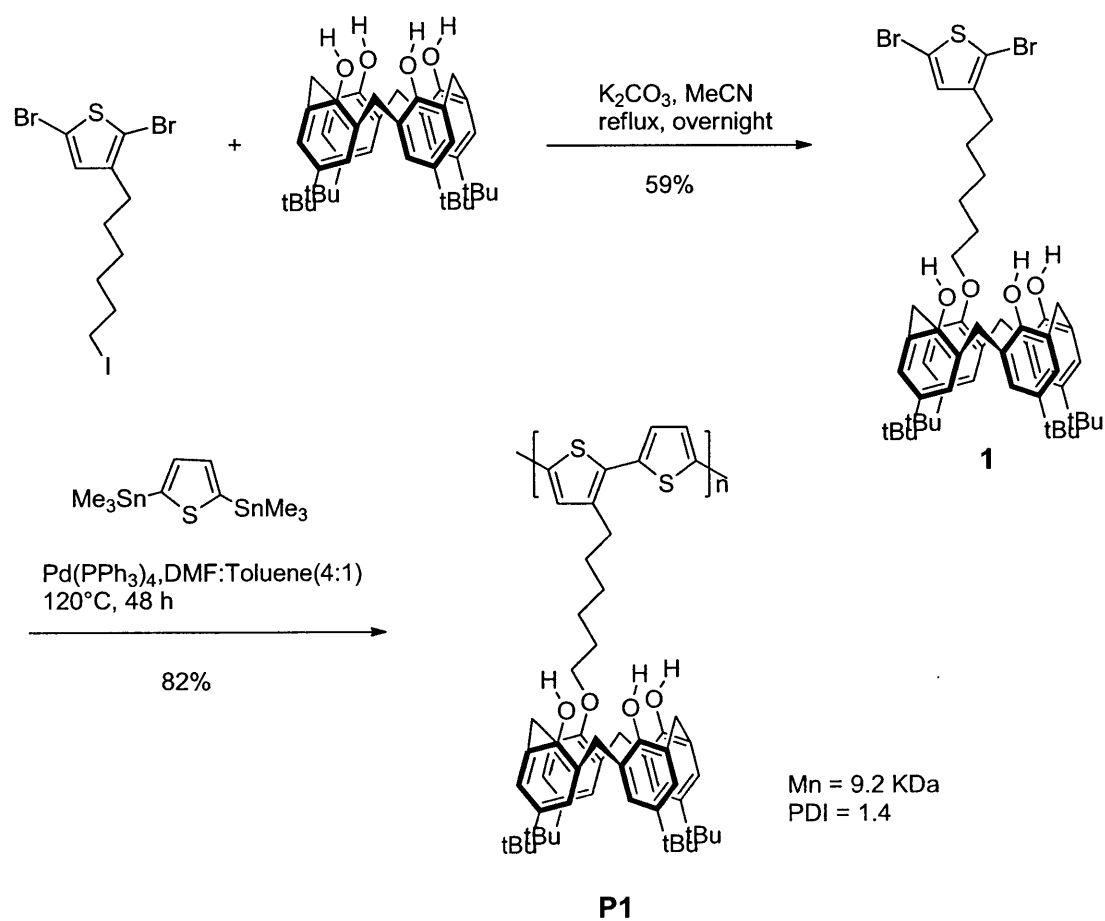
Scheme 3.1. Synthesis of polymer.

3.3 NMR Adsorption Study

To check its selectivity as a recognition group, **P1** powder was exposed to saturated vapor of 1:1:1 mixture of xylene isomers for 10 min and dissolved in CDCl$_3$ (see Supporting Information for details). The proton nuclear magnetic resonance (^{1}H NMR) spectra showed that 0.38 molar equivalent of xylene isomers were adsorbed for each repeating unit of **P1**, with 0.12/0.16/0.10 equivalent of *m-/p-/o-*xylene respectively. As a comparison, poly(3-hexylthiophene) (P3HT), with the same backbone and alkyl sidechain, was exposed to xylene isomers and studied in the same fashion. P3HT adsorbed 0.06 equivalent xylene isomers by each repeating unit, with equal amounts of *m-/p-/o-*xylene. From these measurements it can be concluded that the adsorption selectivity is related to the calixarene.
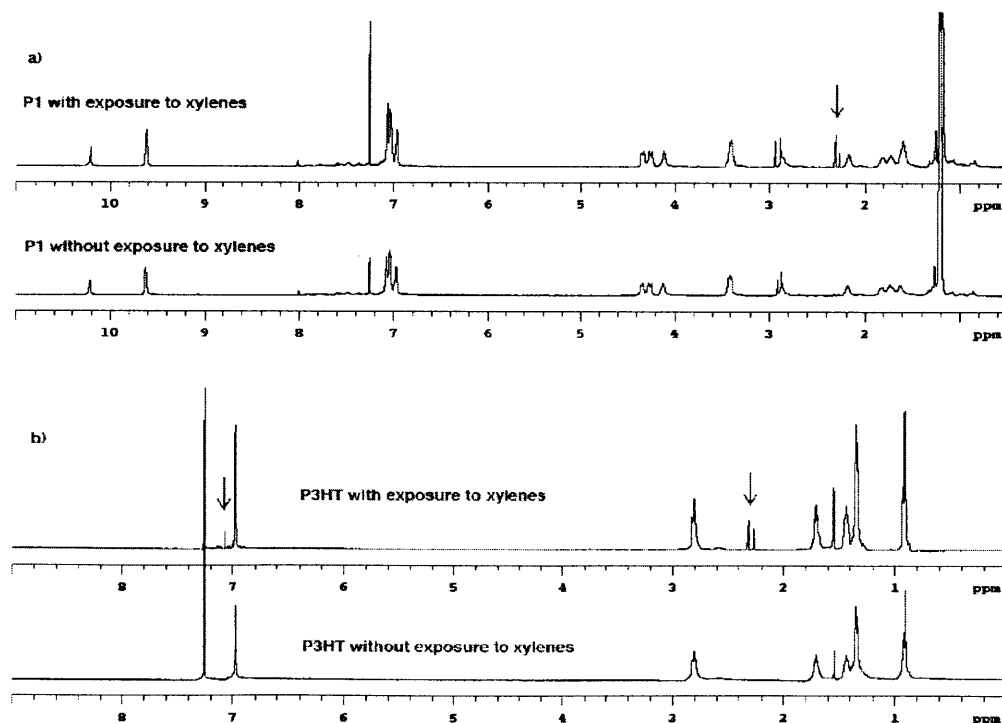
Figure 3.1. ^{1}HNMR of a) **P1** and b) P3HT with and without exposure to xylene vapor.

3.4 Dispersing SWCNT

Stable dispersion of SWCNT in **P1** was obtained by ultra-sonication. As shown in Figure 3.2, transparent solution of **P1**/SWCNT system was obtained. We studied the quality of this SWCNT dispersion by Raman scattering measurement. As shown in Figure 3.3, SWCNT/**P1** in THF solution (red) has a relative lower intensity of the (10, 2) radical breathing mode (RBM) at 266 cm^{-1} than bare SWCNTs (black) and dried SWCNT/**P1** (blue), demonstrating the bundles have been largely decreased by dispersion with **P1**.[16] The fact that the disorder mode and the tangential mode showed no significant change indicates that sonication process has not changed the chemical property of pristine tubes.
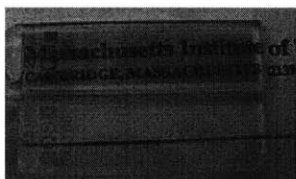
Figure 3.2. Photograph of **P1** (bottom) and SWCNT/**P1** solutions (top, SWCNT~0.05 mg/mL) in THF.
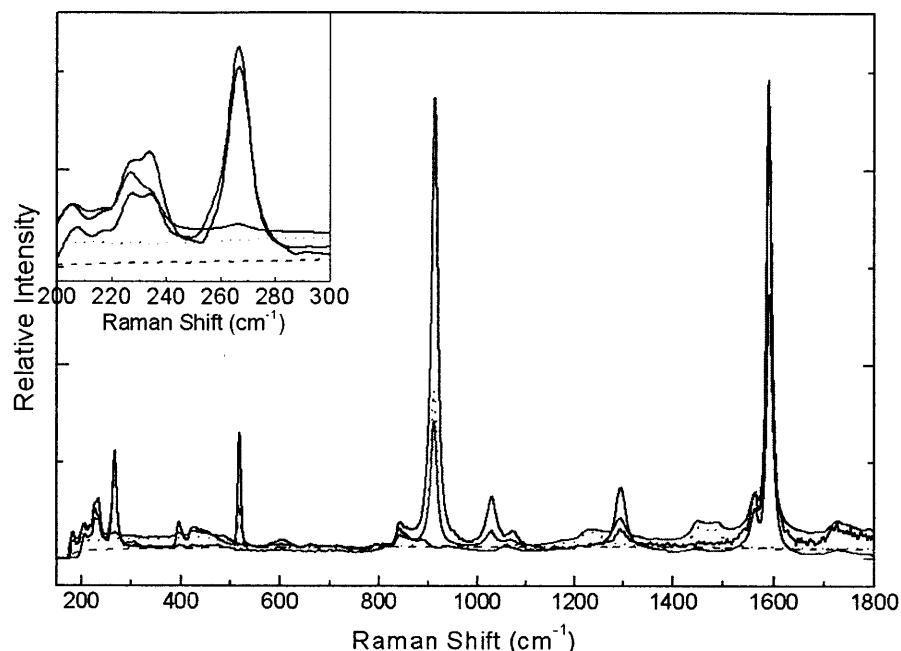
Figure 3.3. Raman spectra of SWCNTs taken from THF suspensions ultra-sonicated for 2h with **P1** (red curve, stable dispersion) and without **P1** (black curve, unstable suspension), and a dried drop of **P1**/SWCNT dispersion (blue). The other grey-colored curves are **P1** without SWCNTs (dotted: solution, dashed: solid). Enlarged spectra in the range of 200-300 nm is shown on the top left. The peaks at 1030 and 914 cm^{-1} are THF solvent peaks. Excitation wavelength is 785 nm.

3.5 Device Fabrication

We fabricated a sensor by spin coating a stable dispersion of **P1** and SWCNTs on top of two gold electrodes (Figure 3.4). Polythiophene is an essential dispersing element and prevents large SWCNT bundles and forms evenly distributed percolative networks in when spin coated. Then we measured the sensory response as the conductance change between the electrodes under a constant bias of 0.02 V in air. As a comparison, a SWCNT/P3HT based sensor was prepared and measured in parallel.
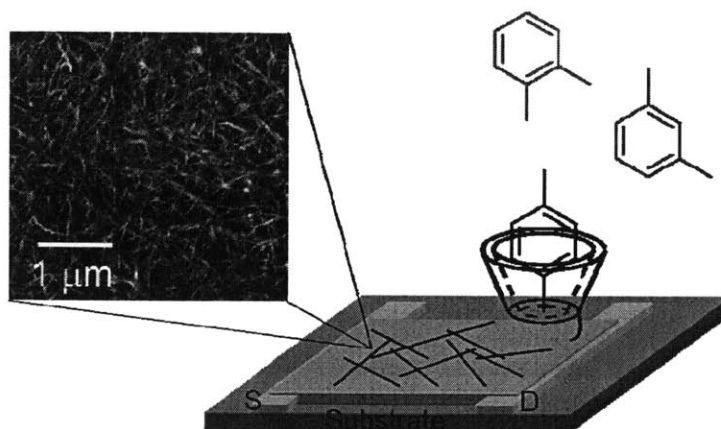
Figure 3.4. Schematic view of the SWCNT/**P1** sensor that selectively adsorbs *p*-xylene. A percolative SWCNT network (5 mm × 5 mm area, 30 nm thick) was deposited between two gold electrodes. An SEM image of the SWCNT network is shown on the top left.

3.6 Sensing Results

As shown in Figure 3.5, the SWCNT/**P1** sensor is very sensitive to the structural differences between the xylene isomers. With 40 s doses of 400 ppm analyte (air was used as carrier gas), we observed a 12% conductance decrease with *p*-xylene, 7% with *m*-xylene and 6% with *o*-xylene. In contrast, the SWCNT/P3HT sensor showed the same response (~6% conductance decrease) to all three isomers. We also found that replacing the carrier gas with nitrogen did not produce any observable change in sensing response for both SWCNT/**P1** and SWCNT/P3HT. Additionally, using air as carrier gas with 30 % relative humidity at 20 °C resulted in only a ~ 0.6% decrease sensitivity without changing the selectivity (see Supporting Information). Considering the fact that SWCNTs sensors are often sensitive to oxygen and moisture[17], in our sensors the polymer may form a protective layer[18] that insulates SWCNTs from undesired environmental influences.
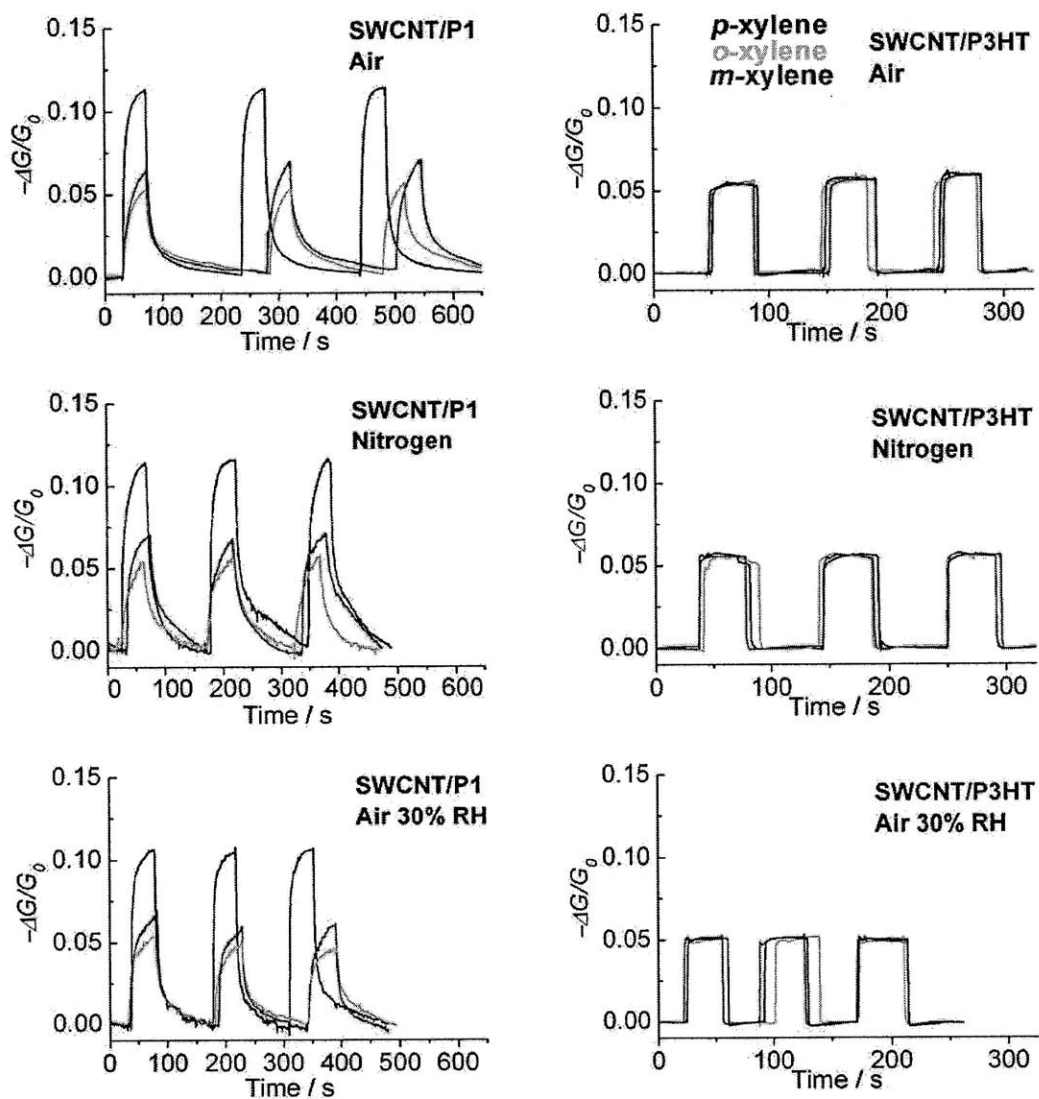
Figure 3.5. Conductance change ($-\Delta G/G_0$) of the SWCNT/**P1** (left column) and SWCNT/P3HT sensors (right column) exposed to 400 ppm of xylene isomers using different carrier gases (top row: air, middle row: nitrogen, bottom row: air with 30 % relative humidity).

3.7 Verification of Selectivity

This selectivity for *p*-xylene was verified by a quartz crystal microbalance (QCM) study at the same analyte concentration and the SWCNT/**P1** film adsorbed more *p*-xylene than *m*- and *o*-xylene, while the SWCNT/P3HT film adsorbed about the same quantities of all three isomers(Figure 3.6). The distinction in QCM measurements is less pronounced than our chemiresistor results because a thicker film was needed to produce a sufficient signal-to-noise ratio. It's also noticeable that SWCNT/P3HT, in both conductance and QCM case, has a faster recovery rate, due to its weaker binding ability with xylenes.
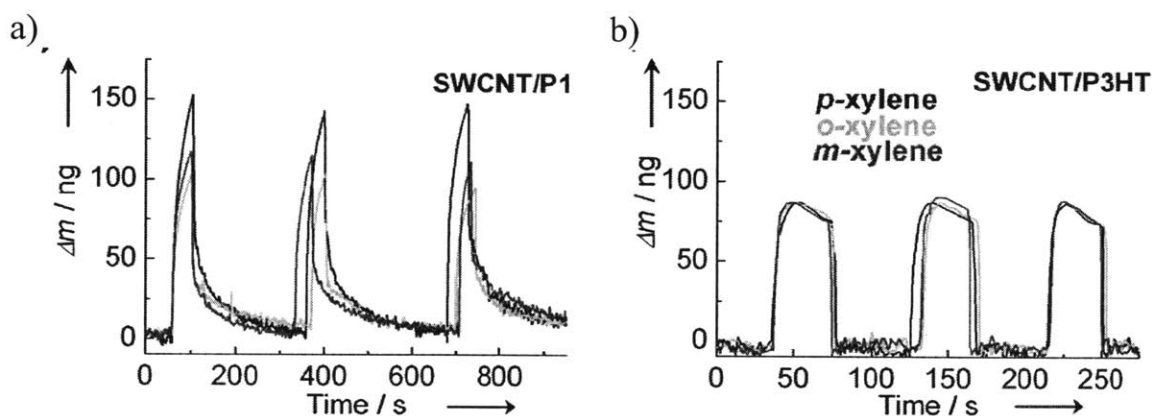
Figure 3.6. The weight increase (Δm) of a)SWCNT/**P1**(9.72 µg) and b) SWCNT/P3HT (11.0 µg) films (0.39 cm^2 area) when exposed to 400 ppm of xylene isomers were also shown to verify the selectivity.

We further monitored the adsorption phenomena by means of fluorescence, since **P1** is an emissive polymer that is senstive to the physical environment.[19,20] **P1** has a fluorescence quantum yield of 36.3% in THF solution with absorption/emission maxima at 454 nm/564 nm, respectively (Figure 3.7, left). However in thin films the absorption/emission maxima shift to

492 nm/597 nm, which is typically observed for conjugated polymers that aggregate and have more planar conformations in the solid state. [20] The emission maxima of **P1** is not shifted in SWCNT dispersions, however the quantum efficiency decreases by 75% (to 9.0%), which suggests that the polymer is closely associated with and quenched by the SWCNTs (Figure 3.7, right).
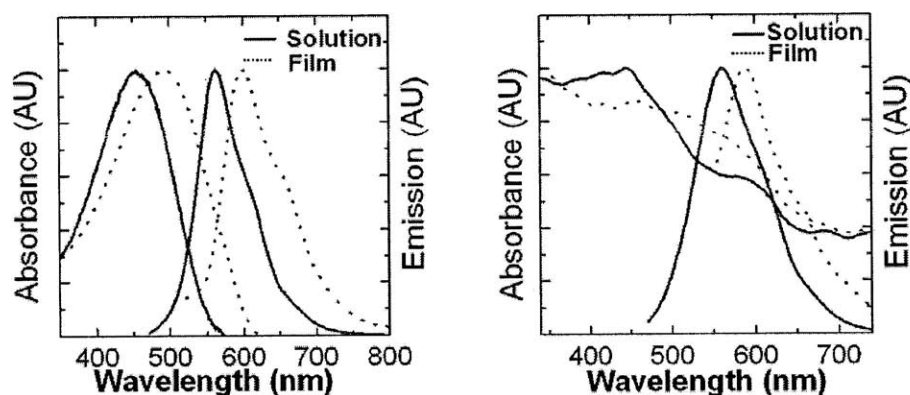
Figure 3.7. UV-vis absorption and fluorescence emission spectra of P1 (left) and SWCNT/**P1** (right) in THF solution (solid lines) and as thin films (dotted lines).

To interrogate the effect of xylene on **P1**, we made films of **P1** and SWCNT/**P1** in the same fashion as the sensory devices and exposed them to saturated vapors of xylene isomers. After 250 s of exposure, the fluorescence of the **P1** film increased by 56.6%, 44.4% and 40.0% for *p-*, *m-*, and *o*-xylene, respectively and the fluorescence of the SWCNT/**P1** film increased by 68.2%, 54.8% and 50.2% for *p-*, *m-*, and *o*-xylene respectively (Figure 3.8). The increase of film fluorescence indicates that the polymer underwent swelling and associated conformational changes, and confirms that more *p*-xylene is adsorbed by the film than *m-* and *o*-xylene. The fact that the SWCNT/**P1** film has a larger relative intensity increase than the **P1** film suggests

that the polymer interactions with the SWCNT are weakened by xylene absorption. It is notable that saturated vapors and prolonged exposures were used in the fluorescence study, thus leading to a larger relative responses than our resistance measurements.
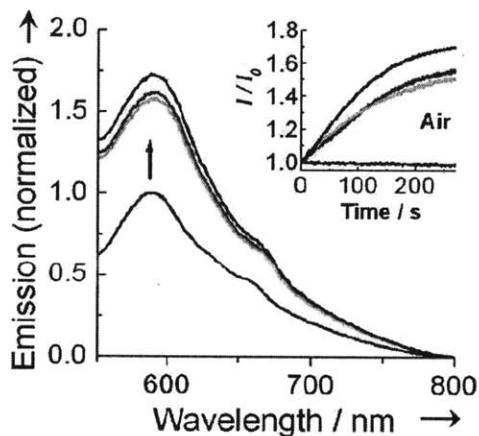
Figure 3.8. Fluorescent emission of SWCNT/**P1** film under air (blue) and with exposure to saturated xylene vapors (black: *p*-xylene, green: *o*-xylene, red: *m*-xylene). Insert: fluorescence intensity changes at 597 nm (I/I_0) vs. exposure time (t) in both conditions. An excitation wavelength of 490 nm was used.

3.8 Mechanistic Study

In addition to NMR, QCM and fluorescence measurements, we further investigated the transduction mechanism by means of Raman spectroscopy, field effect transistor and passivation study. The reduction of SWCNT-SWCNT interactions in SWCNT/**P1** film by xylene exposure was confirmed by Raman spectroscopy, where the relative intensity of 265 cm^{-1} radial breathing mode absorptions decrease by about 10% when the was exposed to *p*-xylene (Figure 3.9). Similar phenomena have also been found with *m*-xylene and *o*-xylene.
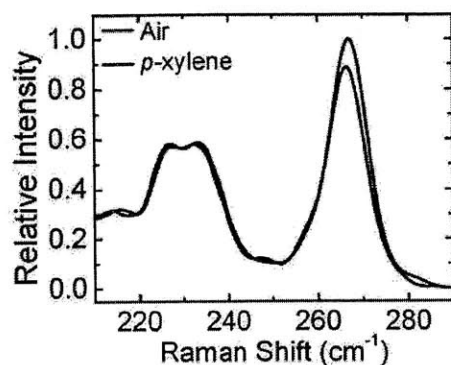
Figure 3.9. Radical breathing modes of SWCNT/P1 film before (blue curve) and after (black curve) exposure to *p*-xylene.

We performed an FET study of SWCNT/**P1** to further investigate the sensing mechanism. The device was fabricated in the same fashion as the sensory device, except that the substrate and gate material were composed of Si with a 100 nm overcoat of SiO_2. As shown in Figure 3.10, the FET has a p-type behavior and small hysteresis. The threshold voltage displayed a negative shift when the device was exposed to xylene isomers, suggesting a charge-transfer process associated with the analyte.

We also passivated the electrode areas of a top-contacted device with 50 μm thick layer of polymethyl methacrylate (PMMA), and found no significant change in sensing response, which indicates the change in the Schottky barrier has a minor contribution to the sensing results. The effectiveness of passivation was demonstrated by passivation of the whole device, which gave no response to the analyte. These observations suggest a combined mechanism of charge transfer and polymer conformational change.
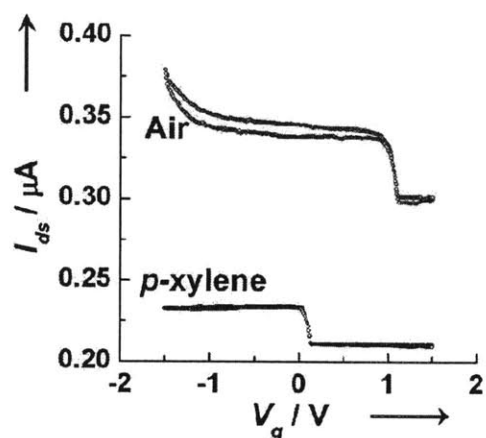
Figure 3.10. The source-drain current (I_{ds}) vs. gate voltage (V_g) of the sensor under conditions of air (blue) and saturated xylene vapors (only *p*-xylene exposure is shown and the same effect was found for the other isomers). The source-drain bias voltage was fixed at 0.1 V. V_g was scanned in a cycle from 1.5 V to -1.5 V.

2.9 Conclusions

In summary, we have developed an SWCNT/calixarene substituted polythiophene based resistance sensor. This sensor shows high sensitivity to minor structural differences in the analytes and a fast response rate. The effectiveness of this approach suggests that SWCNTs dispersed in receptor-functionalized polymers is a promising candidate for low cost, real time selective chemical monitoring based on host-guest chemistry.

3.10 Experimental Section

Materials

All solvents were of spectroscopic grade unless otherwise noted. All chemicals were of reagent grade from Sigma-Aldrich, Alfa Aesar or Acros and used as received. Acetonitrile was dried with molecular sieves 4 Å prior to use. Anhydrous toluene was obtained from J. T. Baker and purified by passing through a Glasscontour dry solvent system. Single-walled carbon nanotubes were acquired from Carbon Nanotechnologies Inc. (CNI lot# R0204) and were synthesized by the high-pressure catalytic decomposition of carbon monoxide (HIPCO) method. 2,5-Dibromo-3-(6-iodohexyl)thiophene was prepared according to the literature procedure.[21,22] 2,5-Bis(trimethylstannayl)thiophene was prepared according to the literature procedure and recrystallized from ethanol.[23]

General Methods and Instrumentation

^{1}H NMR and ^{13}C NMR spectra were obtained with a Varian Mercury (300 MHz). NMR chemical shifts are referenced to residual CD_2Cl_2 (5.32 ppm for ^{1}H, 53.8 ppm for ^{13}C). High-resolution mass spectra (HRMS) were obtained at the MIT Department of Chemistry Instrumentation Facility (DCIF) using a peak-matching protocol to determine the mass and error range of the molecular ion. Polymer molecular weights were determined at room temperature on a HP series 1100 GPC system in THF at 1.0 mL/min (1 mg/mL sample concentrations). UV/Vis spectra were recorded on an Agilent 8453 diode-array spectrophotometer. Emission spectra were acquired on a SPEX Fluorolog fluorometer (model FL-321, 450 W xenon lamp) using either right-angle detection (solution measurements) or front-face detection (thin-film measurements). Fluorescence quantum yields were achieved by

comparison with fluorescien in 0.1 N NaOH as standard.[24] Melting points were measured with a Meltemp II apparatus and are reported uncorrected. Raman spectra were measured with a Kaiser Hololab 5000R Modular Research Raman Spectrometer with Microprobe from MIT Center for Materials Science and Engineering. AFM images were taken with a D3100S-1 atomic force microscope (Digital Instrument). SEM images were taken with a JEOL 6700 scanning electron microscope. Analyte of specific concentration and relative humidity was generated with a KIN-TEK gas-generating system. Source-drain current change in response to analyte was measured with an AUTOLAB PGSTAT 20 potentiostat (Eco Chemie) at constant potential (typically 0.02 V). The source-drain current dependence on gate voltage was measured with a Keithley 4200 semiconductor characterization system. The QCM experiment was performed with a home-built quartz crystal microbalance setup with crystals (10 MHz, Au electrodes) and oscillator from the International Crystal Manufacturing Co. Films were applied by spin-coating SWCNT/P1 or SWCNT/P3HT on both sides of the crystal.

Synthesis of Compound 1

To the suspension of p-$tert$-butylcalix[4]arene (0.32 g, 0.5 mmol) in acetonitrile(10 mL), potassium carbonate (34.5 mg, 0.25 mmol) was added. After refluxing the mixture for 15 min, 2，5-dibromo-3-(6-iodohexyl)thiophene (0.294 g, 1 mmol) was added. The solution became transparent after 1 hour. The mixture was further refluxed for 24 h under Argon atmosphere. After being cooled down to room temperature, the solvent was evaporated under reduced pressure. The residue was extracted with dichloromethane (100 mL), and washed with 1 N HCl (100 mL), H_2O (100 mL×2), and brine (100 mL) sequentially. The solvent was evaporated under reduced pressure, and the residue was purified by column chromatography with

hexane/dichloromethane (2:1) as eluent, providing 0.287 g of a white solid (59%). Mp = 81-84 °C. ^{1}H NMR (300 MHz, CD$_2$Cl$_2$) δ: 9.60 (s, 1H), 9.25 (s, 2H), 7.11 (s, 2H), 7.07 (d, 2H, J = 2.4 Hz), 7.03 (s, 2H), 7.01 (d, 2H, J = 2.4 Hz), 6.89 (s, 1H), 4.32 (d, 2H, J = 12.9 Hz), 4.13 (d, 2H, J = 13.5 Hz), 4.11 (t, 2H, J = 6.9 Hz), 3.41 (d, 4H, J = 13.5 Hz), 2.62 (t, 2H, J = 6.9 Hz), 2.16 (m, 2H), 1.74 (m, 4H), 1.58 (m, 2H), 1.20 (s, 18H), 1.19 (s, 9H), 1.17 (s, 9H). ^{13}C NMR (75 MHz, CDCl$_3$) δ: 149.7, 148.7, 148.5, 147.3, 144.6, 143.6, 143.4, 133.8, 131.6, 128.7, 128.2, 127.9, 126.5, 125.8, 125.8, 125.7, 110.6, 108,4, 77.5, 34.8, 34.5, 34.4, 33.0, 32.5, 31.9, 31.8, 31.7, 30.4, 30.1, 30.0, 29.4, 26.3 HRMS (ESI) m/z 995.3096 for [M +Na]$^+$, calcd for C$_{54}$H$_{68}$Br$_2$O$_4$SNa M 995.3103.

Synthesis of Polymer P1

Into a 50 mL Schlenk tube with a magnetic stirring bar were added 48.65 mg (0.05 mmol) of compound 1, 20.49 mg (0.05 mmol) of 2,5-bis(trimethylstannayl)thiophene. The tube was subjected to 5 successive cycles of evacuation and refilling with nitrogen, then Pd(PPh$_3$)$_4$ (<1 mg) and deoxygenated solution of 1:4 (v/v) DMF/toluene (10 mL) was added. The tube was sealed and heated to 120 °C for 48 h. After cooling to room temperature, the reaction mixture was diluted with dichloromethane (100 mL), and then washed sequentially with ammonium hydroxide solutions (26 %, 20mL), water (100 mL×2) and brine (100 mL) sequentially. After being dried over magnesium sulfate, it was filtered through a 0.2 μm PTFE filter and evaporated to 5 mL under reduced pressure. The polymer solution was then precipitated by slow addition to 40 mL of methanol. The precipitate was isolated by centrifugation and decantation of the supernatant. The precipitate was dissolved in dichloromethane (5 mL) and precipitated into methanol again. The precipitation was repeated

once more. The material was then dissolved in dichloromethane (30 mL) and filtered through a 0.2 μm PTFE filter again. The solvent was evaporated under reduced pressure to yield a dark orange-red solid **P1** (35.6 mg, 82%). GPC (THF): M_n = 9.2K Da, M_w = 12.9K Da. ^{1}H NMR (300 MHz, CD$_2$Cl$_2$) δ: 9.62 (s, 1H), 9.27 (s, 2H), 7.12-7.00 (m, 9H), 4.33 (d, 2H, J = 12.0 Hz), 4.21 (d, 2H, J = 13.4 Hz), 4.11 (t, 2H, J = 6.9 Hz), 3.41 (d, 4H, J = 12.9 Hz), 2.62 (t, 2H, J = 6.9 Hz), 2.18 (m, 2H), 1.79 (m, 4H), 1.66 (m, 2H), 1.19 (s, 18H), 1.18 (s, 9H), 1.17 (s, 9H).

Adsorption Experiment of P1

We prepared saturated vapors of 1:1:1 xylene isomers by adding 1mL of each xylene (3mL in total) into a 25 mL vial. A piece of filter paper was put inside the vial to generate a homogeneous vapor environment. The vial was then sealed, and the system was allowed to equilibrate for 0.5 h before use. Into a small 2 mL vial was added 10 mg of **P1** or P3HT powder. This vial was then put into the 25 mL vial, which was subsequently sealed. After 10 min, the 2 mL vial was taken out. Deuterated chloroform was added right after the removal, and NMR spectra were taken.

Dispersing SWNCTs with HFIP-PT

We prepared SWCNT dispersion in **P1** solution by firstly ultrasoicating purified SWCNT (5 mg) in 5 mL THF for 0.5 h, then adding **P1** (10 mg) in 5 mL THF and further ultrasonicating for 2 hours. The mixture was purified by high speed centrifugation (14.5 rpm, 30 min). The upper 80% of supernatant was collected as uniform dispersion, with ~0.5 mg undisolved SWCNT as precipitation. As shown in Figure S2, transparent solution of **P1**/SWCNT system was obtained.

Sensor Fabrication

The glass substrates were cleaned by sonication in acetone/isopropanol/water succesively and followed by cleaning with oxygen plasma for 5 min. Two gold strip electrodes (50 nm thick) were sputter-coated, and SWCNT/P1 dispersion was spin-coated on top of the gold electrodes. The devices were then annealed in air at 120 °C for 3min.

Raman Spectra Change with Xylene Exposure

The **P1**/SWCNT sample was deposited on Si wafer and was placed in a quartz cuvette with some cotton. To achieve saturated vapor pressure of each xylene isomer, ~0.2 mL of xylene was added into the cuvette and was adsorbed by the cotton. The cuvette was subsequently sealed and was allowed to equilibrate for 10 min before taking the spectra. The Raman spectra were recorded before and after the addition of xylenes.

3.11 References and Notes

(1)   Steed, J. W.; Atwood, J. L. *Supramolecular Chemistry*; 2nd ed.; Wiley, 2009.

(2)   Ariga, K.; Kunitake, T. *Supramolecular Chemistry - Fundamentals and Applications: Advanced Textbook*; 1st ed.; Springer, 2006.

(3)   Dickert, F. L.; Haunschild, A. *Adv. Mater.* **1993**, *5*, 887-895.

(4)   Kong, J.; Franklin, N. R.; Zhou, C.; Chapline, M. G.; Peng, S.; Cho, K.; Dai, H. *Science* **2000**, *287*, 622-625.

(5)   Star, A.; Han, T.; Joshi, V.; Gabriel, J.; Grüner, G. *Adv. Mater.* **2004**, *16*, 2049-2052.

(6)   Snow, E. S.; Perkins, F. K.; Houser, E. J.; Badescu, S. C.; Reinecke, T. L. *Science* **2005**, *307*, 1942-1945.

(7)   Qi, P.; Vermesh, O.; Grecu, M.; Javey, A.; Wang, Q.; Dai, H.; Peng, S.; Cho, K. J. *Nano Lett.* **2003**, *3*, 347-351.

(8)   Kauffman, D. R.; Star, A. *Angew. Chem. Int. Ed.* **2008**, *47*, 6550-6570.

(9)   Star, A.; Gabriel, J. P.; Bradley, K.; Grüner, G. *Nano Lett.* **2003**, *3*, 459-463.

(10)   Allen, B. L.; Kichambare, P.; Star, A. *Adv. Mater.* **2007**, *19*, 1439-1451.

(11)   Kim, S. N.; Rusling, J.; Papadimitrakopoulos, F. *Adv. Mater.* **2007**, *19*, 3214-3228.

(12)   Lide, D. R. *CRC Handbook of Chemistry and Physics, 90th Edition*; 90th ed.; CRC Press, 2009.

(13)   Asfari, Z.; Bohhmer, V.; Harrowfield, J.; Vicens, J. *Calixarenes 2001*; Springer Netherlands, 2009.

(14)   Gutsche, C. Calixarenes Revisited; Royal Society of Chemistry, 1998.

(15)   Vicens, J.; Armah, A. E.; Fujii, S.; Tomita, K. *J. Incl. Phenom. Macro.* **1991**, *10*, 159-163.

(16)   O'Connell, M. J. *Carbon Nanotubes: Properties and Applications*; 1st ed.; CRC Press, 2006.

(17)   Collins, P. G.; Bradley, K.; Ishigami, M.; Zettl, A. *Science* **2000**, *287*, 1801-1804.

(18)   Star, A.; Stoddart, J. F.; Steuerman, D.; Diehl, M.; Boukai, A.; Wong, E. W.; Yang, X.; Chung, S.; Choi, H.; Heath, J. R. *Angew. Chem. Int. Ed.* **2001**, *40*, 1721-1725.

(19)   Kim, J.; Swager, T. M. *Nature* **2001**, *411*, 1030-1034.

(20)   Farchioni, R.; Grosso, G. *Organic Electronic Materials : Conjugated Polymers and Low Molecular Weight Organic Solids*; 1st ed.; Springer, 2001.

(21)   Bäuerle, P.; Würthner, F.; Heid, S. *Angew. Chem. Int. Ed.* **1990**, *29*, 419-420.

(22)   Zhai, L.; Pilston, R. L.; Zaiger, K. L.; Stokes, K. K.; McCullough, R. D. *Macromolecules* **2003**, *36*, 61-64.

(23)   Liu, J.; Kadnikova, E. N.; Liu, Y.; McGehee, M. D.; Fréchet, J. M. J. *J. Am. Chem. Soc.* **2004**, *126*, 9486-9487.

(24)   Lakowicz, J. R. *Principles of Fluorescence Spectroscopy*; 2nd ed.; Springer, 1999.

Chapter 4

Functional Group-Specific Detection of Volatile Organic Compounds Utilizing a Multi-walled Carbon Nanotube Array

4.1 Introduction

Real-time, sensitive detection and identification of volatile organic compounds are critically important to the environment and to human health. Widely used in many industries, many volatile organic chemicals (VOCs) can be toxic or carcinogenic even at relatively low concentrations. More importantly, VOCs in exhaled human breath have long been associated with certain diseases, and their detection and analysis have recently attracted a considerable amount of scientific interest.[1] For example, a number of hydrocarbons that have been detected in the exhaled breath of patients are associated with cancer,[2,3] acetone with uncontrolled diabetes,[4] isoprene with cholesterol metabolism disorders,[5,6] and sulfur-containing compounds with liver disfunctions.[7,8] Breath analysis of exhaled VOCs have several obvious advantages over traditional diagnostic techniques, such as non-invasive sampling, less complexity than blood or other body fluids and the potential of real-time monitoring. However, one of the major limitations that prevent breath analysis from being used as a standard diagnostic technique is the lack of suitable and simple compound detection and identification techniques.[1] Currently, commonly used clinical gas analysis methods include gas chromatography-mass spectroscopy, solid state metal oxide semiconductor sensors, and electrochemical methods, all of which require bulky and expensive instruments as well as considerable expertise to operate.[9]

Carbon nanotube (CNT)-based resistance sensors have generated a tremendous amount of interest over the past decade.[10-13] Resistance sensors generally require low manufacturing cost, low power consumption and simple operation. Due to their low dimensional size requirements, resistance-based sensors can be easily incorporated into other systems. In particular, single-walled CNT (SWCNT) sensors were demonstrated to be ultra-sensitive sensors because their conductance can be drastically changed under different chemical

environments through charge transfer, charge carrier pinning, Schottky barrier changes or CNT network swelling.[10-13] SWCNT gas sensors have been studied for medical detection of organic vapors, including non-polar molecules as cancer markers,[14,15] carbon dioxide,[16] and ethanol.[17] However, there have been no studies based on identifying VOCs by their functional groups with CNTs, which is very important for real-life applications dealing with unknown environmental air compositions or with unidentified diseases.

Chemical or physical modifications of CNT surface are essential for the high sensitivity and selectivity of CNT-based sensors. The Swager research group has recently developed a highly efficient, modular functionalization approach of CNTs and fullerenes.[18,19] The reaction was initiated by a zwitterionic complex between 4-dimethylaminopyridine (DMAP) and disubstituted acetylenedicarboxylates (Scheme 4.1). The functionalization density can be as high as one incorporated functional group per nine carbons for SWCNTs and one per thirty-eight carbons for multi-walled CNTs (MWCNTs). Diverse functionalization can be introduced into the system through charge trapping of the zwitterionic intermediate with added nucleophiles, demethylation reactions, or post-chemical-transformations of CNTs substituted with functional groups such as chloroethyl, allyl and propargyl groups.
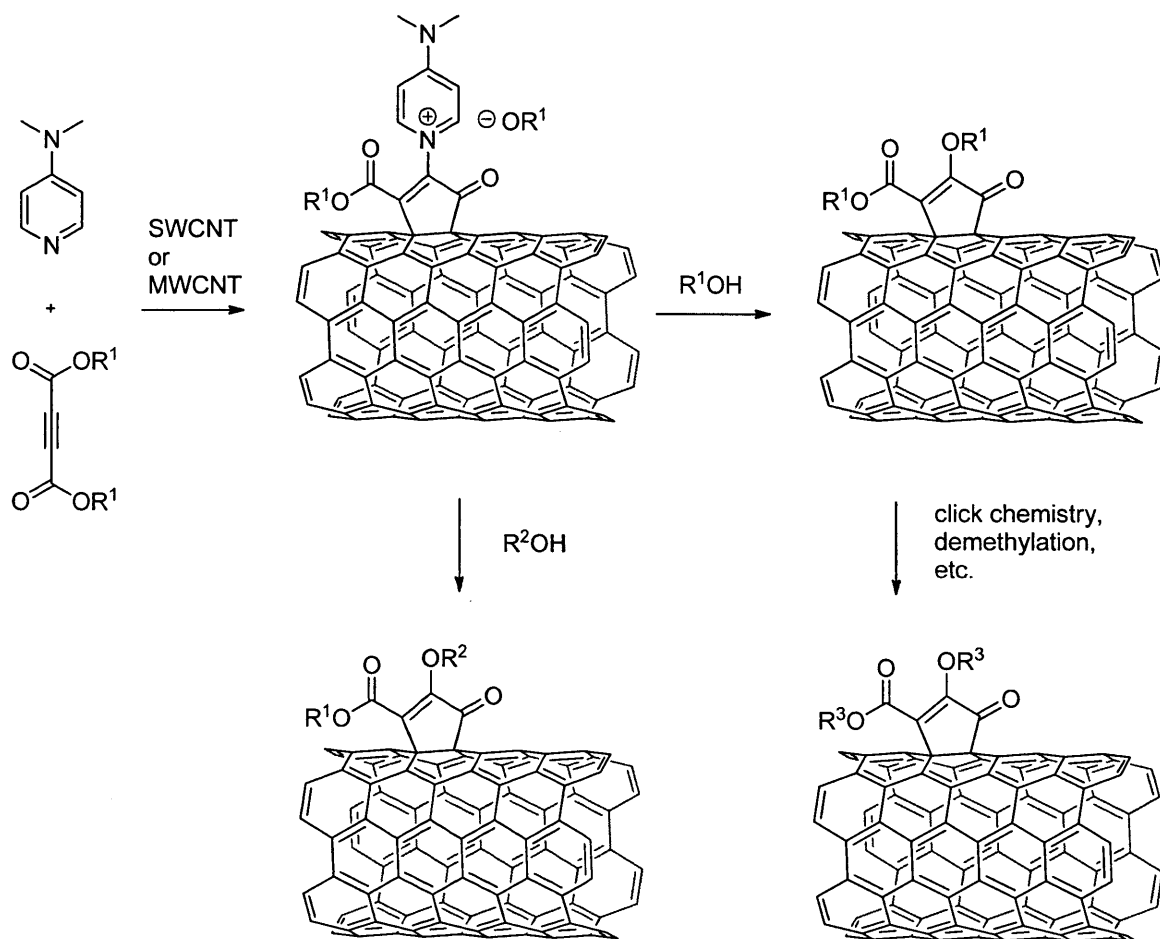
Scheme 4.1. Zwitterion-initiated functionalization of CNTs.

In this chapter we report the first proof-of-concept example of a clear classification of

VOCs based on functional group identification using covalently functionalized MWCNTs. We

functionalized MWCNTs with a series of recognition groups of differencial binding abilities

via the post-transformation synthetic strategy of our zwitterionic approach. We show that the

sensor array has an enhanced sensing response to a variety of VOCs comparing with pristine

MWCNTs. Each chemical has a distinct response pattern. Principal component analysis and

linear discriminant analysis of the sensing data yielded a very clear separation of the VOCs by

their chemical families. We also demonstrated that the incorporation of Pt particles onto triazole functionalized CNTs generated an excellent humidity sensor.

4.2 Design of the Sensor Array

The design of our two-step array sensing is summarized in Figure 4.1. Initially, we observe the real time response of our multiply substituted MWCNT sensor elements to certain VOCs. The obtained responses are then subjected to statistical treatments, according to which the analytes are then identified. Compared with individual sensors, the array sensors have the advantages of responding to a wider range of analytes, improving selectivity and identifying rather than only detecting analyte.[20] Array sensing, which is comprised of multiple receptors and uses pattern recognition process, is very similar to the mammalian olfactory systems and is thus called an "electronic nose."
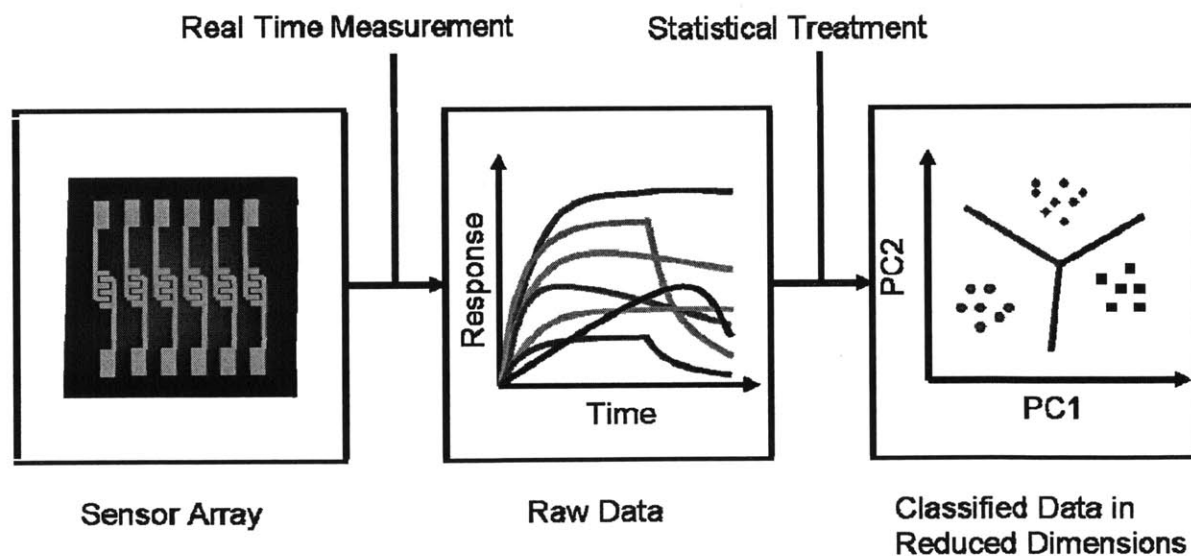
Figure 4.1. Array sensing process.

Table 4.1 summarizes our selections of twenty VOCs as the analytes. Each analyte has different functional groups and different saturated vapor pressures. Unlike many highly reactive toxic gases, which can be sensitively detected by a variety of methods due to their strong chemical interactions such as Lewis acid-base, Bronsted acid-base or redox reactions, these VOCs are rather inert and are much more difficult to detect and identify.[21] As a proof of concept, we chose to detect them in order to demonstrate the superior selectivity of our sensor array.

Table 4.1. Twenty Representative VOCs and Their Vapor Pressures at 298 K.

Analyte Family/ Functional Group	Analyte	Vapor Pressure	
		(mmHg)	(ppmV)
Aliphatic Hydrocarbons	Dodecane	0.0977	128
	Decane	1.132	1489
	Octane	11.17	14697
Aromatic Hydrocarbons	1,3,5-Trimethylbenzene	0.9514	1251
	Xylenes	4.887	6430
	Toluene	22.35	29407
	Benzene	62	81578
Chlorinated Hydrocarbons	Chlorobenzene	9.774	12860
	1,2-Dichloroethane	60.9	80131
	Chloroform	152.9	201184
Ethers	Hexyl Ether	0.06224	81
	Butyl Ether	5.069	6669
	Dioxane	29.63	38986
Ketones	2-Decanone	0.269	353
	Cyclohexanone	2.766	3639
	Methylethylketone	68.88	90631
Alcohols	1-Octanol	0.06366	83
	1-Pentanol	1.545	2032
	1-Butanol	4.49	5907
	Ethanol	49.48	65105

[a] Vapor pressures were obtained and calculated from *Yaws' Handbook of Antoine Coefficients for Vapor Pressure*, or from the EPA's EPI software suite (http://www.epa.gov/opptintr/exposure/docs/episuitedl.htm) and should be taken as approximate only.

We chose MWCNTs as our sensory material because, like SWCNTs, they can provide a rapid response to analytes, good reproducibility, and good reversibility. We did not use SWCNTs for this system because the high functionalization density covalently introduced onto nanotube surfaces to improve sensitivity and selectivity disrupts the effective conjugation and

will destroy the electronic structure of SWCNT.[22] Another reason we did not use SWCNTs is because they are very sensitive to environmental humidity changes, which is a concern for field-based application of these sensors. [23,24]

The recognition groups in our sensor array are designed to provide a variety of non-covalent interactions to the VOCs' functional groups. Researchers from Pacific Northwest National Laboratory developed a linear solvation energy relationship (LSER) theory to quantify the VOC sorption with its contributing interactions.[25] These interactions include hydrogen bonding, dipole-dipole interactions, polarizability and hydrocarbon dispersion interactions. Figure 4.2 summarizes the strategic design of recognition groups according to these interactions and targeted analytes in each case. For hydrogen bonding acidity, we designed a hexafluoroisopropanol (HFIP) group which can maximize hydrogen bonding by its acidic hydroxyl group (*pKa* 9~10, similar to phenols). We also included a carboxylic acid group in our sensors. These two groups are targeted at hydrogen bond basic vapors such as ethers and ketones. For hydrogen bonding basicity, we utilized a structure containing amide and crown-ether groups, which are both very polar and basic. This element is targeted at hydroxyl-containing vapors such as alcohols and acids. The acetylenedicarboxylate ester adduct resulted from the initial zwitterionic functionalization approach is both very polar and hydrogen bond basic itself, and is expected to interact strongly with vapors with large dipoles. Aromatic groups such as our proposed calix[4]arenes have high polarizability, which will favor the adsorption of aromatic and chlorinated hydrocarbons. Moreover, the long chain aliphatic groups such as the proposed dodecyl chains tend to favor dispersion interactions (a balance between the exoergic process and the endoergic cost by entropy change) with aliphatic

hydrocarbons. Finally, we included a humidity indicator which is very sensitive to environmental humidity changes and will be discussed in a later part of this chapter.
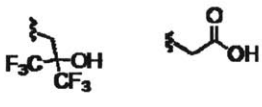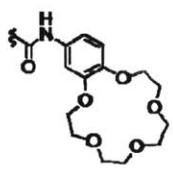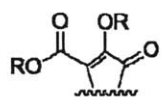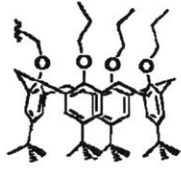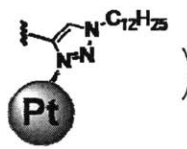
H-bond Acidity	H-bond Basicity	Polarity
Targeted Analytes: H-bond Acceptors such as Ethers, Ketones	Targeted Analytes: H-bond Donors such as Acids, Alcohols	R = allyl or propargyl Targeted Analytes: Vapors with High Polarity Such as Ketones, Ethers
Polarizability	Nonpolar Adsorption	Humidity Response
Targeted Analytes: Aromatic and Chlorinated Hydrocarbons	Targeted Analytes: Aliphatic Hydrocarbons	Humidity Indicator

Figure 4.2. Design of recognition groups based on different interactions and targeted analytes.

4.3 Synthesis of Functionalized MWCNTs

The synthesis of our functionalized MWCNTs is summarized in Scheme 4.2-4.5. Propargyl or allyl groups were initially introduced on to MWCNTs under mild reaction conditions (THF, 60 °C) with dipropargyl or diallyl acetylenedicarboxylate and DMAP, yielding propargyl-MWCNT **1** and allyl-MWCNT **2** (Scheme 4.2).
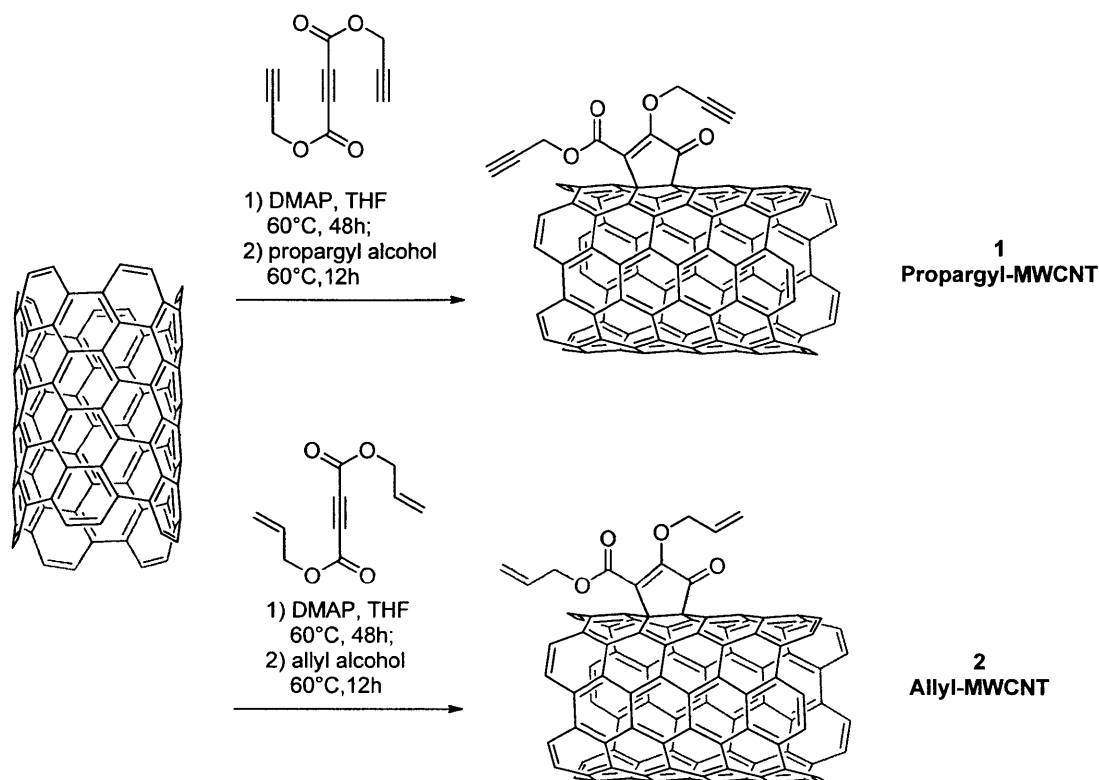
Scheme 4.2. Synthesis of propargyl-MWCNT **1** and allyl-MWCNT **2**.

We further functionalized **1** and **2** via three strategies: 1,3-dipolar cycloaddition (click chemistry), thiol-ene addition and olefin cross-metathesis reactions. The click chemistry and the thiol-ene addition chemistry, which feature high yields and no side products, are widely utilized to modify polymers, nanoscale materials, and biological materials.[26,27] The olefin metathesis reaction, catalyzed by Grubbs ruthenium catalysts, is another important strategy to introduce functional groups, as the reaction generally proceeds in good yield and with high functional group tolerance.[28,29]

Using the click chemistry strategy, dodecyl groups were incorporated onto the propargyl-MWCNTs **1** with dodecyl azide with CuI as the catalyst and diisopropylethylamine

(DIPEA) as the base (Scheme 4.3). After heating the reaction mixture in DMF at 90 °C for 24h,

click-MWCNT **3** was generated with pendant triazole groups.

1
Propargyl-MWCNT

C$_{12}$H$_{25}$N$_3$
CuI, DIPEA
DMF, 90°C, 24h

3
Click-MWCNT
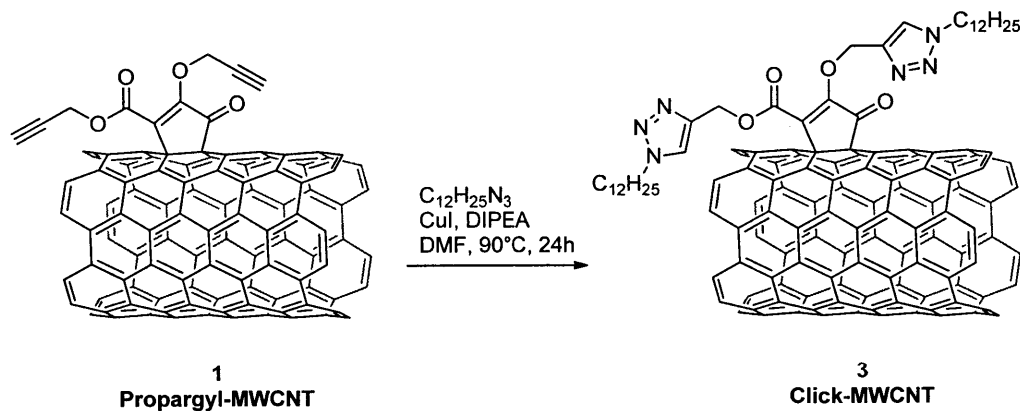
Scheme 4.3. Synthesis of click-MWCNT **3**.

Using the thiol-ene addition strategy, the vinyl group on allyl-MWCNT **2** was reacted

with 1-dodecylthiol or thioglycolic acid under UV irradiation, with 2,2-dimethoxy-2-

phenylacetophenone as an photoinitiator (Scheme 4.4). These thiol-ene addition processes lead

to the formation of thiolchain-MWCNT **4** with pendant dodecyl chain and thiolacid-MWCNT

5 with pendant carboxylic acid groups.
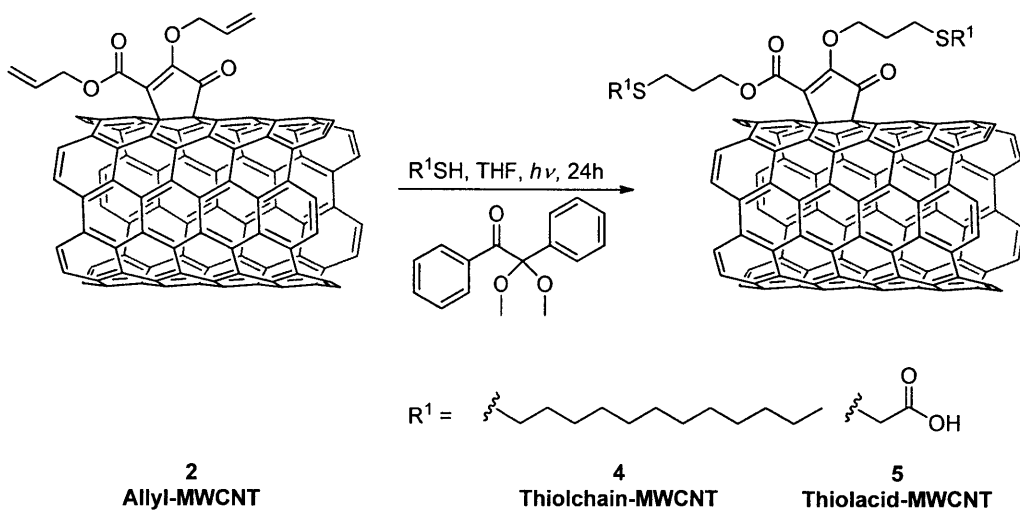
Scheme 4.4. Synthesis of thiolchain-MWCNT **4** and thiolacid-MWCNT **5**.

Finally, a cross metathesis reaction was performed between the allyl-MWCNT **3** and three terminal olefins namely 2-allyl-hexafluoroisopropanol, an allyl substituted calix[4]arene and 4-acryloylamidobenzo-15-crown-5, with Grubbs 2nd generation ruthenium catalyst, leading to HFIP-MWCNT **6**, calix-MWCNT **7** and crown-MWCNT **8**, respectively (Scheme 4.5).

MWCNTs **1** and allyl-MWCNTs **2**, respectively; while the ratio of intensity between D' and G band remained the same (0.3) for all three samples. These results indicated that the zwitterionic functionalization reaction has successfully introduced covalent functionalization onto the MWCNT surface while keeping the inner walls intact.

Figure 4.3. Raman spectra of pristine MWCNTs (black), propargyl-MWCNTs (blue) and allyl-MWCNTs (red). The green lines are fitted peaks and the grey lines are the fitted curves.

While Raman spectroscopy gives evidence on the surface functionalization of nanotubes, Fourier transform infrared (FT-IR) spectroscopy reveals important chemical information regarding the incorporated functional groups.[32] As shown in Figure 4.4, all the

MWCNTs **1** and allyl-MWCNTs **2**, respectively; while the ratio of intensity between D' and G band remained the same (0.3) for all three samples. These results indicated that the zwitterionic functionalization reaction has successfully introduced covalent functionalization onto the MWCNT surface while keeping the inner walls intact.

Figure 4.3. Raman spectra of pristine MWCNTs (black), propargyl-MWCNTs (blue) and allyl-MWCNTs (red). The green lines are fitted peaks and the grey lines are the fitted curves.

While Raman spectroscopy gives evidence on the surface functionalization of nanotubes, Fourier transform infrared (FT-IR) spectroscopy reveals important chemical information regarding the incorporated functional groups.[32] As shown in Figure 4.4, all the

functionalized MWCNTs have strong adsorption bands at 1730 cm^{-1} due to the C=O stretching of the carbonyl group and bands at 1230 and 1020 cm^{-1} due to the C–O stretching of the vinyl alkyl ether. These features are consistent with the acetylenedicarboxylate diester adduct structure. All of the spectra of the functionalized MWCNTs were normalized according to the 1730 cm^{-1} peak.
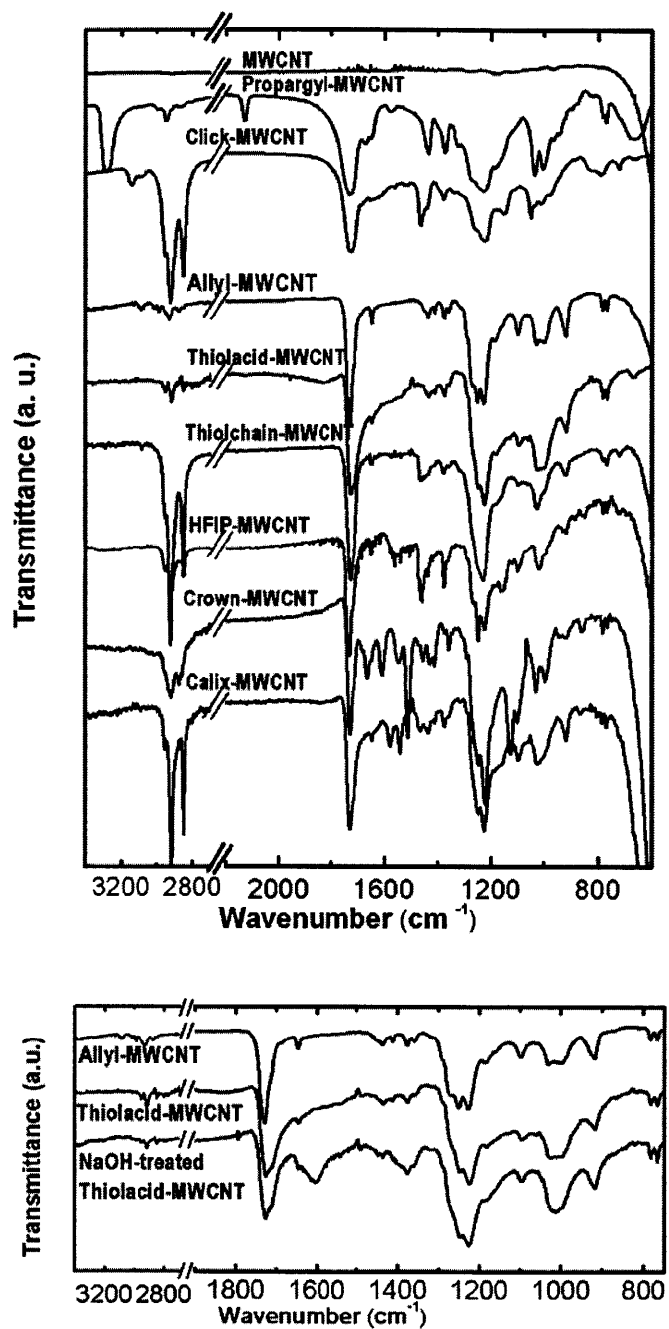
Figure 4.4. FT-IR spectroscopy of pristine and substituted MWCNTs (top). The spectra of thiolacid-MWCNT treated with 0.1 M NaOH is also shown (bottom).

The propargyl-MWCNT showed three characteristic absorption bands at 3285, 2130 and 668 cm^{-1}, corresponding to the terminal $\equiv$C–H stretching, the C$\equiv$C stretching and the –C $\equiv$CH bending of the propargyl group, respectively. After the click chemistry reaction all of these three prominent bands completely disappeared, with concomitant formation of two new bands: the greatly enhanced peaks within the 3000-2800 cm^{-1} region are due to the C–H stretching in the dodecyl groups, while the new peak appearing at 3130 cm^{-1} is associated with the C–H stretching in the 1,2,3-triazole groups. This result indicated that the click reaction proceeded nearly quantitatively.

The allyl-MWCNTs showed characteristic absorption bands of vinyl groups at 3087 and 921 cm^{-1}, corresponding to the =CH$_2$ stretching and the CH$_2$ out-of-plane wagging, respectively. After the thiol-ene addition, both bands of the allyl group had significantly decreased compared to the C=O stretching in the carbonyl group and the C–O stretching in the vinyl alkyl ether, indicating that the vinyl group has in large part reacted. Importantly, the thiolacid-MWCNT became water soluble after washing with 0.1M NaOH, and showed two new broad peaks at 1605 and 1376 cm^{-1}, which are associated with the asymmetric and symmetric stretching of the COO$^-$ group, respectively (Figure 4.4, bottom). We also observed greatly enhanced absorption between 3000 and 2800 cm^{-1} for thiolchain-MWCNTs, which are due to the C–H stretching in the dodecyl group. The large decrease of the vinyl absorption peaks and the appearance of the characteristic peaks of the new functional groups together verified the success of the thiol-ene addition.

Similar to the thiol-ene adducts, the MWCNTs from the metathesis reaction also showed significantly decreased absorption of the vinyl group along with the appearance of characteristic peaks of the new functional groups. Specifically, HFIP-MWCNT showed a new

peak at around 1170 cm^{-1}, corresponding to the C–F stretching in the HFIP group. The crown-MWCNT showed a series of interesting bands: two peaks at 1660 and 1548 cm^{-1} due to the C=O stretching and C–O stretching in the amide group, three peaks at 1610, 1510 and 1456 cm^{-1} due to the aromatic ring stretching of the benzene ring, and a peak at 1125 cm^{-1} due to the C–O–C stretching of the crown ether. The calix-MWCNT showed the appearance of two new peaks at 1580 and 1542 cm^{-1} due to the aromatic ring stretching and a significant increase in the absorptions between 3000 and 2800 cm^{-1} due to the C–H stretching in the *t*-butyl group.

4.5 Quantitative Characterization

We further obtained quantitative evidence on the structure and composition of the functionalized MWCNTs from X-ray photoelectron spectroscopy (XPS) and thermogravimetric analysis (TGA). The XPS spectra (Figure 4.5) were normalized to the C 1s peak at 532 eV. In the TGA experiment (Figure 4.6), pristine MWCNTs cleaned in the same fashion as the functionalized MWCNTs were used as a standard. The weight loss data, which will be discussed in a later part of this paper, are obtained from subtracting the weight loss of the pristine MWCNTs.
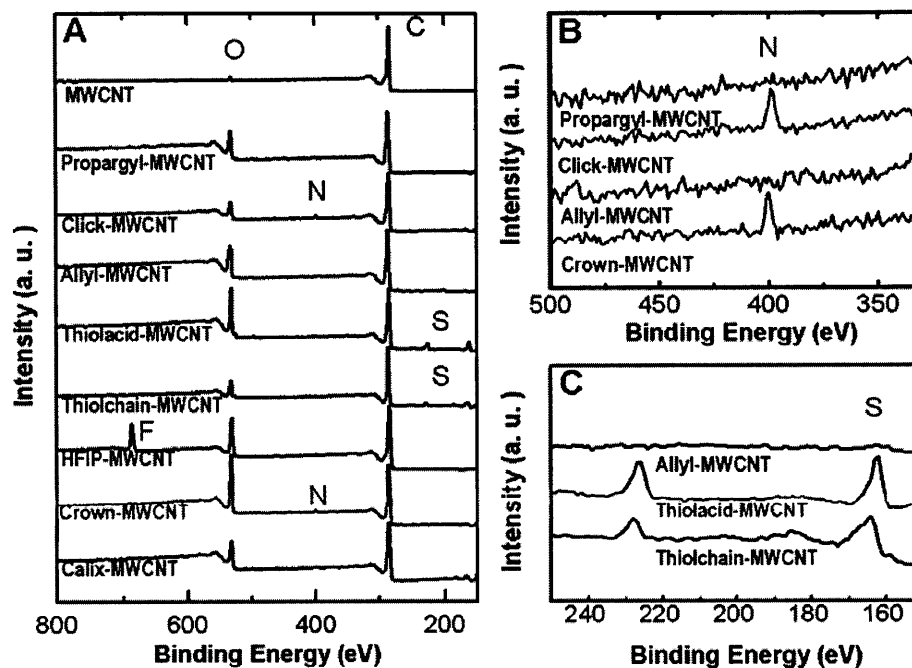
Figure 4.5. XPS of pristine and substituted MWCNTs.

Compared to pristine MWCNTs, both propargyl-MWCNTs and allyl-MWCNTs have increased intensity of oxygen 1s peak at 284 eV, indicating the success of the functionalization. From the oxygen-to-carbon ratio (7 %), the calculated the degree of functionalization density for propargyl-MWCNT is 2 propargyl diester adduct groups per 100 MWCNT carbon atoms. This result agrees with the functionalization density of 2.0 functional groups per 100 MWCNT carbon atoms calculated from the weight loss of 24 % in TGA. Similar calculations were carried out for the allyl-MWCNTs, leading to a density of 3 allyl diester adduct groups per 100 MWCNT carbon atoms by XPS (oxygen-carbon ratio of 8 %) and 2.6 functional groups by TGA (weight loss of 29 %).
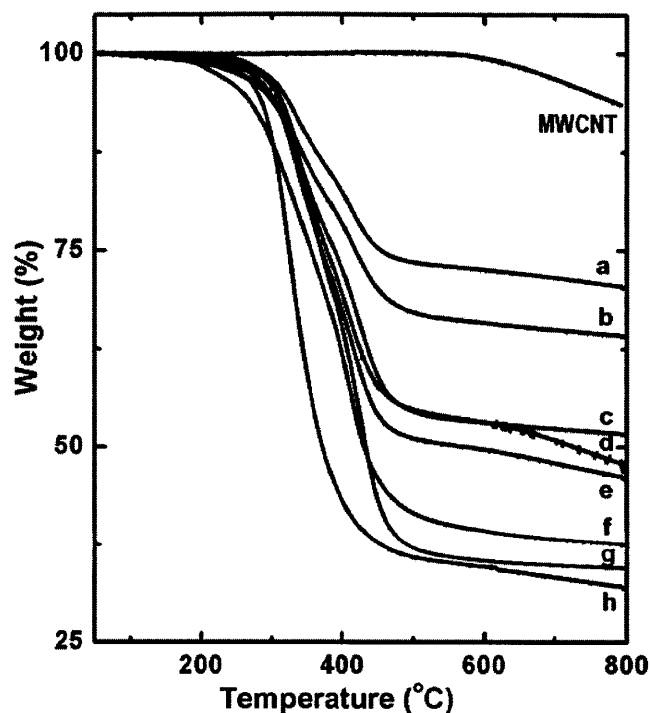
Figure 4.6. TGA of pristine and substituted MWCNTs. a) Propargyl-MWCNT, b) allyl-MWCNT, c) HFIP-MWCNT, d) thiolacid-MWCNT, e) click-MWCNT, f) crown-MWCNT, g) calix-MWCNT, h)thiolchain-MWCNT.

We observed a distinct nitrogen 1s peak at 400 eV in the click-MWCNT sample, and calculated the functionalization density of the triazole group from the oxygen-carbon ratio (5 %) or from the nitrogen-carbon ratio (6 %). The ratios corresponded to 4 triazole groups per 100 MWCNT carbon atoms. The weight loss of 48 %, obtained from TGA measurements, leads to a functionalization density of 3.7 triazole groups per 100 carbon atoms. This high functionalization density indicated that the click chemistry is almost quantitative on propargyl-MWCNTs, which was consistent with our FT-IR observations.

Important information on the elemental composition of other samples was also obtained from XPS. We noticed that the functionalization reaction led to quite different oxygen-nitrogen ratios in each sample. We also observed sulfur 2s and 2p peaks (at 229 and 165 eV, respectively) in thiolacid-MWCNTs and thiolchain-MWCNTs, a fluorine 1s peak at 687 eV in HFIP-MWCNTs, and a nitrogen 1s peak at 400 eV in crown-MWCNTs. Table 4.2 summarizes the functionalization density data calculated from the XPS elemental ratio and from the TGA curves. Compared with other CNT functionalization methods, the functionalization densities are rather high for all the eight MWCNT transformations.

Table 4.2. Functionalization Density Data Calculated from the XPS Elemental Ratio and from the TGA Weight Loss Curves.

Samples	XPS Elemental Ratio (%)		TGA Weight Loss (%)	Density (Numbers of Functional Groups per 100 Carbons)	
	O/C	X/C[a]		by XPS	by TGA
Propargyl-MWCNT	7	-	24	2	2.0
Allyl-MWCNT	8	-	39	3	2.6
Click-MWCNT	5	6	48	4	3.7
Thiolchain-MWCNT	6	3	62	5	5.6
Thiolacid-MWCNT	15	3	45	4	4.6
HFIP-MWCNT	12	7	42	2	1.6
Calix-MWCNT	8	-	59	-[b]	1.3
Crown-MWCNT	17	2	56	2	3.1

[a] X stands for the nitrogen, sulfur or fluorine. [b] XPS data is not used for calculation because functional group has similar oxygen-carbon ratio to parent allyl-MWCNT.

4.6 Morphology and Dispersibility

The scanning electron microscope (SEM) images of functionalized MWCNTs are shown in Figure 4.7. As a comparison, pristine MWCNT were ultra-sonicated and cleaned in

the same fashion as the functionalized MWCNTs, and were used as a standard, ruling out the effect of ultra-sonication and solvent washing. Apparently, the functionalization process greatly reduced the size of the bundles of pristine MWCNTs.
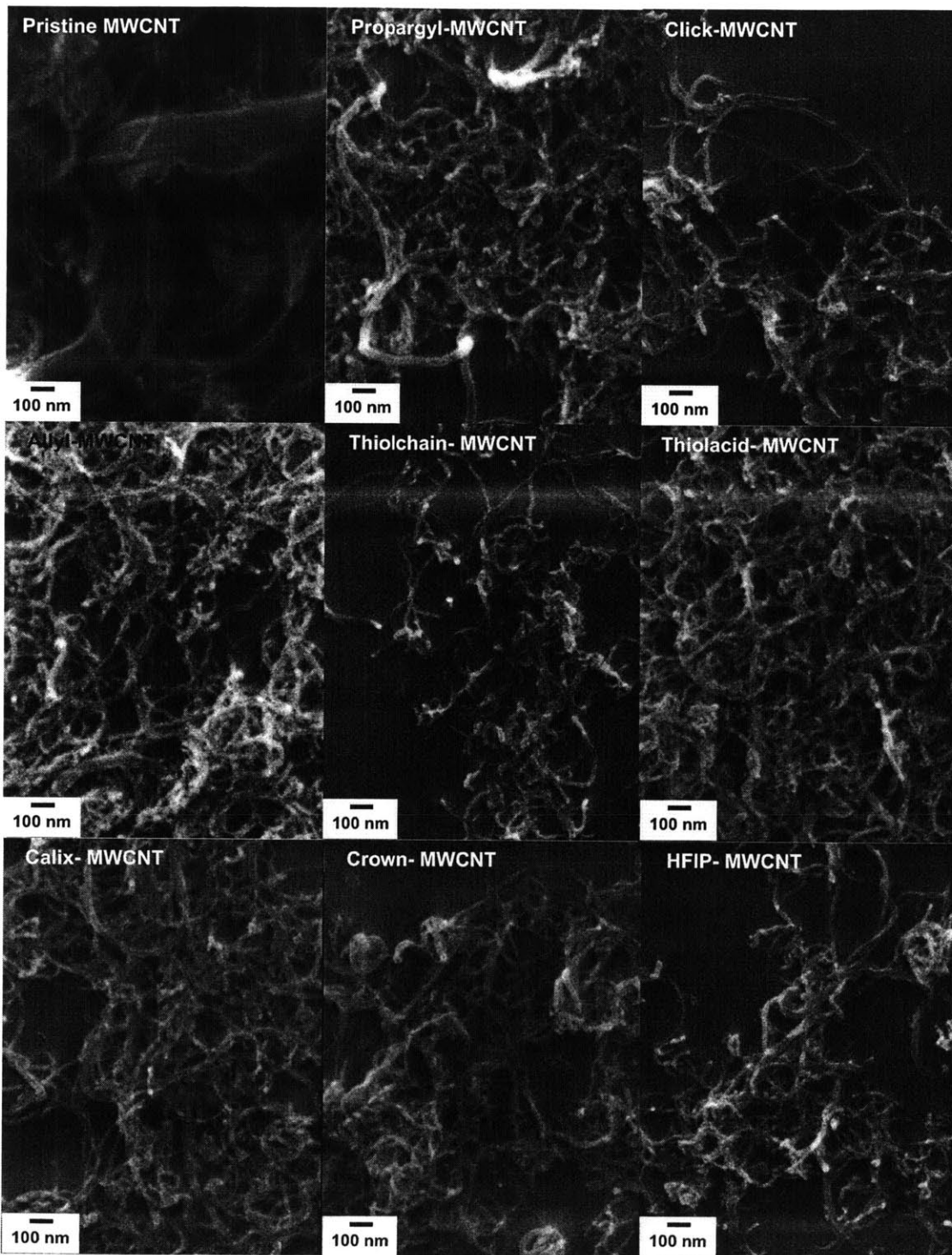
Figure 4.7. SEM images of pristine and substituted MWCNTs.

It was also noticed that chemical treatment greatly enhanced the dispersibility of MWCNTs. For example, after centrifuging thiolchain-MWCNT suspension in dichloromethane at 14.5 K rpm for 5 minutes, most of the tubes still remain in the supernatant layer. This is not surprising, given the high density of long dodecyl chains (5.6 dodecyl groups per 100 MWCNT carbon atoms by TGA), and the debundled nature of functionalized MWCNTs. Similar stable dispersibility was also found with the HFIP-MWCNTs and the thiolacid-MWCNTs in tetrahydrofuran, the crown-MWCNTs in isopropanol, the calix-MWCNTs and the click-MWCNTs in dichloromethane. This good dispersion enables us to achieve a high-quality CNT conductive network, which is critical for our sensor fabrication.

4.7 Sensory Responses of MWCNT Array to VOCs

We fabricated our resistance sensors by spin coating 2 mm x 2 mm MWCNT films on top of two gold electrodes (50 nm thick, 2 mm spacing) on glass stubstrate from a stable dispersion (0.1 mg/mL) of functionalized MWCNTs. The solvents with strong dispersing ability, as mentioned in the morphology section, were used to disperse functionalized MWCNTs. Dimethylformamide was used for dispersing pristine, allyl- and propargyl-MWCNTs. The sensors were then annealed in vacuum at 150 ℃ for 5 minutes before obtaining measurements. The typical thickness of the MWCNT films is in the range of 30-60 nm measured with a profiler. The typical resistance for the MWCNT films is in the range of 0.2 to 0.5 MΩ.

We investigated the sensory response by measuring the relative conductance change $(-\Delta G / G_0)$ of the sensors upon exposure to the 20 VOCs (3 trials each). The current was recorded between the two electrodes under a constant bias voltage (0.05 V) from which the

conductance change was calculated. Our sensor responses were measured sequentially, under the same experimental conditions such as sensor exposure and refreshing time, analyte concentration, temperature, environmental humidity, *etc*.

Representative response curves of the sensor elements (pristine, allyl-, thiolchain- and crown-MWCNTs) to decane (left) and pentanol (right) are shown in Figure 4.8. All the sensors responded to the analyte very rapidly, and the chemical functionalization enhanced the response to both decane and pentanol. It is interesting that the conductance of the thiolchain-MWCNTs decreased by 96 % to decane and 70 % to pentanol, while the conductance of the crown-MWCNTs decreased by 17 % to decane and 97 % to pentanol. This cross-sensitivity is due to the different chemical properties of the sensing elements: the long aliphatic hydrocarbon chains in the thiolchain-MWCNTs lead to a stronger interaction with aliphatic hydrocarbons, while the amide and the crown ether groups in the crown-MWCNTs introduced favorable hydrogen bonding interactions with alcohols.
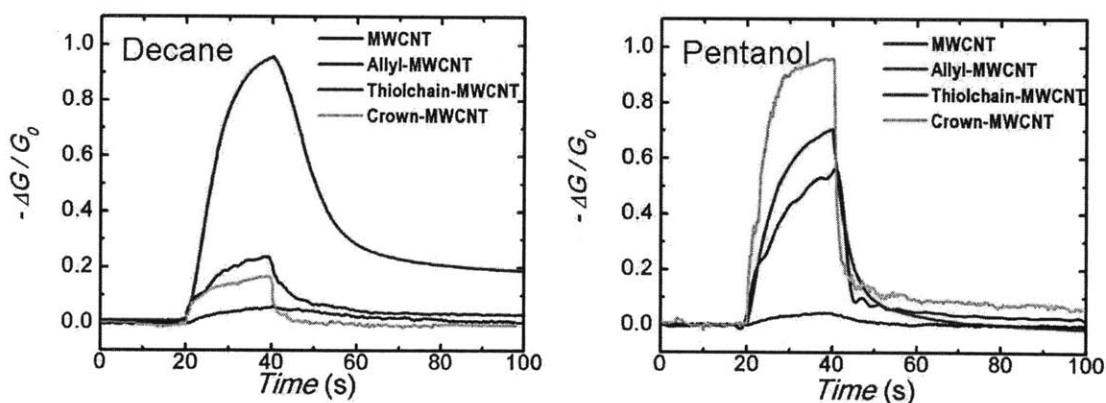
Figure 4.8. Conductance response, $-\Delta G/G_0$, of pristine MWCNT (black line), allyl-MWCNT (dark red line), crown-MWCNT (green line) and thiolchain-MWCNT (red line) resistance sensors to decane (left) and pentanol (right) at their saturated vapor pressures.

Figure 4.9 summarizes the conductance response patterns of pristine and substituted MWCNT based resistance sensors to twenty representative VOCs. Each response is the average of three measurements. For easier visualization, the level of response is shown in color according to the scale bar on the right. As expected, each of the VOCs induced quite different conductance changes in the individual sensors, thus each creating a distinct multi-dimensional response pattern. Compared with pristine MWCNTs, functionalized MWCNTs have much enhanced responses to all the VOCs. This can be attributed to the highly responsive functionalized nanotube surface and the largely debundled CNT network.
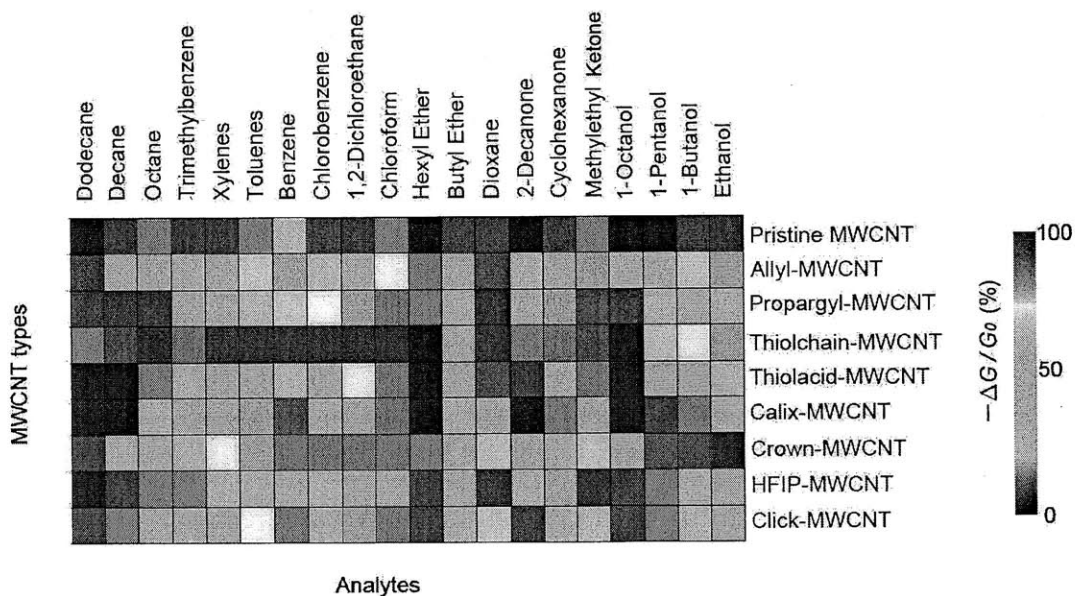
Figure 4.9. Conductance response patterns of pristine and substituted MWCNT based resistance sensors to twenty representative VOCs. Responses are averages of three measurements. For easier visualization, the level of response is showed in color according to the scale bar on the right.

As an example of enhanced selectivity, the HFIP-MWCNT sensor has an increased response to ethers and ketones. It is believed to be associated with the hydrogen bonding acidity of the HFIP group. More interestingly, the HFIP-MWCNT sensor also showed a decreased response to all other VOCs. This can be attributed to the non-favorable interactions between the HFIP's fluorocarbon groups and the hydrocarbon-containning VOCs. As a second example, the thiolchain-MWCNT sensor had a larger response to hydrocarbons with relatively low polarity such as aliphatic, aromatic and chlorinated hydrocarbons. This is most likely due to the favorable dispersion interactions with the aliphatic recognition groups. This effect is also found with the click-MWCNTs. We noticed the enhanced responses of thiolchain-MWCNTs to almost all of the VOCs, which is possibly due to its very high functionalization density (5.6 dodecyl groups per 100 MWCNT carbon atoms by TGA).

We calculated the rate constant k_a for the forward adsorption process from the initial slope of the response curve.[33] As shown in Figure 4.10, the sensor elements exhibit high k_a for aliphatic hydrocarbons and other VOCs with long aliphatic chains.
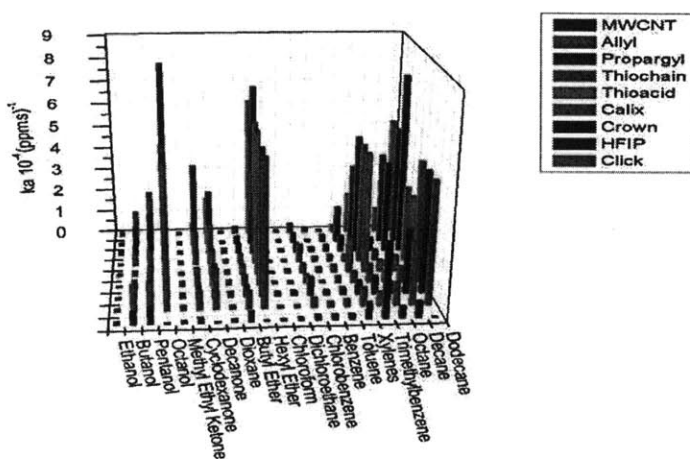
Figure 4.10. Adsorption rate constants of the MWCNT sensors.

4.8 Statistical Analysis

To explore the identifying capabilities of our sensor array, we subjected our sensing results to principal component analysis and linear discriminate analysis. Principal component analysis (PCA) is an unsupervised multivariate analysis method for linear data compression and pattern recognition.[34] Without any prior knowledge of the classification of the analytes, it groups the analytes based on the similarity of their data. The idea of PCA is to find uncorrelated principle components (PCs) which are linear combinations of the original variables (correlated response measurements). These PCs are ranked by the amount of variation they account for. As shown in the Scree plot (Figure 4.11), the PCA of our data set requires 2 PCs to describe 80 % of the total variances and 4 PCs to describe 95 % of the total variances, which is quite different from traditional electronic noses which can achieve 95% discrimination by using only one or two PCs. This effect is due to the large cross-sensitivity of our sensor array and indicates its higher capability for discrimination between similar analytes. The PCA score plot in Figure 4.12 shows a clear classification of the data, utilizing the first two PCs which represent 80 % of the variances. The VOCs were classified into five groups, namely alcohols, ethers/ketones, aliphatic, aromatic and chlorinated hydrocarbons. The fact that both octanol and hexyl ether have long aliphatic chains explains why their results also border the aliphatic hydrocarbon group. Although the ethers and the ketones are very clearly separated from other VOCs, it is difficult to distinguish them from each other because of their similar chemical properties.
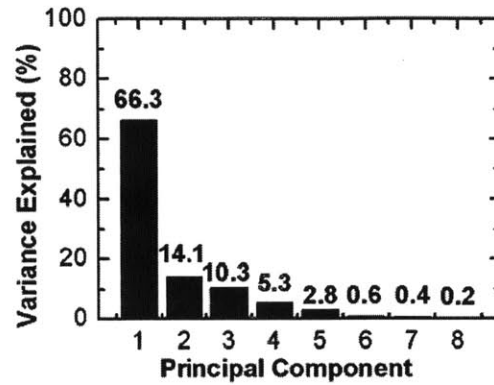
Figure 4.11. Scree plot of the principal component analysis.
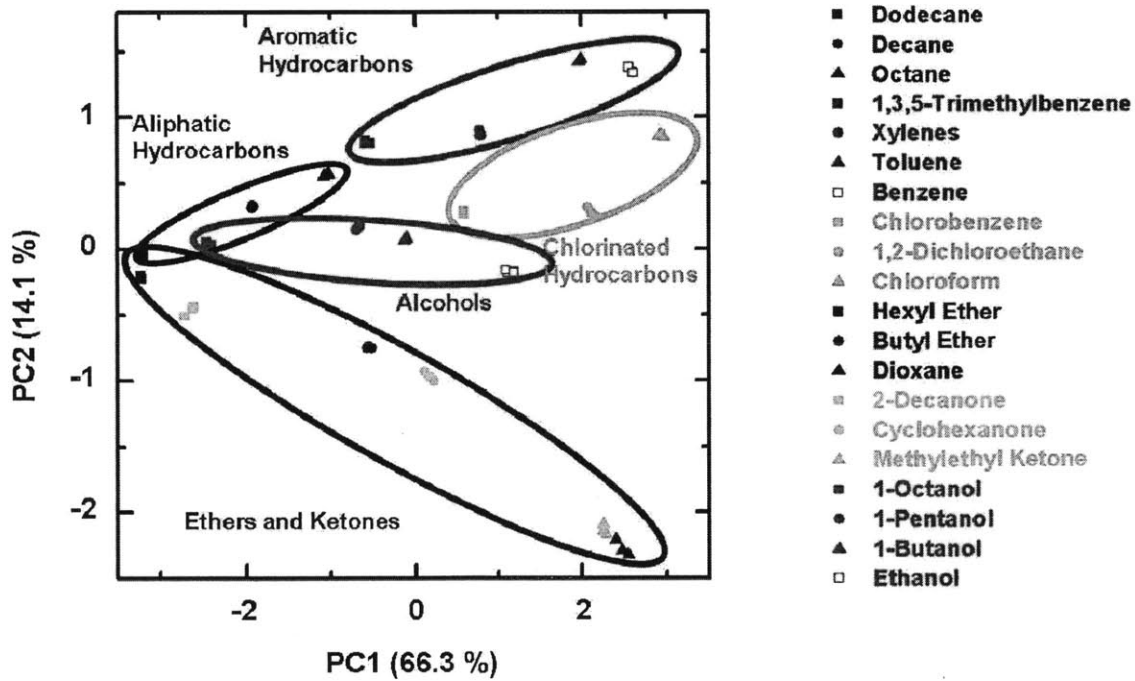
Figure 4.12. Principal component score plots of an array of 8 functionalized MWCNT resistance sensors to 20 representative VOCs (3 trials each).

We also explored the discrimination capability of our sensor with linear discriminant analysis (LDA).[34] LDA is a supervised statistical technique, which utilizes data from known

groups to identify which group a new object belongs to. It is based on the linear discriminant function (LDF), which is a linear combination of the original variables that maximizes the ratio of between-class variance and within-class variance. Specifically, we applied a cross-validation (leave-one-out) routine to compensate for an optimistic apparent error rate. This method calculates the LDF with one observation omitted sequencially, and then classifies the omitted observation with the LDF. After this procedure is repeated for each observation, the success rate is calculated. In our case, the 60 training observations (20 VOCs, 3 trials for each) were separated into the same 5 groups utilized in the PCA classification. As shown in Table 4.3, the cross-validation routine LDA demonstrated 100 % accuracy for all the 60 trials. This result, together with the successful PCA analysis, verified the superior selectivity of our sensor array.

Table 4.3. Summary of Classification with Cross-validation.

Put-into-Group	True Group				
	Chlorinated Hydrocarbons	Ethers / Ketones	Aliphatic Hydrocarbons	Alcohols	Aromatic Hydrocarbons
Chlorinated Hydrocarbons	9	0	0	0	0
Ethers / Ketones	0	18	0	0	0
Aliphatic Hydrocarbons	0	0	9	0	0
Alcohols	0	0	0	12	0
Aromatic Hydrocarbons	0	0	0	0	9
Total N	9	18	9	12	9
N Correct	9	18	9	12	9
Proportion	1.00	1.00	1.00	1.00	1.00

N = 60   N Correct = 60   Proportion Correct = 1.000

4.9 Humidity Sensing

Environmental humidity is always a concern for nanotube based sensors. As shown in Figure 4.13, our sensors have lower responses to humidity compared to their responses to organic molecules such as pentanol, although the saturated vapor pressure of water at $25\,^{\circ}C$ (23.8 mmHg) is 15 times larger than that of pentanol (1.5 mmHg). This fact can be explained by the hydrophobic nature of the incorporated chemical functionalizations.
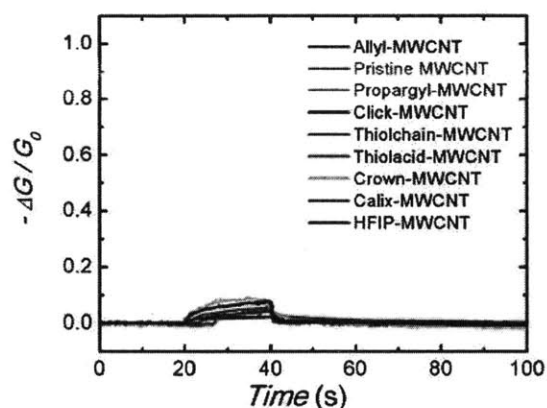
Figure 4.13. Conductance response, $-\Delta G/G_0$, of the pristine and substituted MWCNT based resistance sensors to saturated vapor of water.

In addition to the requirement that MWCNT-based sensors exhibit a low sensitivity to humidity, sensors that can detect environmental changes in humidity are also highly desirable. Previously, the 1,2,3-triazole group has been shown to be a good ligand for platinum.[35] We took advantage of this platinum affinity to grow platinum particles onto the click-MWCNTs by reducing potassium trichloro(ethene)platinate(II) (Zeise's salt) with hydrazine in a dispersion of click-MWCNTs (Figure 4.14).[36,37] As shown in the SEM image in Figure 4.14, the platinum particles grew onto the nanotube surface. We performed an XPS study on this CNT/Pt

composite (Figure 4.15). The peaks at 71.5 and 74.8 eV correspond to metallic platinum $4f_{2/7}$ and $4f_{2/5}$ energies, respectively, indicating that the platinum has been successfully reduced.
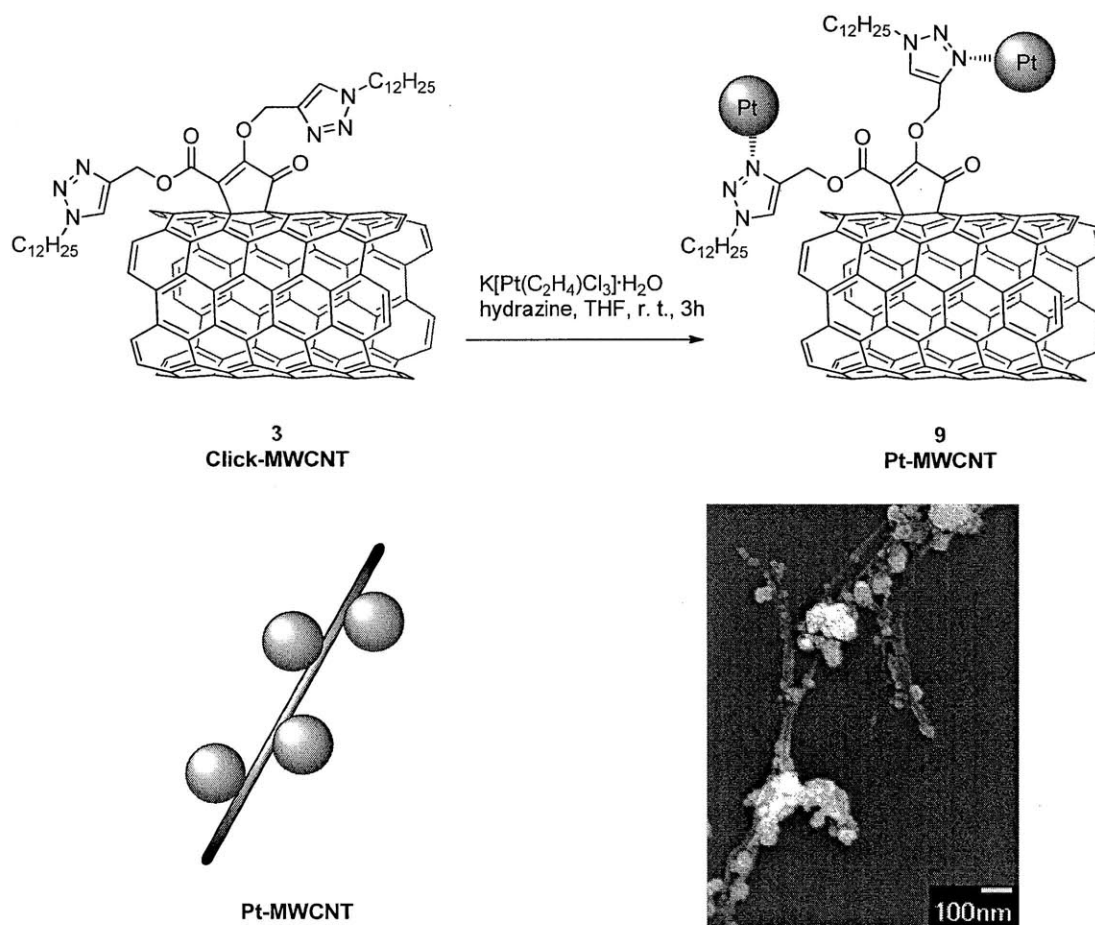
Figure 4.14. Functionalization of the click-MWCNT with platinum particles. Synthetic approach (upper), a cartoon of the structure (lower left) and SEM image (lower right) of the Pt-MWCNT composite.
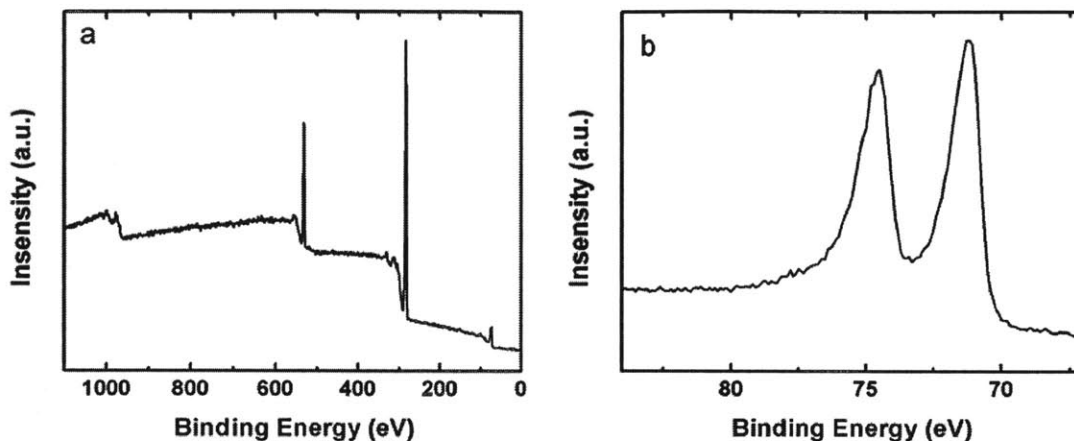
Figure 4.15. XPS spectra of the click-MWCNT/Pt composite. (a) Survey scan spectrum; (b) Pt 4f spectrum.

We also attempted to grow platinum particles within a propargyl-MWCNT media, using the same chemistry as in the click-MWCNT case. In contrast, the platinum particles that formed were located both on the nanotube and away from the nanotube surface (Figure 4.16). It is likely that the platinum(II) ions that were coordinated to the surface of click-MWCNTs initiated the nucleation process, and the platinum particles grew preferentially onto the nanotube surface during the reduction process. In contrast, due to the much weaker interactions between platinum and the propargyl-MWCNTs, there is no referred location for the platinum particles to nucleate and grow. Therefore, click-MWCNTs are superior materials for controllable incorporation of platinum particles.
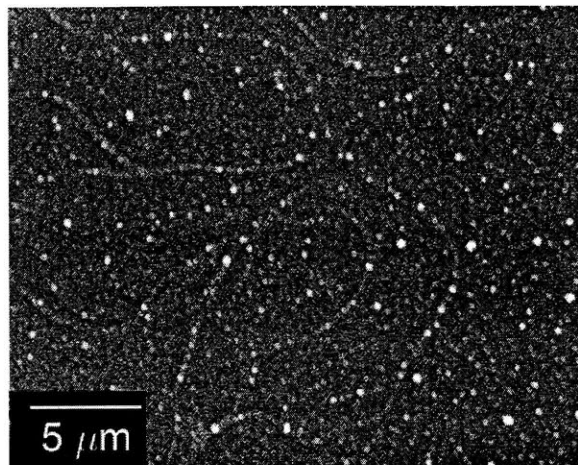
Figure 4.16. SEM image of platinum reduced in the propargyl-MWCNT media.

We fabricated a sensor with the click-MWCNT/Pt composite and measured its conductance changes in the same fashion as the other MWCNT sensors. As shown in Figure 4.17, the conductance of the Pt/nanotube composite increased 40 % at 30 % relative humidity (RH), 400 % at 60 % RH and 1100 % at 100 % RH.
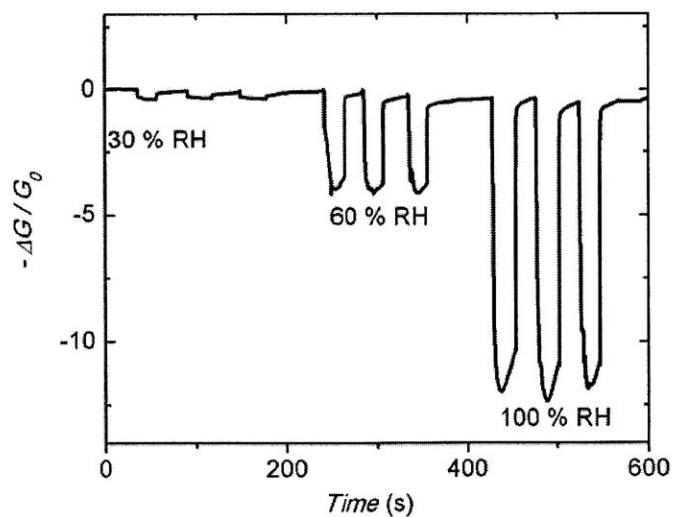
Figure 4.17. Conductance response, $-\Delta G/G_0$, of Pt/CNT based resistance sensor to water.

As a comparison, we synthesized platinum particles without CNTs using the same chemistry as in the click-MWCNT case, and fabricated sensor from this material. However, only a 3 % decrease in conductance was observed when the sensor was exposed to 100 % RH (Figure 4.18). Considering the magnitude of the response, the MWCNT/Pt composite generated 366 times larger response than pure platinum material.
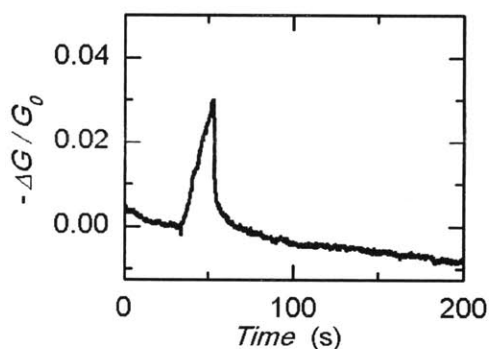
Figure 4.18. Conductance response, $-\Delta G/G_0$, of Pt based sensor to saturated water vapor.

The enhanced response of Pt/CNT based resistance sensor to water can be explained by the catalytic activity of the platinum surface. Platinum surfaces are known to bind and activate water, generating protons and electrons.[38]

$$x\ H_2O + Pt^* \ (M) \longrightarrow (M)\ Pt\text{-}[OH]_x + x\ H^+ + x\ e^- \tag{1}$$
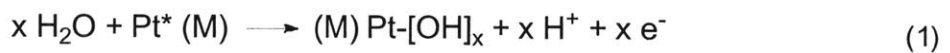
Our proposed mechanism is that water binds to the platinum surfaces on the click-MWCNT/Pt composite, and then dissociates according to equation (1). The electrons generated from this process doped the nanotubes, thus increasing the conductivity of the device. In the case without CNTs, no such doping effect takes place, so the conductance was decreased by the adsorbed water.

4.10 Conclusions

A MWCNT-based sensor array was developed as the first proof-of-concept of identifying VOCs by their functional groups with nanotubes. Functionalized MWCNTs with a series of cross-sensitive recognition groups were successfully synthesized via zwitterionic and post-transformation synthetic approaches. The incorporated chemical functional groups on MWCNT surfaces introduced greatly increased sensitivity and selectivity to the targeted analytes. The distinct response pattern of each chemical was subjected to statistical treatments, which led to a clear separation and accurate identification of 100 % of the VOCs. Further incorporation of platinum particles onto triazole-functionalized MWCNTs generated a highly sensitive humidity detector. We believe this MWCNT-based sensor array is a promising approach for low-cost, real time detection and identification of VOCs.

4.11 Experimental Section

Materials.

All chemicals were of reagent grade from Sigma-Aldrich, Alfa Aesar or Acros and used as received. All solvents were of spectroscopic grade unless otherwise noted. Dimethylformamide was stirred over CaH_2 and distilled thereafter. Anhydrous tetrahydrofuran and dichloromethane were obtained from J. T. Baker and purified by passing through a Glasscontour dry solvent system. Multi-walled carbon nanotubes were acquired from Sigma-Aldrich. (> 99 MWCNT, O.D. 6-13 nm X 2.5-20 μm). Diallyl acetylenedicarboxylate and dipropargyl acetylenedicarboxylate were prepared according to literature procedures. 5,11,17,23-Tetrakis(*t*-butyl)-25-allyl-26,27,28-tripropyl-calix[4]arene was prepared according to literature procedure.

General Methods and Instrumentation.

Raman spectra were measured with a Kaiser Hololab 5000R Modular Research Raman Spectrometer with Microprobe from MIT Center for Materials Science and Engineering. FT-IR spectra were recorded on a Perkin Elmer Model 2000 FT-IT spectrometer by drop-casting the material on a KBr disk. TGA analyses were performed with a TGA Q50 apparatus (TA instruments). Experiments were carried out under nitrogen. Samples were heated at 5 °C/min from 30 °C to 800 °C. XPS spectra were recorded on a Kratos AXIS Ultra X-ray Photoelectron Spectrometer. SEM images were taken with a JEOL 6700 Scanning Electron Microscope. Gold layer was coated from a Polaron SC7620 sputter coater. The substrates were cleaned with a Harrick Plasma PDC-32G Plasma Cleaner. Film thicknesses were measured with a Veeco Dektak 6M Stylus Profiler.

All synthetic manipulations were carried out under an argon atmosphere using standard Schlenk techniques unless otherwise noted. Glassware was oven-baked and cooled under N_2 atmosphere. Analyte of specific concentration and relative humidity was generated with a KIN-TEK gas-generating system. Source-drain current change in response to analyte was measured with an AUTOLAB PGSTAT 20 potentiostat (Eco Chemie) at constant potential (typically 0.05 V). The statistical treatment was performed with a Minitab software (version 15) using multivariate analysis methods.

Synthesis of Propargyl-MWCNTs 1.

A suspension of MWCNTs (48.0 mg, 4.0 mmol of carbon) in THF (40 mL) was sonicated for 5 min using an ultrasonic probe yielding a black suspension. To the MWCNT suspension were added activated molecular sieves (4 Å) to remove moisture introduced by the sonication process, and left overnight. The heterogeneous solution was then transferred to a dry flask through a cannula and was heated at 60 °C. To the MWCNT suspension were added simultaneously a solution of dipropargyl acetylenedicarboxylate (3.80 g, 20.0 mmol) in THF (20 mL) and a solution of 4-dimethylaminopyridine (2.44 g, 20.0 mmol) in THF (20 mL) via syringe pump within 48h. To the reaction mixture was added propargyl alcohol (1.5 mL), and the resulting mixture was stirred at 65 °C for another 12 h. The reaction mixture was cooled to room temperature, and centrifuged at 14,500 rpm for 15 min. The supernatant was discarded and the residue was dispersed in DMF for 3 min using an ultrasonic bath. The mixture was centrifuged and the supernatant was discarded. The same sequence was repeated five times with DMF and five times with acetone. The ropargyl-MWCNTs 1 were dried under vacuum overnight. See Figure 4.3 for Raman spectra, Figure 4.4 for FT-IR spectra, Figure 4.5 for XPS

spectra, Figure 4.6 for TGA weight loss curve, and Figure 4.7 for SEM image.

Synthesis of Allyl-MWCNTs 2.

A suspension of MWCNTs (48.0 mg, 4.0 mmol of carbon) in THF (40 mL) was sonicated for 5 min using an ultrasonic probe yielding a black suspension. To the MWCNT suspension were added activated molecular sieves (4 Å) to remove moisture introduced by the sonication process, and left overnight. The heterogeneous solution was then transferred to a dry flask through a cannula and was heated at 60 °C. To the MWCNT suspension were added simultaneously a solution of diallyl acetylenedicarboxylate (3.88 g, 20.0 mmol) in THF (20 mL) and a solution of 4-dimethylaminopyridine (2.44 g, 20.0 mmol) in THF (20 mL) via syringe pump within 48h. To the reaction mixture was added allyl alcohol (1.5 mL), and the resulting mixture was stirred at 65 °C for another 12 h. The reaction mixture was cooled to room temperature, and centrifuged at 14,500 rpm for 15 min. The supernatant was discarded and the residue was dispersed in DMF for 3 min using an ultrasonic bath. The mixture was centrifuged and the supernatant was discarded. The same sequence was repeated five times with DMF and five times with acetone. The allyl-MWCNTs **1** were dried under vacuum overnight. See Figure 4.4 for FT-IR spectra, Figure 4.5 for XPS spectra, Figure 4.6 for TGA weight loss curve, and Figure 4.7 for SEM image.

Synthesis of click-MWCNTs 3.

To a 10 mL Schlenk flash was added propargyl-MWCNTs **1** (10 mg) and CuI (38 mg, 0.2 mmol), followed by sequentially vacuuming and refilling with argon for three times. Then dodecyl azide (0.22 g, 1 mmol), diisopropylethylamine (2 mL) and dimethylformamide (2 mL)

was added via syringe. The mixture was sonicated in a sonication bath for 30 min, followed by stirring at 90 °C for 24 h. The reaction mixture was cooled to room temperature, and washed with ammonium hydroxide for five times to remove copper. Interestingly, the MWCNTs are well dispersed in the diisopropylethylamine phase during the washing process, so a 25 mL separation funnel was used to collect the diisopropylethylamine phase. The dispersion was further washed with water for three times to remove residue ammonium hydroxide. The dispersion was added to methanol and centrifuged at 14,500 rpm for 15 min. The supernatant was discarded and the residue was dispersed in acetone for 3 min using an ultrasonic bath. The mixture was centrifuged and the supernatant was discarded. The same sequence was repeated five times with acetone. The click-MWCNTs **3** were dried under vacuum overnight. See Figure 4.3 for Raman spectra, Figure 4.4 for FT-IR spectra, Figure 4.5 for XPS spectra, Figure 4.6 for TGA weight loss curve, and Figure 4.7 for SEM image.

Synthesis of thiolchain-MWCNTs 4.

To a 10 mL Schlenk flask was added allyl-MWCNTs **2** (10 mg) and 2,2-dimethoxy-2-phenylacetophenone (DMPA) (26 mg, 0.1 mmol), followed by sequentially vacuuming and refilling with argon for three times. Then *n*-dodecylthiol (0.40 g, 2 mmol) and tetrahydrofuran (2 mL) was added via syringe. The mixture was sonicated in a sonication bath for 30 min, followed by stirring under UV irradiation at room temperature for 24 h. The reaction mixture was then diluted with acetone and centrifuged at 14,500 rpm for 15 min. The supernatant was discarded and the residue was dispersed in acetone for 3 min using an ultrasonic bath. The mixture was centrifuged and the supernatant was discarded. The same sequence was repeated five times with acetone. The thiolchain-MWCNTs **4** were dried under vacuum overnight. See

Figure 4.4 for FT-IR spectra, Figure 4.5 for XPS spectra, Figure 4.6 for TGA weight loss curve, and Figure 4.7 for SEM image.

Synthesis of thiolacid-MWCNTs 5.

To a 10 mL Schlenk flash was added allyl-MWCNTs **2** (10 mg) and 2,2-dimethoxy-2-phenylacetophenone (DMPA) (26 mg, 0.1 mmol), followed by sequentially vacuuming and refilling with argon for three times. Then thioglycolic acid (0.18 g, 2 mmol) and tetrahydrofuran (2 mL) was added via syringe. The mixture was sonicated in a sonication bath for 30 min, followed by stirring under UV irradiation at room temperature for 24 h. The reaction mixture was then diluted with acetone and centrifuged at 14,500 rpm for 15 min. The supernatant was discarded and the residue was dispersed in acetone for 3 min using an ultrasonic bath. The mixture was centrifuged and the supernatant was discarded. The same sequence was repeated five times with acetone. The thiolacid-MWCNTs **5** were dried under vacuum overnight. See Figure 4.4 for FT-IR spectra, Figure 4.5 for XPS spectra, Figure 4.6 for TGA weight loss curve, and Figure 4.7 for SEM image.

Synthesis of HFIP-MWCNTs 6.

To a 10 mL Schlenk flash was added allyl-MWCNTs **2** (10 mg) and Grubbs second generation ruthenium catalyst (8 mg, 0.01 mmol), followed by sequentially vacuuming and refilling with argon for three times. Then 2-allyl-hexafluoroisopropanol (0.4 g, 2 mmol) and dichloromethane (2 mL) was added via syringe. The mixture was sonicated in a sonication bath for 30 min, followed by stirring at 40 °C for 48 h. The reaction mixture was then diluted with acetone and centrifuged at 14,500 rpm for 15 min. The supernatant was discarded and the

residue was dispersed in acetone for 3 min using an ultrasonic bath. The mixture was centrifuged and the supernatant was discarded. The same sequence was repeated five times with acetone. The HFIP-MWCNTs **6** were dried under vacuum overnight. See Figure 4.4 for FT-IR spectra, Figure 4.5 for XPS spectra, Figure 4.6 for TGA weight loss curve, and Figure 4.7 for SEM image.

Synthesis of Calix-MWCNTs 7.

To a 10 mL Schlenk flash was added allyl-MWCNTs **2** (10 mg), Grubbs second generation ruthenium catalyst (8 mg, 0.01 mmol) and 5,11,17,23-Tetrakis(*t*-butyl)-25-allyl-26,27,28-tripropyl-calix[4]arene (0.16 g, 0.2 mmol) followed by sequentially vacuuming and refilling with argon for three times. Then dichloromethane (2 mL) was added via syringe. The mixture was sonicated in a sonication bath for 30 min, followed by stirring at 40 °C for 48 h. The reaction mixture was then diluted with acetone and centrifuged at 14,500 rpm for 15 min. The supernatant was discarded and the residue was dispersed in acetone for 3 min using an ultrasonic bath. The mixture was centrifuged and the supernatant was discarded. The same sequence was repeated five times with acetone. The calix-MWCNTs **7** were dried under vacuum overnight. See Figure 4.4 for FT-IR spectra, Figure 4.5 for XPS spectra, Figure 4.6 for TGA weight loss curve, and Figure 4.7 for SEM image.

Synthesis of Crown-MWCNTs 8.

To a 10 mL Schlenk flash was added allyl-MWCNTs **2** (10 mg), Grubbs second generation ruthenium catalyst (8 mg, 0.01 mmol) and 4-acryloylamidobenzo-15-crown-5 (0.14 g, 0.4 mmol) followed by sequentially vacuuming and refilling with argon for three times.

Then dichloromethane (2 mL) was added via syringe. The mixture was sonicated in a sonication bath for 30 min, followed by stirring at 40 °C for 48 h. The reaction mixture was then diluted with acetone and centrifuged at 14,500 rpm for 15 min. The supernatant was discarded and the residue was dispersed in acetone for 3 min using an ultrasonic bath. The mixture was centrifuged and the supernatant was discarded. The same sequence was repeated five times with acetone. The crown-MWCNTs **8** were dried under vacuum overnight. See Figure 4.4 for FT-IR spectra, Figure 4.5 for XPS spectra, Figure 4.6 for TGA weight loss curve, and Figure 4.7 for SEM image.

Synthesis of Pt-MWCNT Composite 9

To a 25 mL vial click-MWCNTs **3** (2 mg) and tetrahydrofuran (10 mL). The mixture was sonicated in a sonication bath for 30 min, yielding a stable dispersion. To another vial was added potassium trichloro(ethene)palatinate (II) monohydrate (2 mg, 0.005 mmol) dissolved in 2 mL tetrahydrofuran, then dropwisely added the propargyl-MWCNT dispersion. The mixture was stirred at room temperature for 30 min. Then a hydrazine solution in tetrahydrofuran (0.001 M, 1 mL) was added dropwisely to the mixture. The mixture was then further stirred for 3 h. The reaction mixture was then centrifuged at 14,500 rpm for 1 min. The supernatant was discarded and the residue was dispersed in tetrahydrofuran for 1 min using an ultrasonic bath. The mixture was centrifuged and the supernatant was discarded. The composite was dried under vacuum overnight. See Figure 4.13 for SEM image and Figure 4.14 for XPS spectra.

Device Fabrication.

The glass substrates were cleaned by sonication in acetone/isopropanol/water successively and followed by cleaning with oxygen plasma for 5 min. Two gold strip electrodes (50 nm thick, 2 mm spacing) were sputter-coated, and MWCNT dispersions were spin-coated on top of the gold electrodes. The devices were then annealed under vacuum at 150 °C for 5 min. The typical thickness of the MWCNT films is in the range of 30-60 nm measured with a profiler. The typical resistance for the MWCNT films is in the range of 0.2-0.5 MΩ.

Device measurement.

We investigated the sensory response by measuring the relative conductance change ($-\Delta G / G_0$) of the sensors upon exposure to the 20 VOCs (3 trials each). The current was recorded between the two electrodes under a constant bias voltage (0.05 V) from which the conductance change was calculated. Our sensor response is taken one at a time, under the same experimental conditions such as sensor exposure and refreshing time, analyte concentration, temperature, environmental humidity, *etc.*

4.12 References and Notes

(1)   Buszewski, B.; Keogonsy, M.; Ligor, T.; Amann, A. *Biomed. Chromatogr.* **2007**, *21*, 553-566.

(2)   O'Neill, H. J.; Gordon, S. M.; O'Neill, M. H.; Gibbons, R. D.; Szidon, J. P. *Clin. Chem* **1988**, *34*, 1613-1618.

(3)   Phillips, M.; Gleeson, K.; Hughes, J. M. B.; Greenberg, J.; Cataneo, R. N.; Baker, L.; McVay, W. P. *Lancet* **1999**, *353*, 1930-1933.

(4)   Deng, C.; Zhang, J.; Yu, X.; Zhang, W.; Zhang, X. *J. Chromatogr. B* **2004**, *810*, 269-275.

(5)   Miekisch, W.; Schubert, J. K.; Noeldge-Schomburg, G. F. E. *Clin. Chim. Acta* **2004**, *347*, 25-39.

(6)   Stone, B.; Besse, T.; Duane, W.; Dean Evans, C.; DeMaster, E. *Lipids* **1993**, *28*, 705-708.

(7)   Di Francesco, F.; Fuoco, R.; Trivella, M.; Ceccarini, A. *Microchem. J.* **2005**, *79*, 405-410.

(8)   Libardoni, M.; Stevens, P.; Waite, J. H.; Sacks, R. *J. Chromatogr. B* **2006**, *842*, 13-21.

(9)   Amann, A.; Smith, D. *Breath Analysis for Clinical Diagnosis And Therapeutic Monitoring*; World Scientific Publishing Company, 2005.

(10)   Allen, B. L.; Kichambare, P.; Star, A. *Adv. Mater.* **2007**, *19*, 1439-1451.

(11)   Kauffman, D. R.; Star, A. *Angew. Chem. Int. Ed.* **2008**, *47*, 6550-6570.

(12)   Kim, S. N.; Rusling, J.; Papadimitrakopoulos, F. *Adv. Mater.* **2007**, *19*, 3214-3228.

(13)   Snow, E. S.; Perkins, F. K.; Robinson, J. A. *Chem. Soc. Rev.* **2006**, *35*, 790-798.

(14)   Peng, G.; Trock, E.; Haick, H. *Nano Lett.* **2008**, *8*, 3631-3635.

(15)   Peng, G.; Tisch, U.; Haick, H. *Nano Lett.* **2009**, *9*, 1362-1368.

(16)   Star, A.; Han, T.; Joshi, V.; Gabriel, J.; Grüner, G. *Adv. Mater.* **2004**, *16*, 2049-2052.

(17)   Someya, T.; Small, J.; Kim, P.; Nuckolls, C.; Yardley, J. T. *Nano Lett.* **2003**, *3*, 877-881.

(18) Zhang, W.; Swager, T. M. *J. Am. Chem. Soc.* **2007**, *129*, 7714-7715.

(19) Zhang, W.; Sprafke, J. K.; Ma, M.; Tsui, E. Y.; Sydlik, S. A.; Rutledge, G. C.; Swager, T. M. *J. Am. Chem. Soc.* **2009**, *131*, 8446-8454.

(20) Albert, K. J.; Lewis, N. S.; Schauer, C. L.; Sotzing, G. A.; Stitzel, S. E.; Vaid, T. P.; Walt, D. R. *Chem. Rev.* **2000**, *100*, 2595-2626.

(21) Lim, S. H.; Feng, L.; Kemling, J. W.; Musto, C. J.; Suslick, K. S. *Nat. Chem.* **2009**, *1*, 562-567.

(22) Balasubramanian, K.; Burghard, M. *Small* **2005**, *1*, 180-192.

(23) Kim, W.; Javey, A.; Vermesh, O.; Wang, Q.; Li, Y.; Dai, H. *Nano Lett.* **2003**, *3*, 193-198.

(24) Zahab, A.; Spina, L.; Poncharal, P.; Marli□re, C. *Phys. Rev. B* **2000**, *62*, 10000.

(25) Grate, J. W. *Chem. Rev.* **2000**, *100*, 2627-2648.

(26) Kolb, H. C.; Finn, M. G.; Sharpless, K. B. *Angew. Chem. Int. Ed.* **2001**, *40*, 2004-2021.

(27) Dondoni, A. *Angew. Chem. Int. Ed.* **2008**, *47*, 8995-8997.

(28) Chatterjee, A. K.; Choi, T.; Sanders, D. P.; Grubbs, R. H. *J. Am. Chem. Soc.* **2003**, *125*, 11360-11370.

(29) Trnka, T. M.; Grubbs, R. H. *Acc. Chem. Res.* **2001**, *34*, 18-29.

(30) Osswald, S.; Havel, M.; Gogotsi, Y. *J. Raman Spectrosc.* **2007**, *38*, 728-736.

(31) Amer, M. *Raman Spectroscopy, Fullerenes and Nanotechnology*; Royal Society of Chemistry, 2010.

(32) Crews, P.; Jaspars, M.; Rodríguez, J. *Organic Structure Analysis*; Oxford University Press, 2009.

(33) Lee, C. Y.; Strano, M. S. *Langmuir* **2005**, *21*, 5192-5196.

(34) Jurs, P. C.; Bakken, G. A.; McClelland, H. E. *Chem. Rev.* **2000**, *100*, 2649-2678.

(35) Suijkerbuijk, B. M. J. M.; Aerts, B. N. H.; Dijkstra, H. P.; Lutz, M.; Spek, A. L.; Koten, G. V.; Gebbink, R. J. M. K. *Dalton Trans.* **2007**, 1273-1276.

(36) Härelind Ingelsten, H.; Béziat, J.; Bergkvist, K.; Palmqvist, A.; Skoglundh, M.; Qiuhong, H.; Falk, L. K. L.; Holmberg, K. *Langmuir* **2002**, *18*, 1811-1818.

(37) Damle, C.; Biswas, K.; Sastry, M. *Langmuir* **2001**, *17*, 7156-7159.

(38) Murthi, V. S.; Urian, R. C.; Mukerjee, S. *J. Phys. Chem. B* **2004**, *108*, 11011-11023.

Chapter 5

Hydrogen Bonding-Based Interfacial Engineering

in Polythiophene / PCBM Hybrid Materials

5.1 Introduction

Organic electronics[1] have attracted a tremendous amount of interest over the past few decades. Compared to traditional metal-based and silicon-based electronics, the cost of organic electronics is much lower, and the fabrication process is largely simplified. Another distinct advantage of the organic-based devices is their ultra-thin and flexible nature. Typical organic electronic devices include organic light-emitting diodes (OLEDs),[2,3] thin film transistors (TFTs),[4] and organic photovoltaics (OPVs).[5,6] Since they are generally composed of one or more organic layers sandwiched between metal or oxide electrodes, the properties of the metal-organic[7] and the organic-organic interfaces[8] are critical to charge transport[9] and to charge carrier dissociation/recombination processes.[10] However, these complicated interfacial behaviors are not yet fully understood, even though much work has been done.

In the previous chapters, we have demonstrated that molecular interactions, including hydrogen bonding, host-guest chemistry, and solvation interactions, can significantly improve the performance of resistance-based chemical sensors. We are interested in learning how these molecular interactions can affect the performance of organic electronics.

We are interested in polythiophenes, whose synthesis,[11] structure, and electronic properties[12,13] have been extensively investigated. Organic photovoltaic devices based on polythiophenes have been extensively explored, and the most widely studied donor-acceptor pair is poly(3-hexylthiophene) (P3HT) and phenyl-C61-butyric acid methyl ester (PCBM) (Scheme 5.1).[14-16]

P3HT   **PCBM**
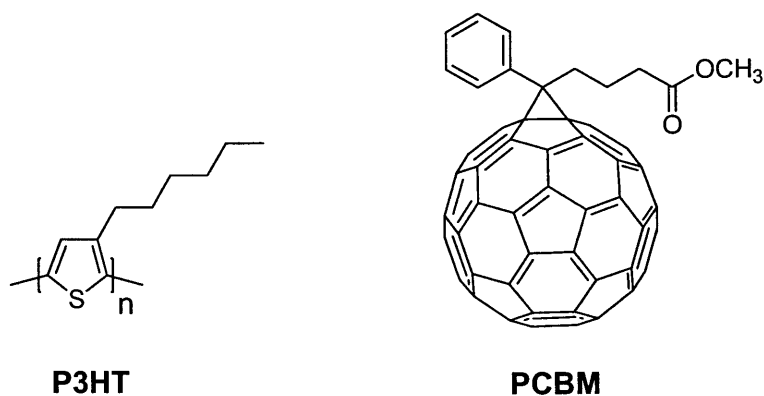
Scheme 5.1. Structures of P3HT and PCBM.

In this chapter, we synthesized several hexafluoroisopropanol (HFIP)-containing polythiophenes, and utilized them to study the effect of hydrogen bonding on charge transfer processes and morphological phenomena. The fluorescence quenching interactions between these polymers and PCBM indicated that the hydrogen bonding can facilitate the charge transfer processes from the polymers to PCBM. The XRD data of the polymers and their mixtures with PCBM demonstrated that the HFIP substitution prevented clean phase separation between the polythiophene and the PCBM.

5.2 Synthesis of Monomers

The polymers of interest are the HFIP-functionalized polythiophenes. As discussed in previous chapters, the HFIP group has very strong hydrogen bond acidity[17,18] and tends to interact strongly with PCBM. Scheme 5.2 summarizes the structures of the monomers used in this chapter. In monomer **1**, the HFIP group was directly connected to the thiophene, while in monomer **2** the HFIP group was connected to the thiophene via a C6 chain. In order to achieve

high solubility of the polymers in organic solvents, copolymers with 3-hexylthiophene **3** were made.
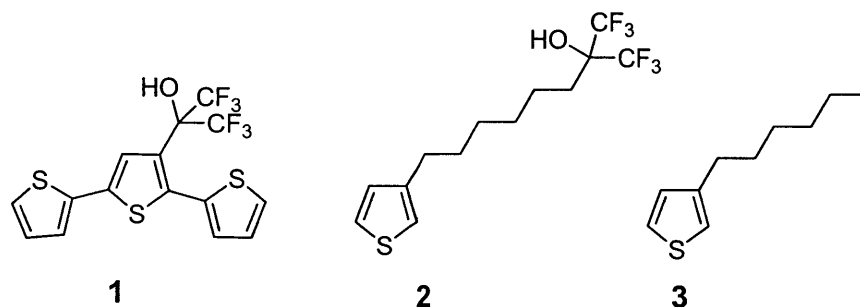
Scheme 5.2. Structures of monomers.

The synthesis of monomer **2** is summarized in Scheme 5.3. 5-bromo-1-pentene **4** readily reacted with magnesium to yield corresponding Grignard compound. The intermediate then underwent nickel catalyzed Grignard coupling with 3-bromothiophene in the presence of 0.1 mol % [1,3-bis(diphenylphosphino)propane]Ni(II) chloride (NiDPPPCl$_2$) as catalyst in refluxing ether, leading to the 3-(4-pentenyl)thiophene **5.** Olefin cross-metathesis between precursor **5** and a HFIP substituted terminal olefin with Grubbs' second generation ruthenium catalyst,[19,20] and subsequent reduction with H$_2$/Pd proceeded to give monomer **2**, with a pendant HFIP group, in good yield (65 %). The synthesis of monomer **1** was discussed in Chapter 1 and monomer **3** is commercially available.
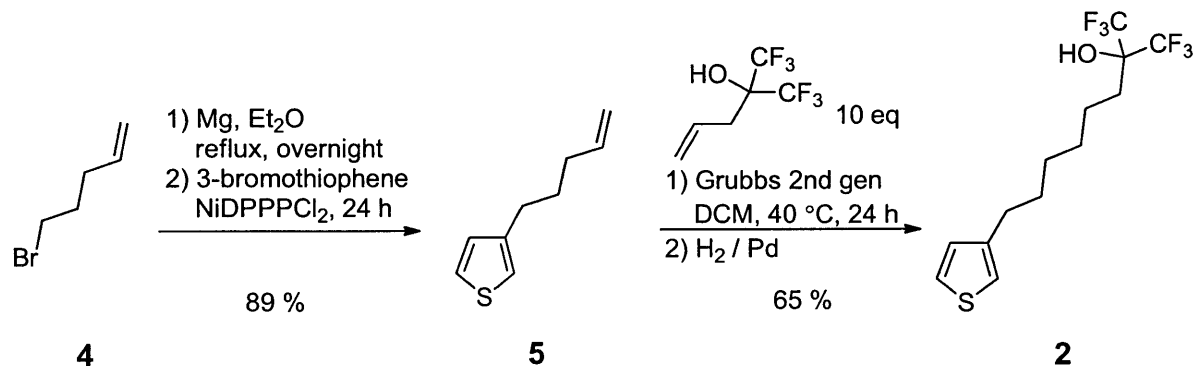
Scheme 5.3. Synthesis of monomer **2**.

5.3 Synthesis of Polymers

The synthesis of copolymer **P1** is summarized in Scheme 5.4. We used anhydrous chloroform and 4 equivalents of the iron chloride catalyst to maintain maximum catalytic activity during the polymer synthesis. In order to achieve high molecular weights, we fractionated the polymer by sequentially precipitating it in solvent mixtures containing increasing amounts of a 'good' solvent, *i.e.* hexane, hexane/ethyl acetate (16:1) and hexane/ethyl acetate (6:1). In this way, we produced a random co-polymer of HFIP monomer **1** and 3-hexylthiophene monomer **3** of number average molecular weights as high as 109,700. Using a similar method, we synthesized a random co-polymer of HFIP monomer **2** and 3-hexylthiophene monomer **3** to study the effect of the position of the HFIP group (Scheme 5.5). In this case, we were able to produce polymers with a number average molecular weight of 76,000.
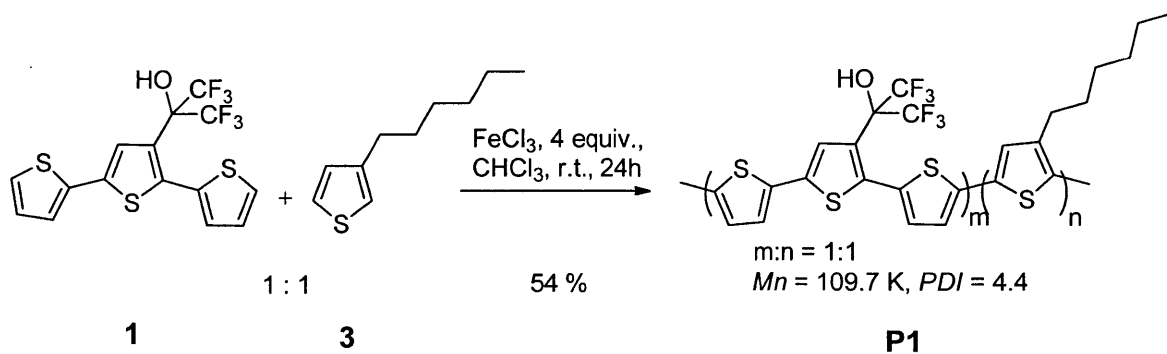
Scheme 5.4. Synthesis of polymer **P1**.
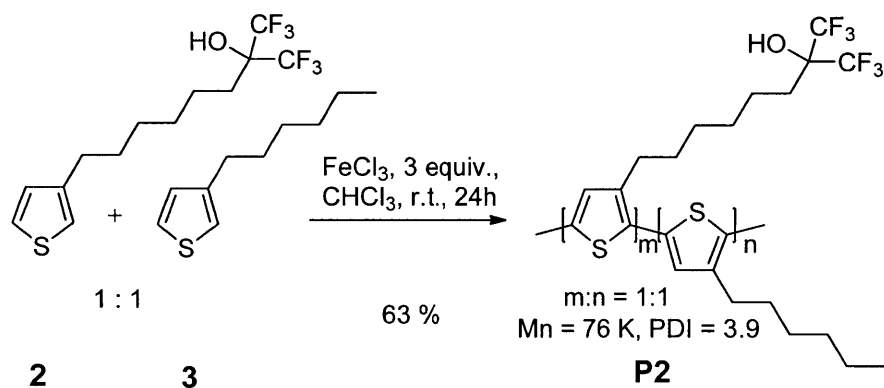
Scheme 5.5. Synthesis of polymer **P2**.

5.4 Photophysical Characterizations

The photophysical properties of **P1** and **P2** were characterized and the results are summarized in Figure 5.1 and Table 5.1. The data of P3HT are also listed for comparison. From the data, we find that the presence of the functionalized HFIP groups results in no major perturbation to the photophysical properties of the polythiophenes, including the shape of the

absorption and emission spectra, extinction coefficients, quantum yields and fluorescence lifetimes. The only change is the blue-shifted absorption and emission maxima of polymers **P1** and **P2** compared to P3HT. This effect may be attributed to the electron-withdrawing properties of the HFIP functional group that increases the band gap of the conjugated system. Given the fact that the molecular weight of **P1** and **P2** are significantly larger than that of P3HT, the blue shift may be also attributed to the regio-random structures of **P1** and **P2** that might cause a minor twist to the conjugated back bones of polythiophenes.

Table 5.1. Photophysical Data of Polymers **P1**, **P2** and P3HT.[a]

Polymers	M_n (PDI)	Absorption maxima (nm)	Emission maxima (nm)	Extinction coefficients[b] ($10^3 M^{-1}cm^{-1}$)	Quantum yield[c]	Lifetime (ns)
P1	109 (4.4)	430	558	5.4	31 %	0.60
P2	76 (3.9)	434	558	5.2	35 %	0.58
P3HT	24 (1.5)	451	571	5.3	33 %	0.66

[a] The absorption and emission spectra, extinction coefficients, quantum yields and lifetimes were all measured in anhydrous toluene solution. [b] Extinction coefficients were calculated based on each thiophene ring on the polymer backbone as a monomer. [c] Fluorescence quantum yields were achieved by comparison with fluorescein in 0.1 N NaOH as a standard.
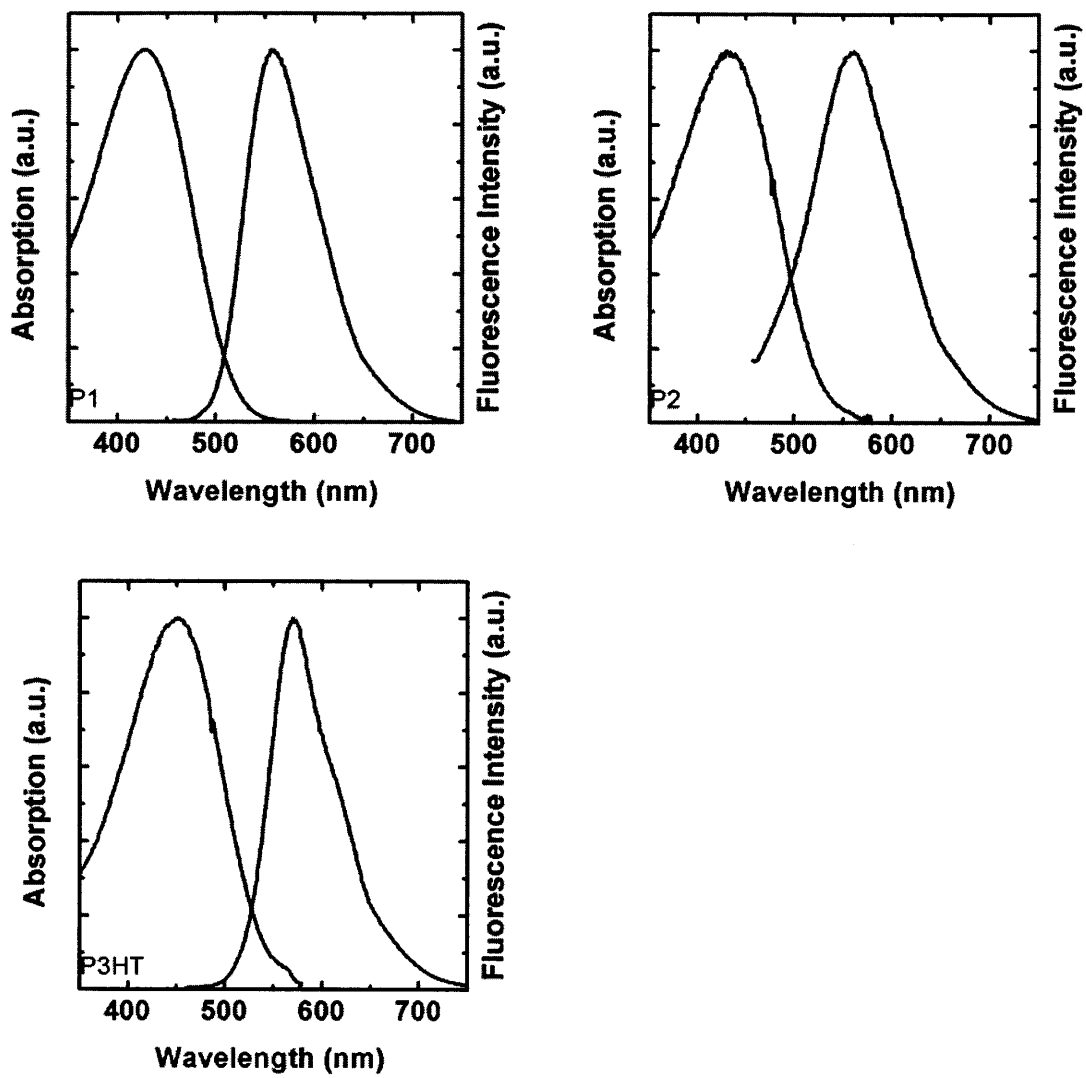
Figure 5.1. Absorption and fluorescence spectra of **P1** (top left), **P2** (top right) and **P3HT** (bottom right) in anhydrous toluene.

5.5 Solution Fluorescence Quenching Studies

Herein we explored the fluorescence quenching of the polymers in dilute solution to understand the interaction between the functionalized polythiophenes and PCBM on a molecular level. Anhydrous toluene was used as the solvent, and was bubbled with argon for 30 min before use.

The fluorescence quenching properties were investigated by measuring the fluorescence intensity changes of the polymer solutions with the addition of PCBM. PCBM was dissolved in a polymer solution with the same concentration as the initial solution, so that the polymer concentration remained constant throughout the experiment. Figure 5.2 shows typical fluorescence spectra of P1 with the addition of increasing amount of PCBM. Similar data were obtained for **P2** and P3HT. No new emission bands were observed with these three polymers during the quenching studies.

Figure 5.2. Fluorescence of **P1** solution $(1.2 \times 10^{-5}\,M)$ quenched by PCBM. [PCBM] $= 0 -$ $7.7 \times 10^{-5}\,M$ (from top to bottom).

Representative UV-Vis absorption spectra of the polymer **P1**, PCBM and the mixed solution are shown in Figure 5.3. Apparently, there is a competitive absorption of PCBM at the excitation and emission wavelengths of **P1**. To account for this effect, the measured fluorescence was corrected by equation (1).[21]
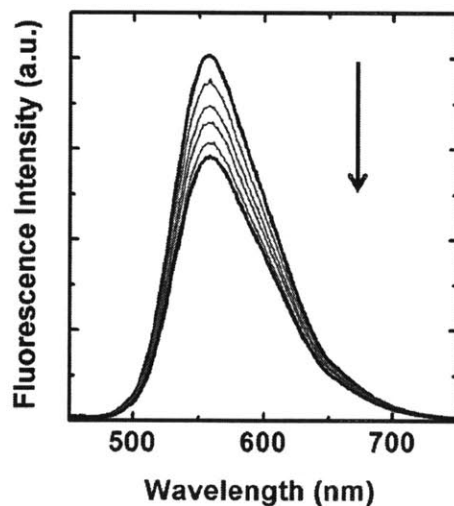
$$F = F_{em} \times \frac{1-e^{-\varepsilon_1 C_1 l}}{\varepsilon_1 C_1 l} \times \frac{\varepsilon_1 C_1 l + \varepsilon_2 C_2 l}{1-e^{-(\varepsilon_1 C_1 + \varepsilon_2 C_2)l}} \times \frac{\varepsilon_3 C_2 l}{1-e^{-\varepsilon_3 C_2 l}} \qquad (1)$$

In this equation, F_{em} denotes the experimental fluorescence intensity, F demotes the corrected fluorescence intensity, C_1 is the molar concentration of polythiophene, C_2 is the molar concentrations of PCBM, ε_1 is the molar extinction coefficient of a polythiophene at its excitation wavelength (451 nm for P3HT), ε_2 is the molar extinction coefficient of PCBM at the excitation wavelength of the polymer (451 nm for P3HT), ε_3 is the molar extinction coefficient of PCBM at the emission maxima of the polymer (471 nm for P3HT), and l is the thickness of the cell.

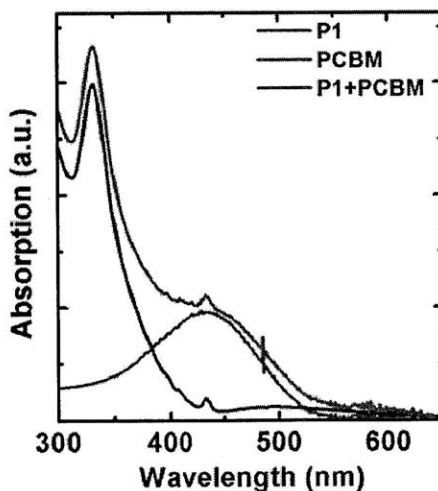**Figure 5.3.** Absorption spectra of toluene solutions of **P1** (1.2×10^{-5} M, blue), PCBM (1.7×10^{-5} M, black) and **P1** (1.2×10^{-5} M, blue) / PCBM (1.7×10^{-5} M, black) mixture.

Figure 5.4 shows the relative changes of the corrected fluorescence intensities of **P1** as a function of PCBM concentration. The change in the lifetime of **P1** is shown in red. Both the relative fluorescence intensity change and the lifetime changes have a linear relationship with the PCBM concentration. The fact that the fluorescence intensity and lifetime have different slopes indicates that the quenching process is a combined process of dynamic quenching and static quenching.[22] Since dynamic quenching is due to diffusive collisions between the photoluminescence emitter and the quencher, the lifetime will change in the same fashion as the fluorescence intensity. In contrast, since static quenching occurs through the formation of a ground state complex, the lifetime of the polymer is not affected.
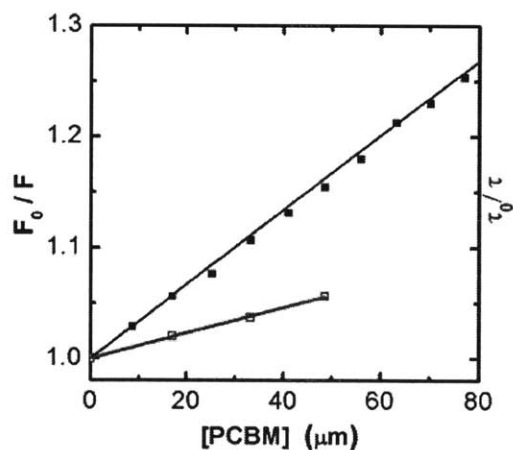

Figure 5.4. Stern-Volmer plots of P1 in anhydrous toluene in response to PCBM: F_0/F (black solid square), τ_0/τ (red hollow square), fitting of experimental data to equations (3) and (4) with K_D and Ks determined to be $1.2 \times 10^3 \, M^{-1}$ and $2.2 \times 10^3 \, M^{-1}$, respectively.

The quenching effect can be quantitatively described by Stern-Volmer equation (2).[22]

$$\frac{F_0}{F} = (1 + K_D[Q])(1 + K_S[Q])$$ (2)

In this equation, F_0 and F are the fluorescence intensities in the absence and presence of quencher Q, respectively. K_D is the dynamic quenching constant, K_S is the static quenching constant and [Q] is the quencher concentration. At low quencher concentrations, equation (2) can be simplified into a linear equation (3).

$$\frac{F_0}{F} = 1 + (K_D + K_S)[Q]$$ (3)

The value for $(K_D + K_S)$ can be obtained as the slope of the Stern-Volmer plot, while the dynamic quenching constant K_D can be determined by lifetime measurements:

$$\frac{\tau_0}{\tau} = K_D[Q]$$ (4)

where τ_0 and τ are the lifetime of polymers in the absence and presence of quencher Q, respectively.

By fitting the quenching data of **P1** with equations (3) and (4), K_D and K_S were determined to be $1.2 \times 10^3 \ M^{-1}$ and $2.2 \times 10^3 \ M^{-1}$, respectively. Large dynamic quenching constants have also been observed with a poly(phenylvinylene) quenched by PCBM,[23] and can be explained based on the efficient exciton diffusion that occurs in conjugated polmers.[24] Given the hydrogen bonding acidity of the HFIP group, the large value of static quenching constant can be attributed to the closely associated hydrogen bond complex between the HFIP functionalized **P1** and the PCBM. The enhancement of fluorescence quenching, induced by specific chemical bindings, has been conceptualized as a "molecular wire" effect, which finds widespread applications in fluorescence based chemical sensing.[25,26]

Interestingly, the same quenching experiment of **P1** was repeated using 1% tetrahydrofuran in anhydrous toluene as a solvent, and remarkably different results were obtained (Figure 5.5). We observed a comparable K_D value ($1.3 \times 10^3 \, M^{-1}$) but a largely decreased Ks value ($1.2 \times 10^3 \, M^{-1}$). The decrease in static quenching constant can be attributed to the fact that tetrahydrofuran, a very strong hydrogen bond acceptor, binds strongly with the HFIP group and hinders the formation of a complex between HFIP and PCBM.
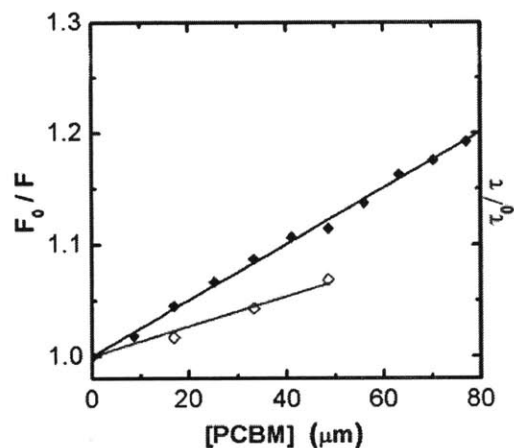
Figure 5.5. Stern-Volmer plots of **P1** in anhydrous toluene in response to PCBM: F_0/F (black solid diamond), τ_0/τ (red hollow diamond), fitting of experimental data to equations (3) and (4) with K_D and Ks determined to be $1.3 \times 10^3 \, M^{-1}$ and $1.2 \times 10^3 \, M^{-1}$, respectively.

Quenching experiments with **P2** and P3HT were performed both in anhydrous toluene and in 1% tetrahydrofuran/toluene solvents, and the results are summarized in Figures 5.6-5.7 and Table 5.2. Similar to **P1**, the presence of tetrahydrofuran decreased the static quenching constant of **P2**, but did not influence the quenching behavior of the P3HT-PCBM system. The

fact that P3HT experiments yielded almost the same the slope for fluorescence changes and lifetime changes indicates that the quenching of P3HT is dynamic in nature.

Figure 5.6. Stern-Volmer plots of **P2** in anhydrous toluene (left) and in 1% tetrahydrofuran/toluene (right) in response to PCBM: F_0/F (black labels), τ_0/τ (red labels).

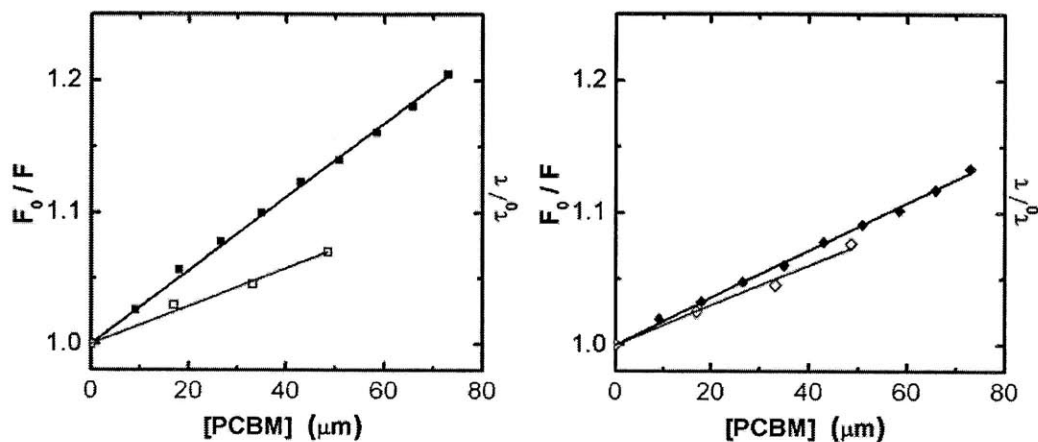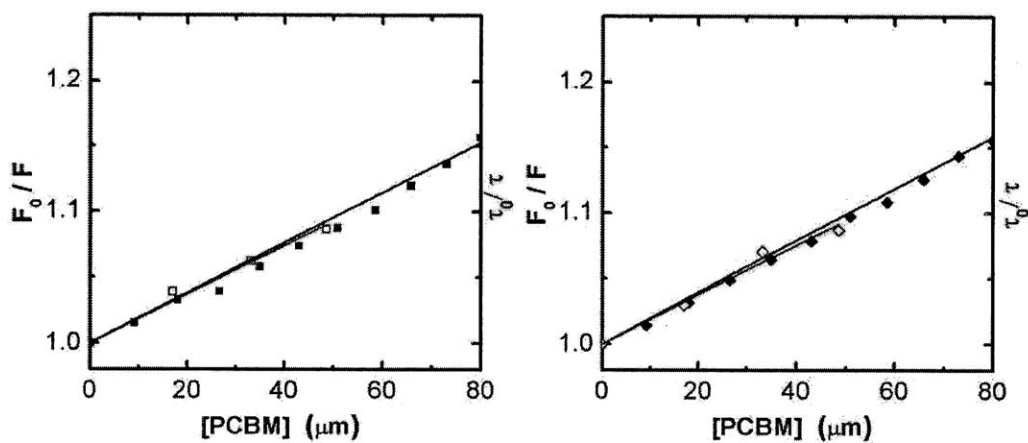

Figure 5.7. Stern-Volmer plots of P3HT in anhydrous toluene (left) and in 1% tetrahydrofuran/toluene (right) in response to PCBM: F_0/F (black labels), τ_0/τ (red labels).

Table 5.2. Quenching Constant Data of polymers **P1**, **P2** and P3HT.[a]

Polymers	In Anhydrous Toluene			In 1% Tetrahydrofuran/Toluene		
	$K_S + K_D$ $(10^3 M^{-1})$	K_S $(10^3 M^{-1})$	K_D $(10^3 M^{-1})$	$K_S + K_D$ $(10^3 M^{-1})$	K_S $(10^3 M^{-1})$	K_D $(10^3 M^{-1})$
P1	3.4	2.2	1.2	2.4	0.9	1.5
P2	2.8	1.4	1.4	1.8	0.3	1.5
P3HT	1.9	0	1.9	1.9	0	1.9

[a] All dynamic quenching constants were determined by fitting the experimental data of the lifetime changes to equation (4). All static quenching constants were determined by fitting the experimental data of the fluorescence intensity changes to equation (3) and by subtracting the dynamic quenching constants.

As shown in Table 5.2, the HFIP functionalized polythiophenes generally have smaller dynamic quenching constants than P3HT. Considering the electron-withdrawing properties of the HFIP group, it is likely that the energy levels of the HFIP-containing polymers are less favorable for charge-transfer to the PCBM than that of P3HT. Another possible reason, especially in the case of **P2** where the HFIP is not directly connected to the conjugated backbone, is that the bulky HFIP group may hinder the collisions of PCBM with the polythiophene backbone. However, these HFIP-polymers still have larger total quenching constants than P3HT in anhydrous toluene due to the contribution of hydrogen bonding-induced static quenching.

5.6 Crystallinity of the Polymers

The crystallinity of the polymers was investigated by X-ray Diffraction (XRD). Figure 5.8 shows the XRD data of P3HT after annealing in vacuum at 140° C for 1 hour. A typical lamellar structure (d_{layer} = 16.3 Å) is observed with these samples.[14] The two new sharp peaks

that appeared at 16 and 20° (2θ) in the polymer/PCBM mixtures are assigned to the PCBM

phase.
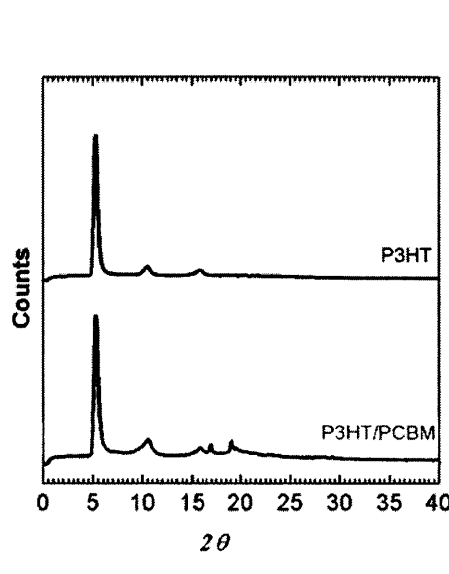
Figure 5.8. XRD patterns of P3HT in pure form and with PCBM (1:1 by weight), after

annealing in vacuum at 140 °C for 1 hour.

As shown in Figure 5.9, **P1** and **P2** have less ordered structures than region-regular

P3HT. The direct functionalization of the HFIP on the polythiophene backbone creates an

amorphous material of **P1**. **P2**, with pendant HFIP groups, has an ordered structure with a

sharp peak at d = 11.0 Å. This peak can be explained by a layered structure with

interpenetrating chains. However, this order is completely lost in the 1:1 composition with

PCBM. This suggests that the binding of the HFIP group leads to a homogenous dispersion of

the polymer and PCBM. It appears that the interaction of the HFIP group with PCBM prevents
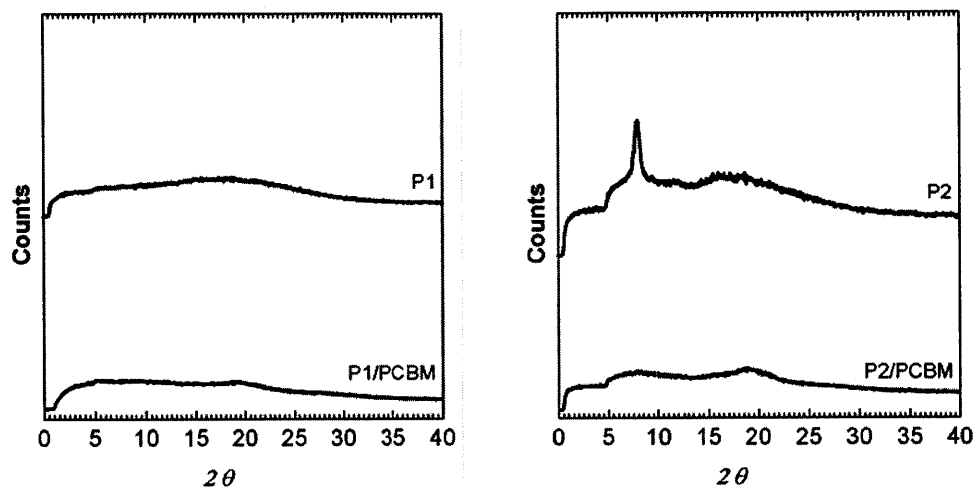
phase separation.

Figure 5.9. XRD patterns of **P1** and **P2** in pure form and with PCBM (1:1 by weight), after annealing in vacuum at 140 °C for 1 hour.

5.7 Conclusions

Several HFIP-containing polythiophenes have been designed and synthesized. Their photophysical properties and the fluorescence quenching phenomena have been systematically investigated. An interesting enhancement of the energy transfer constants was observed with these polymers, and was demonstrated to result from the strong hydrogen bonding between the HFIP group and PCBM. The XRD data of the polymers and their mixtures with PCBM demonstrated that the HFIP substitution prevents clean phase separation between the polythiophene and the PCBM. These results together proved the power of molecular interactions in changing the donor-acceptor interactions and in controlling the polymer morphology. Our future plans are to use this effect to create controlled interfaces between P3HT and PCBM by blending HFIP-containing polythiophenes with P3HT. In this way, we have the potential to control the morphology and also facilitate the charge separation processes in our systems.

5.8 Experimental Section

Materials.

All chemicals were of reagent grade from Sigma-Aldrich, Alfa Aesar or Acros and used as received. All solvents were of spectroscopic grade unless otherwise noted. Anhydrous tetrahydrofuran and toluene were obtained from J. T. Baker and purified by passing through a Glasscontour dry solvent system.

General Methods and Instrumentation.

All synthetic manipulations were carried out under an argon atmosphere using standard Schlenk techniques unless otherwise noted. Glassware was oven-baked and cooled under N_2 atmosphere. ^1H NMR spectra were recorded on a Varian Mercury-300 MHz or a Varian Unity-500 MHz instrument. Polymer molecular weights were determined by gel permeation chromatography using an HP series 1100 GPC system running at a flow rate at 1.0 mL/min in THF and a diode detector. The molecular weights are reported relative the polystyrene standards purchased from Polysciences. UV-vis spectra were recorded with an Agilent 8453 diode-array or Cary 50 UV-vis spectrophotometer, corrected for baseline with a solvent-filled cuvette. Emission spectra were acquired on a SPEX Fluorolog-τ3 fluorometer. The spectra in solution were obtained at room temperature using a quartz cuvette with a path length of 1 cm at right angle detection. The absorbance of all samples used for fluorescence studies were equal to or below 0.1. Lifetime experiments were performed using a SPEX MF^2 Multi-Frequency Fluorometer equipped with a 365 nm LED. Time decay of fluorescence was determined by a phase-modulation method, using frequencies between 10 and 250 MHz. Lifetimes were calculated relative to POPOP in ethanol, which has a lifetime of 1.35 ns. X-ray data were

collected using an Inel CPS 120 position sensitive detector using an XRG 3000 generator (Cu Kα)

Synthesis of Compound 5.

Into a 25 mL three-neck flask was added magnesium turnings (0.79 g, 33 mmol) followed by sequentially vacuuming and refilling with argon for three times. 3 mL ether was then added to the flask via syringe. 4-pentenyl bromide **4** in 10 mL ether was then added dropwisely to the reaction mixture with an addition funnel. After refluxing overnight, the reaction mixture was then transferred via cannula to a second addition funnel, and added dropwisely to a mixture of NiDPPPCl$_2$ (15 mg, 0.1 mol %) and 3-bromothiophene (2.3 mL, 25 mmol) in 10 mL ether under argon at 0 °C over 1 h. After refluxing for 24 h, the reaction mixture was cooled down to room temperature and was hydrolyzed by 10 mL 1 N HCl and 30 mL ice water. The mixture was then extracted with ether for 3 times. The combined organic phases was then washed to neutrality, and dried over MgSO$_4$. After removal of the solvent, the crude product was purified by column chromatography (hexane) to yield 3.4 g (89 %) of a colorless liquid. ^{1}H NMR (300 MHz, CD$_2$Cl$_2$): δ 7.26 (dd, 1 H, J = 3, 5), 6.97 (d, 1 H, J = 5), 6.96 (d, 1 H, J = 3), 5.85 (m, 1 H), 5.06 (m, 1 H), 5.00 (m, 1 H), 2.65 (t, 2 H, J = 7), 2.11 (m, 2 H), 1.72 (m, 2 H).

Synthesis of Compound 2.

Into a 25 mL Schlenk flask was added compound **5** (0.38 g, 2.5 mmol) and 0.01 g (0.01 mmol) of Grubbs' second generation ruthenium catalyst followed by sequentially vacuuming and refilling with argon for three times. A solution of 1,1,1-trifluoro-2-(trifluoromethyl)-pent-

4-en-2-ol (5 g, 24 mmol) in 5 mL dichloromethane was added to the flask via syringe. The reaction mixture was heated to 40 °C for 24 h. After cooling to room temperature, the solvent was removed and the crude product was separated with column chromatography (hexane : dichloromethane = 2 : 1). The compound with RF of 0.3 was collected. Removal of the solvent yielded 0.62 g of a colorless liquid. The liquid was dissolved in ethanol and then subjected hydrogenation with Pd as catalyst (0.1 g of 10% Pd on carbon) at 40 PSI overnight. The reaction mixture was filtered through of a pad of celite. After removal of the solvent, the crude product was purified with column chromatography (hexane : dichloromethane = 2 : 1) and yielded 0.54 g (65 %) of a colorless liquid. ^{1}H NMR (300 MHz, CD_2Cl_2): δ 7.25 (dd, 1 H, J = 3, 5), 6.96 (d, 1 H, J = 5), 6.94 (d, 1 H, J = 3), 2.99 (s, 1 H), 2.63 (t, 2 H, J = 7), 1.94 (t, 2 H, J = 8), 1.62 (m, 2 H), 1.42-1.26 (m, 2 H). ^{19}F NMR (282 MHz, CD_2Cl_2): δ -77.32.

Synthesis of Polymer P1

To a 25 mL round-bottom flask with anhydrous iron trichloride (0.13 g, 0.8 mmol) in chloroform (15 mL) was added monomer **1** (41 mg, 0.1 mmol) and monomer **3** (17 mg, 0.1 mmol) in a chloroform solution (1 mL). The mixture was sonicated for 2 h, and then stirred at room temperature for 24 h. It was then diluted with tetrahydrofuran (100 mL), reduced with sodium thiosulphate (0.5 g), then washed sequentially with water (100 mL), 0.1 M hydrazine aqueous solution (100 mL), water (100 mL), brine (100 mL), dried over MgSO4, filtered with a 0.2 μ m PTFE filter and evaporated to 10 mL under reduced pressure. The polymer solution was then precipitated into 60 mL of hexane. The precipitate was isolated by centrifugation and decantation of the liquid. The precipitate was dissolved in tetrahydrofuran (10 mL) and precipitated into hexane/ethyl acetate (16:1, 60 mL in total). The precipitate was isolated by

centrifugation and decantation of the liquid. The precipitate was dissolved in tetrahydrofuran (10 mL) and precipitated into hexane/ethyl acetate (6:1, 60 mL in total). The material was dried under vacuum to yield an dark-red solid (31 mg, 54 %). According to gel-permeation chromatography (with tetrahydrofuran as eluent and with polystyrene standards), polymer **P1** has a number average molecular weight (Mn) = 109.7 K and a polydispersity index (PDI) = 4.4. ^{1}H NMR (300 MHz, THF) δ: 7.69 (1 H), 7.34 (2 H), 7.25 (2 H), 7.20 (1 H), 7.09 (1 H),   2.85 (2 H), 1.77 (2 H), 1.47 (2 H), 1.35 (2 H), 0.92 (3H). ^{19}F NMR (282 MHz, THF) δ: -76.36.

Synthesis of Polymer P2

To a 50 mL round-bottom flask with anhydrous iron trichloride (0.19 g, 1.2 mmol) in chloroform (20 mL) was added monomer **2** (67 mg, 0.2 mmol) and monomer **3** (34 mg, 0.2 mmol) in a chloroform solution (2 mL). The mixture was sonicated for 2 h, and then stirred at room temperature for 24 h. It was then diluted with tetrahydrofuran (100 mL), reduced with sodium thiosulphate (0.5 g), then washed sequentially with water (100 mL), 0.1 M hydrazine aqueous solution (100 mL), water (100 mL), brine (100 mL), dried over MgSO4, filtered with a 0.2 μ m PTFE filter and evaporated to 10 mL under reduced pressure. The polymer solution was then precipitated into 60 mL of hexane. The precipitate was isolated by centrifugation and decantation of the liquid. The precipitate was dissolved in tetrahydrofuran (10 mL) and precipitated into hexane/ethyl acetate (16:1, 60 mL in total). The precipitate was isolated by centrifugation and decantation of the liquid. The precipitate was dissolved in tetrahydrofuran (10 mL) and precipitated into hexane/ethyl acetate (6:1, 60 mL in total). The material was dried under vacuum to yield a black solid (65 mg, 63 %). According to gel-permeation chromatography (with tetrahydrofuran as eluent and with polystyrene standards), polymer **P2**

has a Mn = 76 K and a PDI = 3.9. ^{1}H NMR (300 MHz, THF) δ: 6.99 (2 H), 2.97-2.42 (4 H), 1.93 (2 H), 1.80-1.62 (4 H), 1.62-1.07 (13 H), 0.91 (3H). ^{19}F NMR (282 MHz, CDCl$_3$) δ: -77.04.

5.9 References and Notes

(1)   Forrest, S. R. *Nature* **2004**, *428*, 911-918.

(2)   Burroughes, J. H.; Bradley, D. D. C.; Brown, A. R.; Marks, R. N.; Mackay, K.; Friend, R. H.; Burns, P. L.; Holmes, A. B. *Nature* **1990**, *347*, 539-541.

(3)   Friend, R. H.; Gymer, R. W.; Holmes, A. B.; Burroughes, J. H.; Marks, R. N.; Taliani, C.; Bradley, D. D. C.; Santos, D. A. D.; Bredas, J. L.; Logdlund, M.; Salaneck, W. R. *Nature* **1999**, *397*, 121-128.

(4)   Joseph Kline, R.; McGehee, M. D.; Toney, M. F. *Nat. Mater.* **2006**, *5*, 222-228.

(5)   Nelson, J. *Mater. Today* **2002**, *5*, 20-27.

(6)   Brabec, C. J.; Sariciftci, N. S.; Hummelen, J. C. *Adv. Func. Mater.* **2001**, *11*, 15-26.

(7)   Vitali, L.; Levita, G.; Ohmann, R.; Comisso, A.; De Vita, A.; Kern, K. *Nat. Mater.* **2010**, *9*, 320-323.

(8)   Matyba, P.; Maturova, K.; Kemerink, M.; Robinson, N. D.; Edman, L. *Nat. Mater.* **2009**, *8*, 672-676.

(9)   Tao, N. J. *Nat. Nano.* **2006**, *1*, 173-181.

(10)   Halls, J. J. M.; Walsh, C. A.; Greenham, N. C.; Marseglia, E. A.; Friend, R. H.; Moratti, S. C.; Holmes, A. B. *Nature* **1995**, *376*, 498-500.

(11)   Roncali, J. *Chem. Rev.* **1992**, *92*, 711-738.

(12)   Perepichka, I. F.; Perepichka, D.; Meng, H.; Wudl, F. *Adv. Mater.* **2005**, *17*, 2281-2305.

(13)   Leclerc, M.; Faid, K. *Adv. Mater.* **1997**, *9*, 1087-1094.

(14)   Kim, Y.; Cook, S.; Tuladhar, S. M.; Choulis, S. A.; Nelson, J.; Durrant, J. R.; Bradley, D. D. C.; Giles, M.; McCulloch, I.; Ha, C.; Ree, M. *Nat. Mater.* **2006**, *5*, 197-203.

(15)   Kim, Y.; Choulis, S. A.; Nelson, J.; Bradley, D. D. C.; Cook, S.; Durrant, J. R. *Appl.*

         Phys. Lett. **2005**, *86*, 063502.

(16)   Reyes-Reyes, M.; Kim, K.; Carroll, D. L. *Appl. Phys. Lett.* **2005**, *87*, 083506.

(17)   Grate, J. W. *Chem. Rev.* **2000**, *100*, 2627-2648.

(18)   Grate, J. W. *Chem. Rev.* **2008**, *108*, 726-745.

(19)   Chatterjee, A. K.; Choi, T.; Sanders, D. P.; Grubbs, R. H. *J. Am. Chem. Soc.* **2003**, *125*,

         11360-11370.

(20)   Trnka, T. M.; Grubbs, R. H. *Acc. Chem. Res.* **2001**, *34*, 18-29.

(21)   Zheng, M.; Bai, F.; Li, F.; Li, Y.; Zhu, D. *J. Appl. Polym. Sci.* **1998**, *70*, 599-603.

(22)   Lakowicz, J. R. *Principles of Fluorescence Spectroscopy*; 2nd ed.; Springer, 1999.

(23)   Wang, J.; Wang, D.; Moses, D.; Heeger, A. J. *J. Appl. Polym. Sci.* **2001**, *82*, 2553-2557.

(24)   Lin, H.; Weng, Y.; Huang, H.; He, Q.; Zheng, M.; Bai, F. *Appl. Phys. Lett.* **2004**, *84*,

         2980.

(25)   Swager, T. M. *Acc. Chem. Res.* **1998**, *31*, 201-207.

(26)   Zhou, Q.; Swager, T. M. *J. Am. Chem. Soc.* **1995**, *117*, 7017-7018.
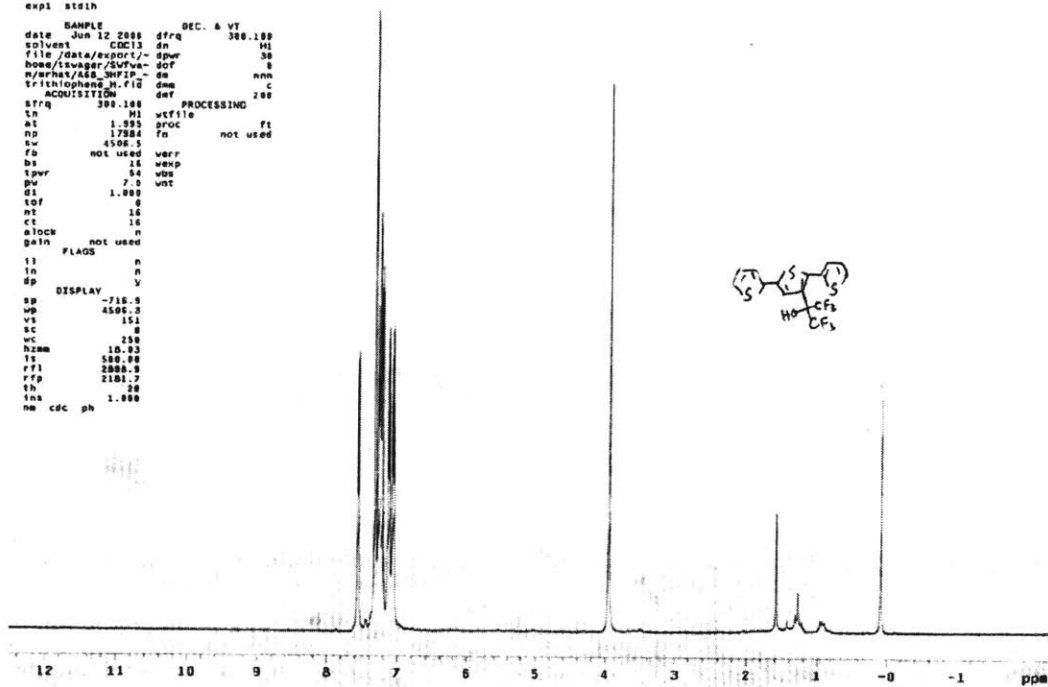
Appendix 1

NMR Spectra for Chapter 2
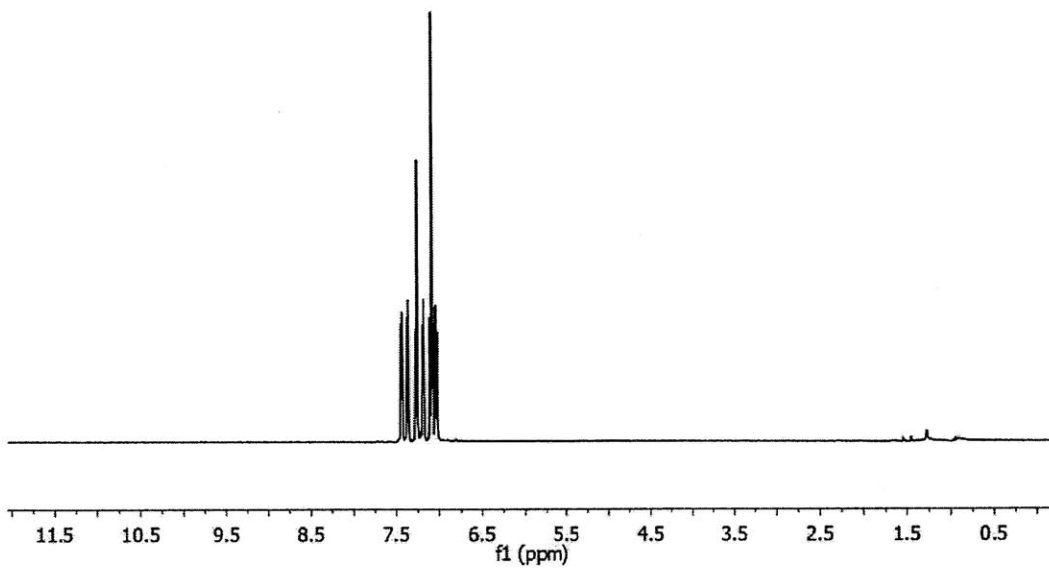
^{1}H NMR of **2** (300 MHz, CDCl$_3$)
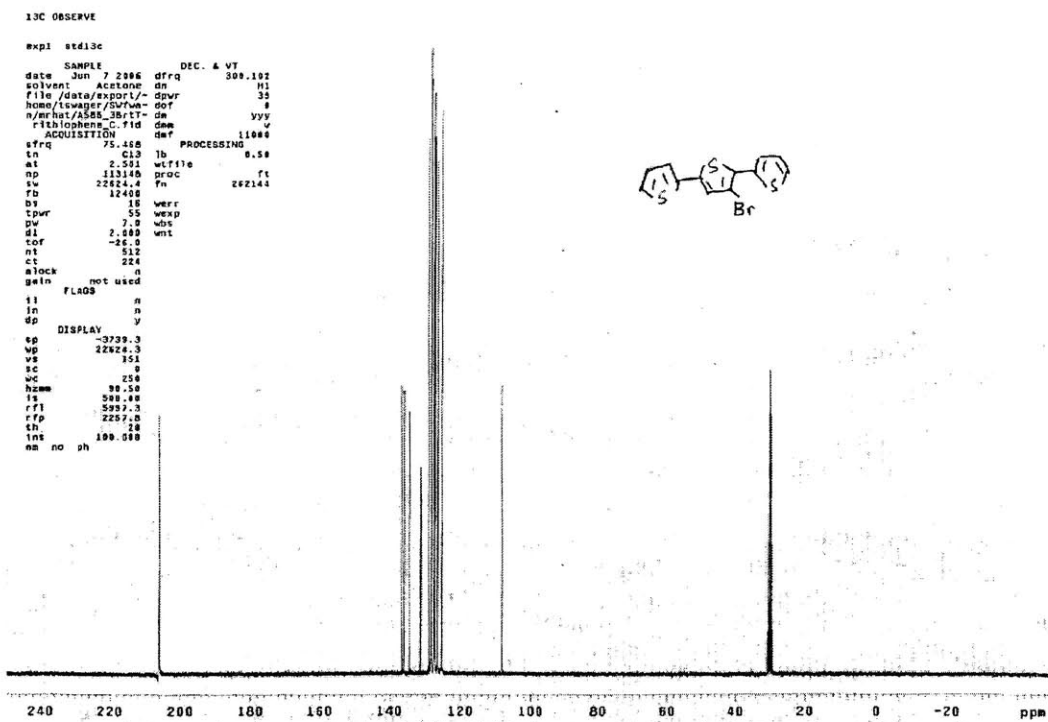
^{13}C NMR of **2** (300 MHz, Acetone)

^{1}H NMR of **3** (300 MHz, CDCl$_3$)

^{13}C NMR of **3** (300 MHz, CDCl$_3$)

19F OBSERVE
STANDARD PARAMETERS

expl s2pul
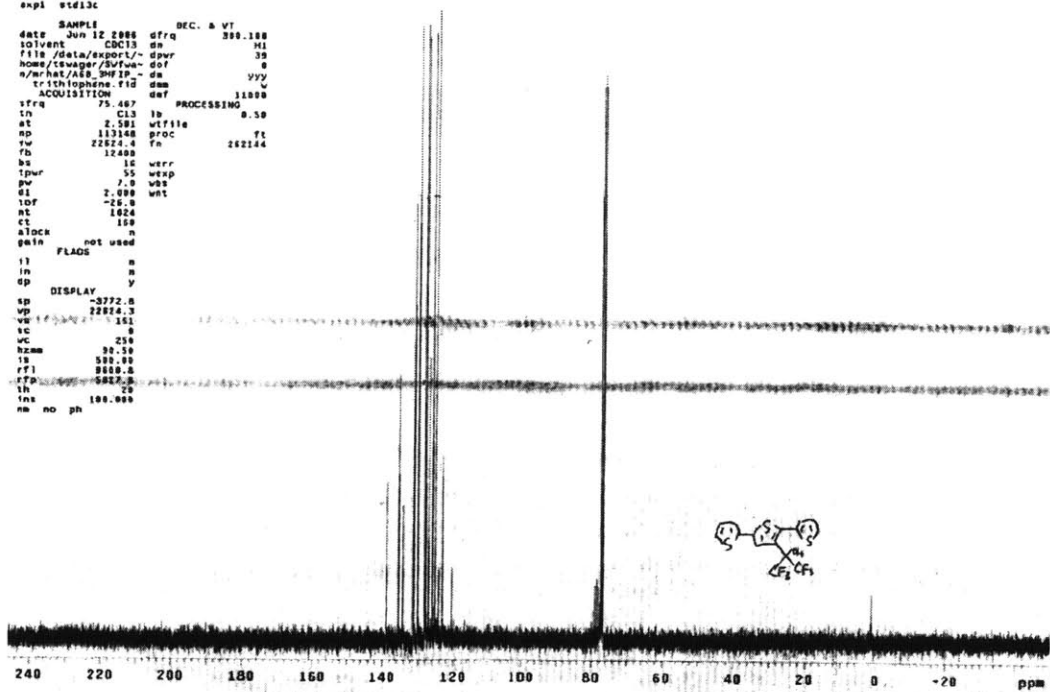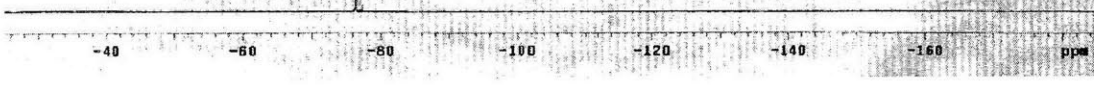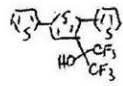   SAMPLE   DEC. & VT
date   Jun 12 2006   dfrq   300.100
solvent   CDCl3   dn   H1
file /data/export/~   dpwr   30
home/tswager/SVfwa~   dof   0
n/arhat/A&A_3HFIP_~   dm   nnn
  trithiophene.fid   dmm   c
    ACQUISITION   dmf   200
sfrq   282.346   PROCESSING
tn   F19   lb   0.30
at   0.300   wtfile
np   27230   proc   ft
sw   45454.5   fn   not used
fb   not used
bs   4   werr
tpwr   56   wexp
pw   5.8   wbs
d1   4.000   wnt
tof   0
nt   16
ct   16
alock   n
gain   0
      FLAGS
il   n
in   n
dp   y
    DISPLAY
sp   -52876.4
wp   45451.8
vs   151
sc   0
wc   250
hzmm   181.82
is   500.00
rfl   52079.2
rfp   0
th   20
ins   100.000
nm   no   ph

^{19}F NMR of **3** (282 MHz, CDCl$_3$)
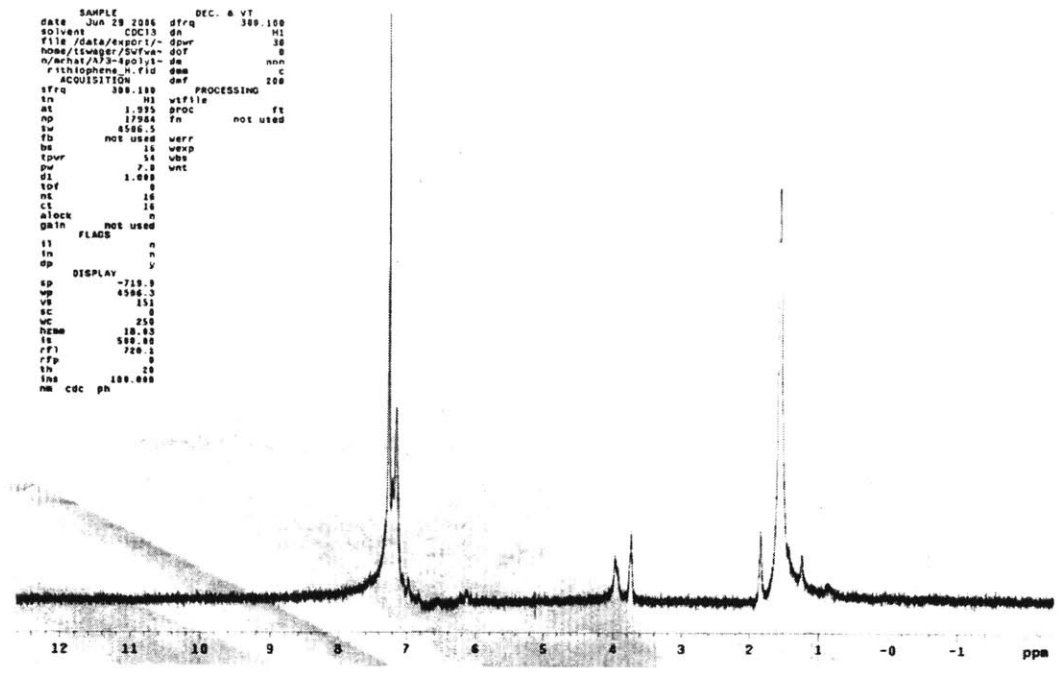
STANDARD 1H OBSERVE

exp1 std1h

        SAMPLE   DEC. & VT
date   Jun 29 2006   dfrq   300.100
solvent   CDCl3   dn   H1
file /data/export/~   dpwr   30
home/tiwager/Swfwa~   dof   0
n/mrhat/A73-4polyt~   dm   nnn
  rithiophene_H.fid   dmm   c
     ACQUISITION   dmf   200
sfrq   300.100   PROCESSING
tn   H1   wtfile
at   1.995   proc   ft
np   17984   fn   not used
sw   4506.5
fb   not used   werr
bs   16   wexp
tpwr   54   wbs
pw   7.3   wnt
d1   1.000
tof   0
nt   16
ct   16
alock   n
gain   not used
       FLAGS
il   n
in   n
dp   y
      DISPLAY
sp   -719.9
wp   4506.3
vs   151
sc   0
wc   250
hzmm   18.03
is   500.00
rfl   720.1
rfp   0
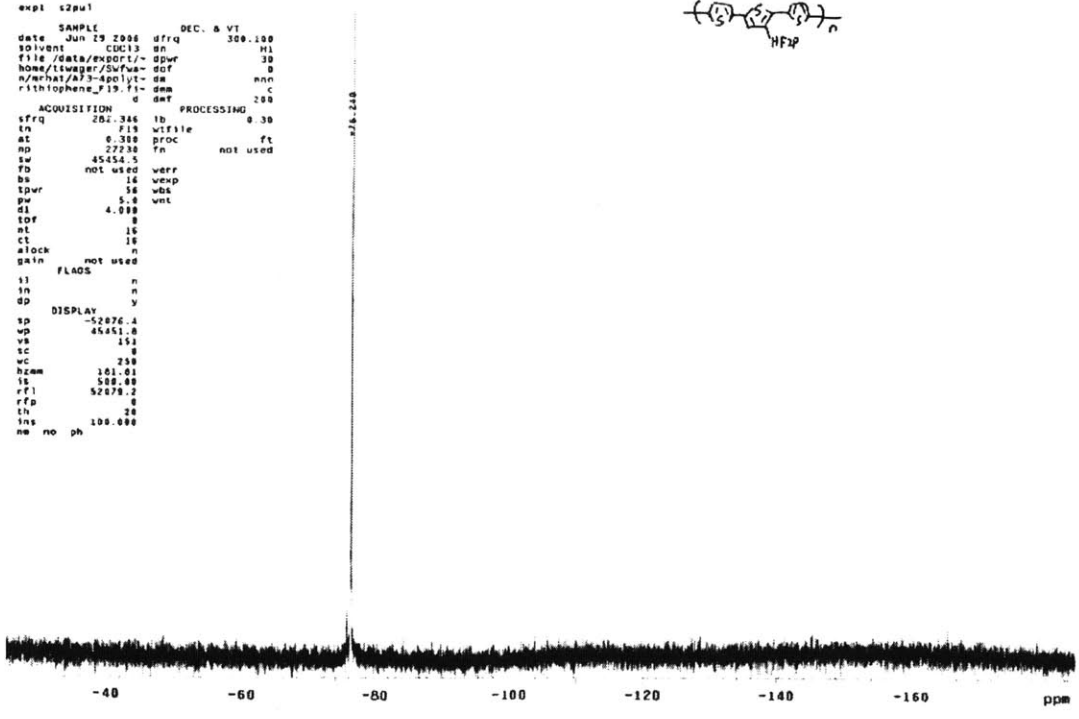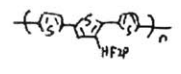th   20
ins   100.000
nm cdc ph

¹H NMR of **P1** (300 MHz, CDCl₃)

19F OBSERVE
STANDARD PARAMETERS

exp1 s2pul

        SAMPLE   DEC. & VT
date   Jun 29 2006   dfrq   300.100
solvent   CDCl3   dn   H1
file /data/export/~   dpwr   30
home/tiwager/Swfwa~   dof   0
n/mrhat/A73-4polyt~   dm   nnn
  rithiophene_F19.fi~ dmm   c
           d   dmf   200
     ACQUISITION   PROCESSING
sfrq   282.346   lb   0.30
tn   F19   wtfile
at   0.300   proc   ft
np   27230   fn   not used
sw   45454.5
fb   not used   werr
bs   16   wexp
tpwr   56   wbs
pw   5.0   wnt
d1   4.000
tof   0
nt   16
ct   16
alock   n
gain   not used
       FLAGS
il   n
in   n
dp   y
      DISPLAY
sp   -52076.4
wp   45451.8
vs   151
sc   0
wc   250
hzmm   161.81
is   500.00
rfl   52079.2
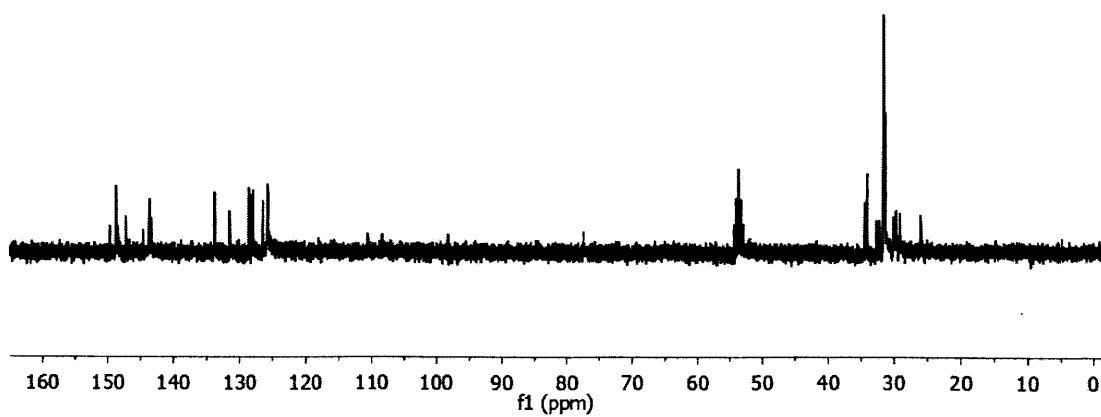rfp   0
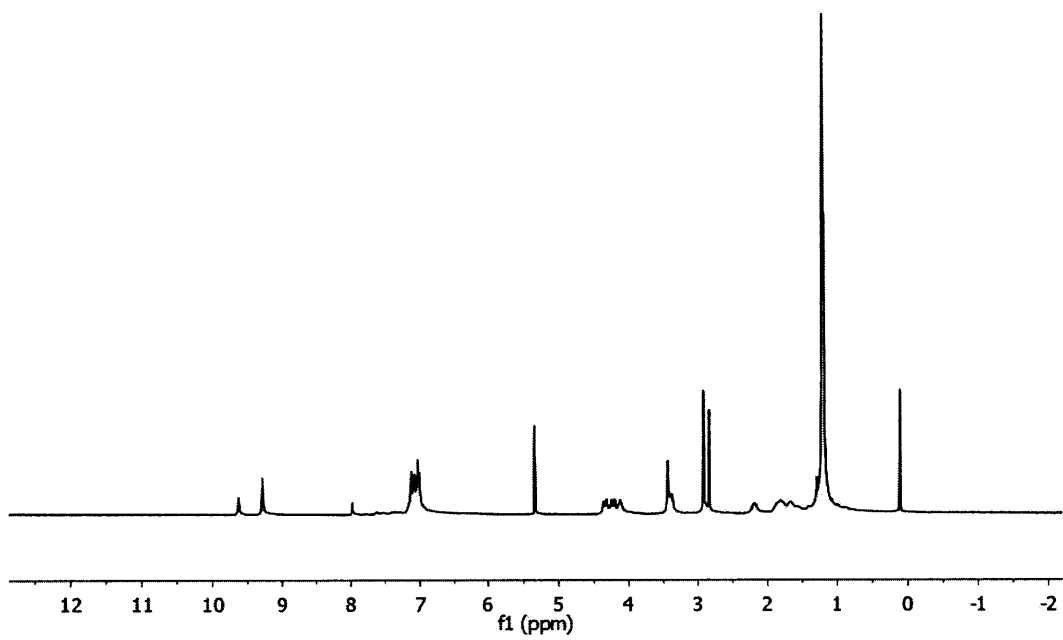th   20
ins   100.000
nm   no ph

¹⁹F NMR of **P1** (300 MHz, CDCl₃)

- 151 -

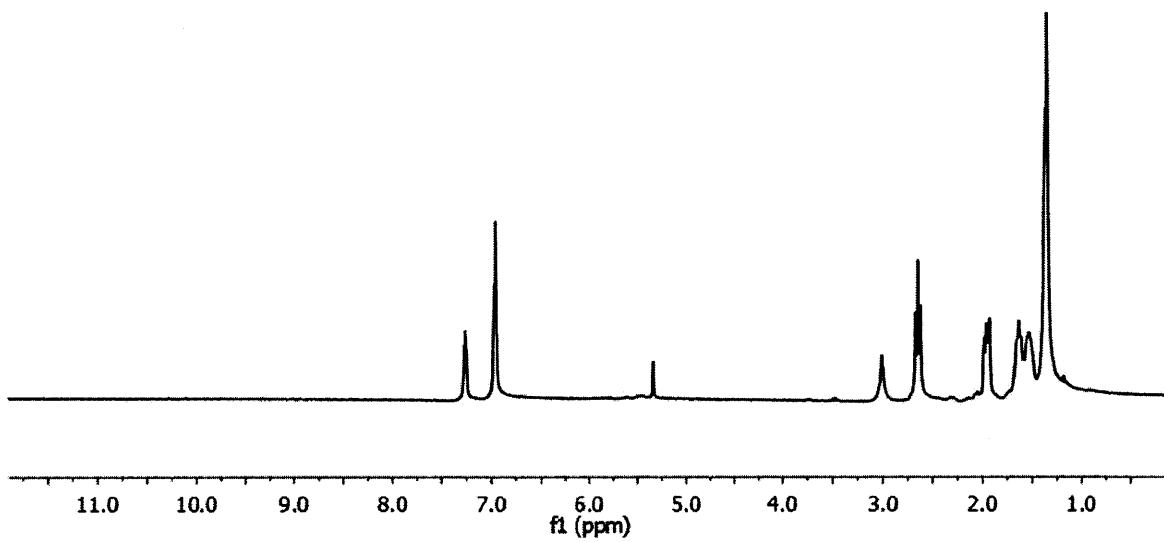# Appendix 2

NMR Spectra for Chapter 3
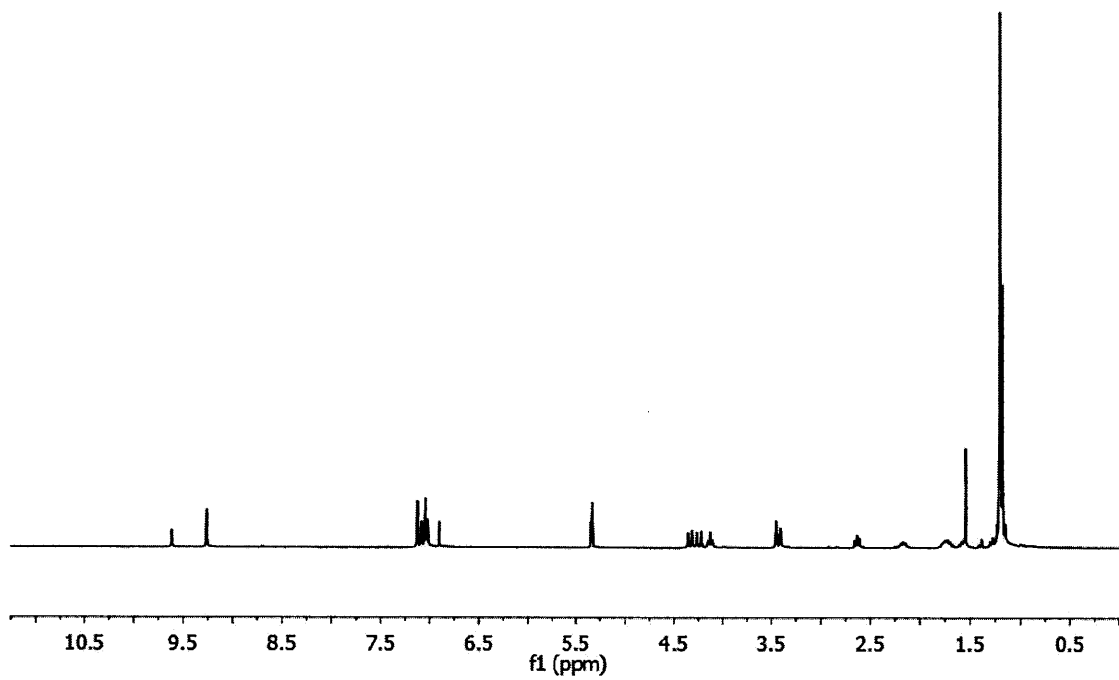
^{1}H NMR of **1** (300 MHz, CD$_2$Cl$_2$)

^{13}C NMR of **1** (300 MHz, CD$_2$Cl$_2$)
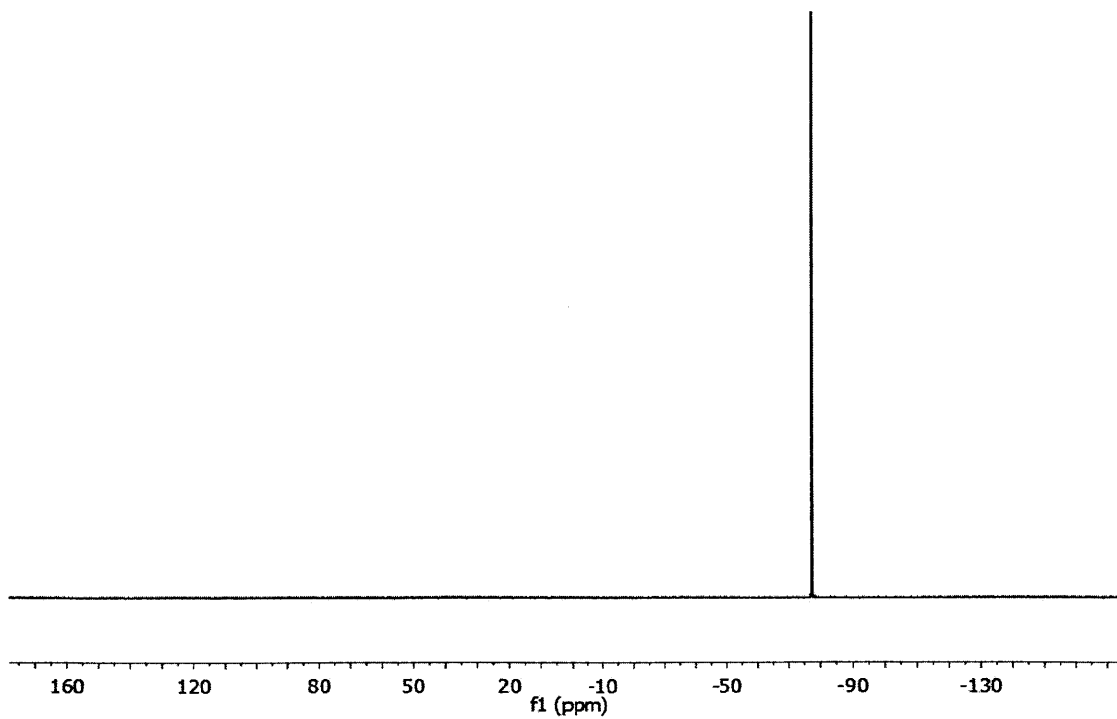
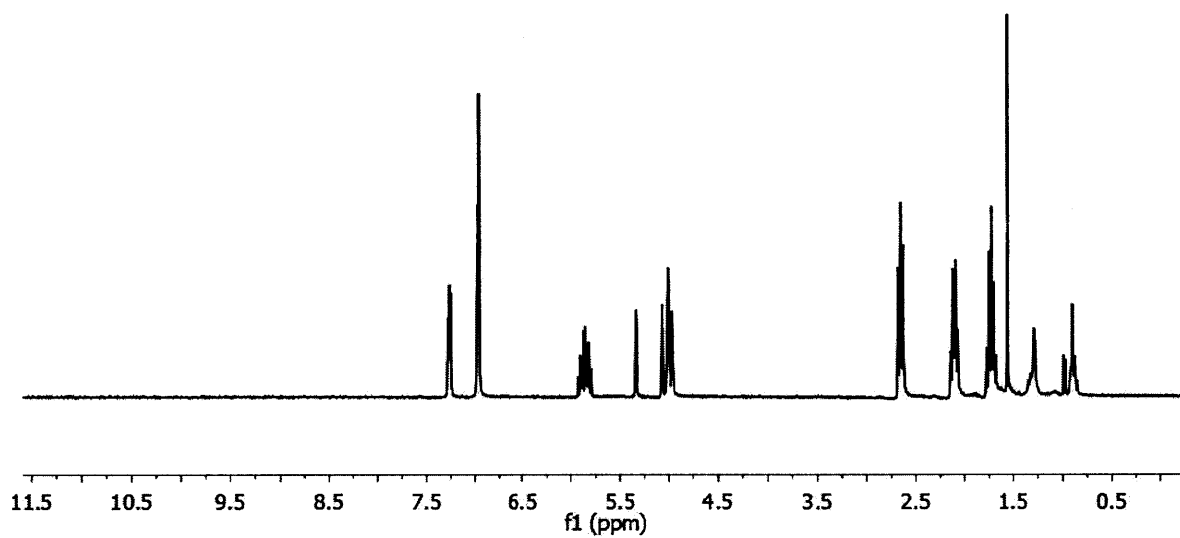^{1}H NMR of **P1** (300 MHz, CD$_2$Cl$_2$)

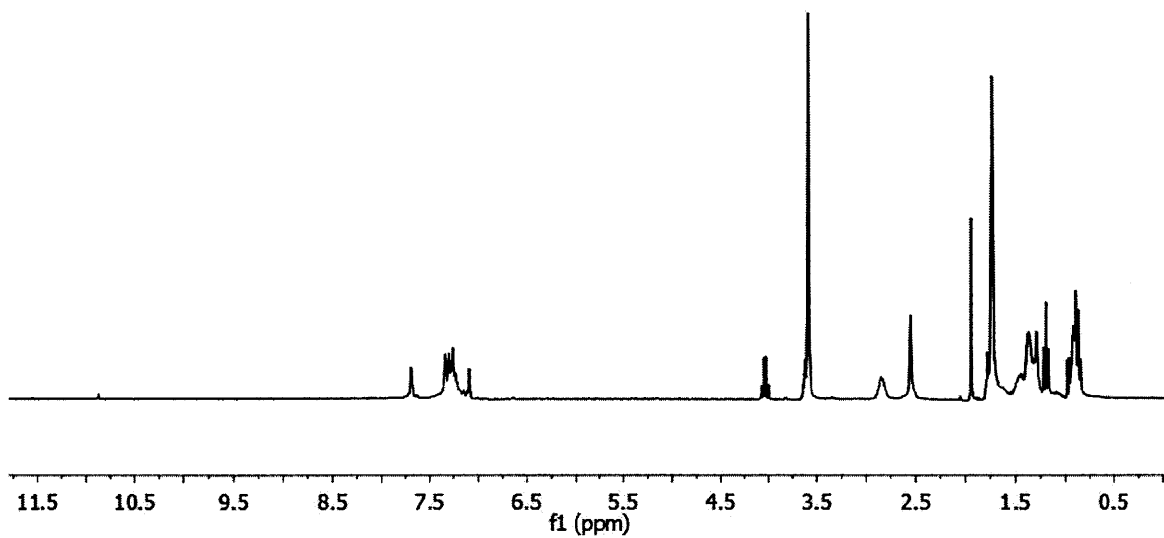# Appendix 3

NMR Spectra for Chapter 5

^{1}H NMR of **2** (300 MHz, CD$_2$Cl$_2$)
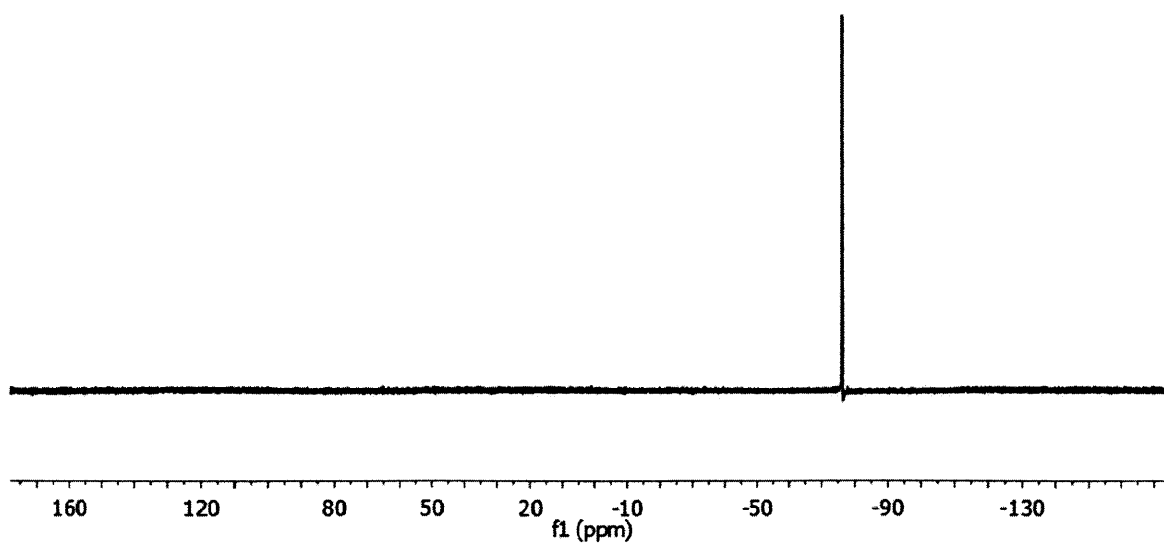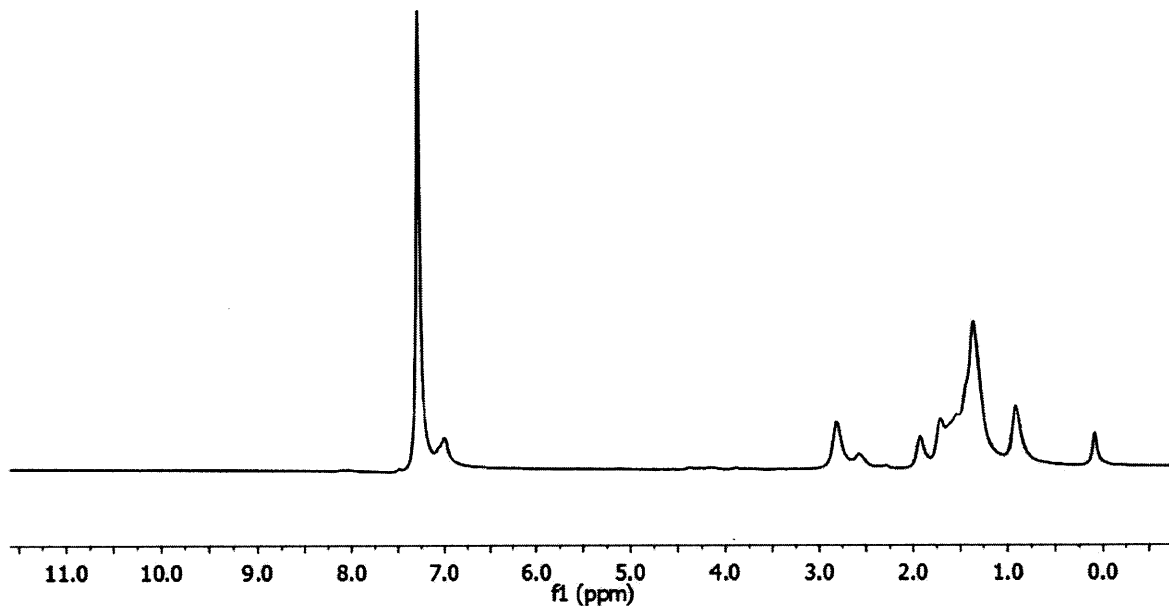

^{19}F NMR of **2** (282 MHz, CD$_2$Cl$_2$)

^{1}H NMR of **5** (300 MHz, CD$_2$Cl$_2$)

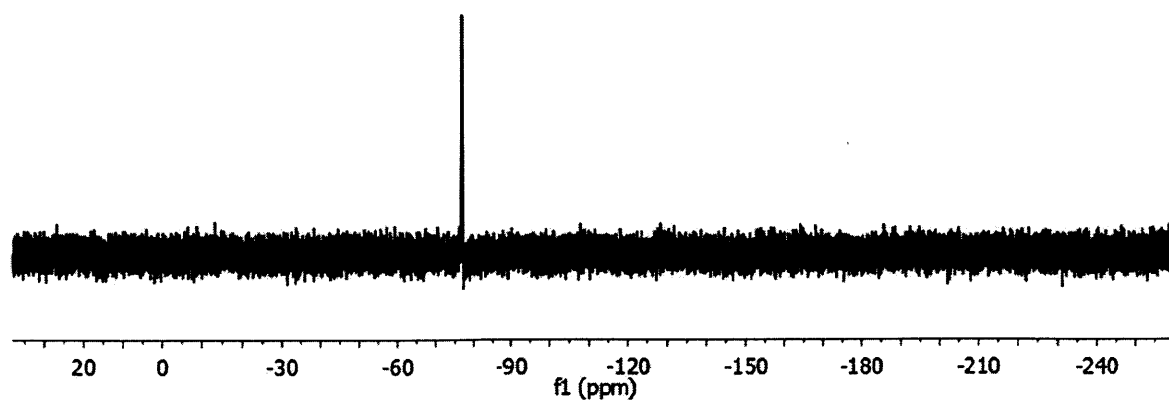^{1}H NMR of **P1** (300 MHz, THF)

^{19}F NMR of **P1** (282 MHz, THF)

^{1}H NMR of **P2** (500 MHz, CDCl$_3$)

^{19}F NMR of **P2** (470 MHz, CDCl$_3$)

Fei Wang

Education **MASSACHUSETTS INSTITUTE OF TECHNOLOGY (MIT)**   **CAMBRIDGE, MA**
Ph.D. in Materials Science and Engineering   **May 2010**
Concentration: Program in Polymer Science and Technology
Thesis: Polymer and Carbon Nanotube Materials for Chemical Sensors and Organic Electronics.
PEKING UNIVERSITY   **BEIJING, CHINA**
B.S. in Chemistry with Highest Honor (GPA: 3.85/4.00, Class Rank 2/170)   **2005**

Experience **MIT, DEPARTMENT OF CHEMISTRY**   **CAMBRIDGE, MA**
Graduate Research Assistant   2005–present
- Designed, synthesized and characterized several novel polymers and carbon nanotubes for high performance chemical sensing and organic photovoltaics.
- Established a sensory platform for ultra sensitive and selective, low-cost chemical detections, which resulted in 2 peer-reviewed papers, 1 co-authored paper, 1 patent, and 5 conference presentations to over 100 audiences each.
- Developed distributed sensors and improved their durability with MIT Lincoln Laboratory.
- Achieved extensive background in polymer science and engineering, including synthesis, physical chemistry, biomaterials, colloidal science, solid and fluid mechanics and statistical mechanics.

PEKING UNIVERSITY, DEPARTMENT OF CHEMISTRY   **BEIJING, CHINA**
Undergraduate Research Assistant   2003–2005
- Co-authored a paper on effective synthesis of aminosulfonic acids.
- Synthesized water-soluble inorganic nanoparticles as novel bio-marker materials.

Publications
- Alcazar, D.; **Wang, F.**; Swager, T. M.; Thomas E. L. "Gel Processing for Highly Oriented Conjugated Polymer Films." *Macromolecules* **2008**, *41*, 9863-9868.
- **Wang, F.**; Yang, Y.; Swager, T. M. "Molecular Recognition for High Selectivity in Carbon Nanotube/ Polythiophene Chemiresistors." *Angew. Chem. Int. Ed.* **2008**, *120*, 8522-8524.
- **Wang, F.**; Gu, H.; Swager, T. M. "Carbon Nanotube/Polythiophene Chemiresistive Sensors for Chemical Warfare Agents." *J. Am. Chem. Soc.* **2008**, *130*, 5392-5393.
- Huang, J.; **Wang, F.**; Xu, J. "A new and expeditious synthesis of 1-substituted and cyclic taurines." *Synthesis* **2005**, 2122-2128.

Conferences
- **Wang, F.**; **Swager, T. M.** "High performance nanotube sensor arrays." Oral presentation in Materials Research Society Meeting, Boston, MA, December **2009**
- **Wang, F.**; Swager, T. M. "Highly selective polythiophene/nanotube sensors." Oral presentation in Materials Research Society Meeting, Boston, MA, December **2008**
- **Wang, F.**; Swager, T. M. "Carbon nanotube networks as selective chemical sensors." Poster in Julius Springer Forum on Applied Physics, Cambridge, MA, September **2008** (**invited poster**)
- **Wang, F.**; Swager, T. M. "Carbon nanotube/polythiophene hybrid materials for high-performance chemical sensors." Oral presentation in Materials Research Society Meeting, San Francisco, CA, March **2008**
- **Wang, F.**; Yang, Y.; Swager, T. M. "Polythiophene/carbon nanotube chemiresistors as high-performance chemical sensors." Oral presentation in 234th American Chemical Society Meeting, Boston, MA, August **2007**
- **Wang, F.** "New fluorinated electronic polymers." Oral presentation in DuPont-MIT Alliance Student Symposium, MIT, Cambridge, MA, September **2006**

Awards
- **Ronald A Kurtz Fellowship** for Outstanding Academic Performance, MIT   2005
- **DuPont Scholarship** for Best Performance in Chemistry, Peking University   2004
- **Canon Scholarship** for Outstanding Academic Performance, Peking University   2003

Acknowledgements

The experience at MIT has left me with so many fond memories. I would like to take this opportunity to express my sincere appreciation to many of the people who helped and supported me throughout my time here.

I would like to start by thanking my research advisor, Professor Timothy M. Swager. His enthusiasm to science is a perfect role-model of how a great scientist could be, and has positively influenced many of his students including me. I am grateful for his guidance, including his inexhaustible ideas, insightful suggestions and the large freedom of research. I very much appreciate all that Tim has done for me. The experience of working with him is tremendously rewarding and enjoyable for me, and I will miss him as my supervisor.

I would also like to thank my thesis committee, Professor Michael Rubner, Professor Francesco Stellacci and Professor Michael Strano, for their valuable suggestions and strong support throughout my studies here.

It is a great opportunity to collaborate with so many intelligent colleagues on different areas. I would like to thank Hongwei who taught me how to disperse nanotubes and gave me many valuable advises. I thank Yong who worked with me on the molecular recognition project for his effort on polymer synthesis and helpful discussions. I thank Jill for helping me testing the photovoltaic performances of many of my polymers. I thank Daniel for finding interesting structural properties of the HFIP-PT. I thank Christina, Derek and Mindy from Lincoln Lab for collaboration on the distributive sensors. I thank Raul, Katsuhiro, Gaku, Tomoyuki and Yossi who collaborated with me on many nanotube projects.

It has been a very enjoyable experience working in Swager group. I thank Shuang for lots of joy working together and lots of help, Julian for many proof reading and discussions, and Mindy for proof reading my thesis, suggestions on jobseeking and joyful chattings. I thank Koushik, Jean and Becca for being great baymates. I will miss our office and bay. I also thank Bill and Yossi for proof reading the array sensing chapter. I thank John and Hongwei who spent a lot of time helping me getting oriented to the techniques used in the lab. I thank Jan for helping with XPS measurements and many nanotube samples. I thank Kathy, Caitlin and Becky for their assistance. I thank Dahui, Wei, Zhihua, Jean, Jessica, Andrew, Changsik, Anne, Stef, Daisuke, Paul, Trisha, Jose, Inja, Kazu and Arisa for scientific discussions. I also thank Scott, Eric, Jeewoo, Brett, Olisa, Joel, Jason, Dave, Birgit, Armando, Carlos and Joe for making the lab fun to work.

I was under the PPST program at MIT. I would like to thank Professor Gareth McKinley for recruiting me into this program. I thank Seung Woo, Erik, Carlos and Al for helping each other with the extensive curriculum of the first year. I also thank Yana, Yuki and many others for sharing their experience of PPST with me.

最后，我要感谢父母一直以来的关爱，教导和支持，感谢公婆克服重重困难万里迢迢来帮我们照顾牛牛。感谢晓成这些年来同甘共苦，共同成长和进步，希望我们的明天更美好。